



**MONASH** University

# **Modified soft elastomers for cardiac tissue engineering**

A thesis submitted for the degree of *Doctor of Philosophy* at  
Monash University in (2016)  
Department of Material Science and Engineering  
Faculty of Engineering  
Monash University  
Clayton VIC 3800  
Australia

# Copyright notice

© Chenghao Zhu (2016). Except as provided in the Copyright Act 1968, this thesis may not be reproduced in any form without the written permission of the author.

I certify that I have made all reasonable efforts to secure copyright permissions for third-party content included in this thesis and have not knowingly added copyright content to my work without the owner's permission.

# Abstract

Poly (glycerol sebacate) (PGS) is a biodegradable crosslinked polyester elastomer. Due to its hemocompatibility, biodegradability, soft and flexible mechanical properties, PGS has been studied to replace or repair soft tissues in mechanically dynamic environments such as myocardial tissue. In this project, PGS based scaffolds were designed and fabricated to address some of the drawbacks of PGS and enhance the performance of cardiomyocytes which is the main component of myocardial tissue.

The properties of PGS were modified by blending and/or copolymerizing PGS with another biocompatible polymer, poly(3-hydroxybutyrate-4-hydroxybutyrate) (P34HB). These blends provided a wider range of mechanical properties without losing the elastomeric characteristics of PGS. The degradation rates of the blends were also reduced in comparison with PGS. Since a patient's recovery from myocardial infarction (MI) is a long process, slower degradation rates can provide more enduring mechanical support for myocardial tissue.

In the second part of this thesis, micropatterns exhibiting repetitive grooves and crests were fabricated on the surface of PGS substrates. More aligned cardiomyocytes, better beating behavior and higher amplitude of  $\text{Ca}^{2+}$  transients could be achieved using


substrates with such topographical features. Cardiomyocytes were confined by the grooves, and formed anisotropic structures reminiscent of natural myocardial tissue.

Brain derived neurotrophic factor (BDNF) small molecule mimetic was copolymerized into the PGS network and slowly released from the polymer during its bio-degradation. Recent studies showed that BDNF is an important factor for cardiomyocytes normal contraction and relaxation, not only in conditions such as hypoxia and ischemia, but during normal physiological function. The contractile force of myocardium is controlled by intracellular  $\text{Ca}^{2+}$  concentration and  $\text{Ca}^{2+}$  transients regulation regulates beating and provides a constant cardiac output. The amplitude of calcium transients of cardiomyocytes was elevated in the presence of BDNF mimetic, similar to BDNF full protein. Thus BDNF mimetic copolymerized in the PGS network could provide a potential therapy for insufficient cardiac output.

# Declaration

*All Students should reproduce this section in their thesis verbatim*

This thesis contains no material which has been accepted for the award of any other degree or diploma at any university or equivalent institution and that, to the best of my knowledge and belief, this thesis contains no material previously published or written by another person, except where due reference is made in the text of the thesis.

Signature:  ..

Print Name: Chenghao Zhu

Date: .....19<sup>th</sup>/08/2016.....

# Publication during the enrolment

**Zhu C**, Andrew R, Zhou K, John MH, Bing Wang<sup>3</sup>, Cook WD, Forsythe J, Micropatterned tissue-like bioelastomers improve cardiomyocyte alignment and beating homogeneity Biofabrication Submitted.

Xu B, Cook WD, **Zhu C**, Chen Q. Aligned core/shell electrospinning of poly (glycerol sebacate)/poly (l - lactic acid) with tuneable structural and mechanical properties. Polymer International 2016.

Xu B, Li Y, **Zhu C**, Cook WD, Forsythe J, Chen Q. Fabrication, mechanical properties and cytocompatibility of elastomeric nanofibrous mats of poly (glycerol sebacate). European Polymer Journal 2015; 64:79-92.

**Zhu C**, Chen Q. Polyhydroxyalkanoate-Based Biomaterials for Applications in Biomedical Engineering. Advanced Healthcare Materials 2014:439-64.

Chen Q, **Zhu C**, Thouas GA. Progress and challenges in biomaterials used for bone tissue engineering: bioactive glasses and elastomeric composites. Progress in Biomaterials 2012; 1:1-22.

---

# Acknowledgements

I would like to express my deepest gratitude to my advisors, A/Prof. John Forsythe, Prof. Wayne Cook and A/Prof. Binghui Wang, for their guidance and inspiration. Their enthusiasm for this project, dedication to academic research and rigorous attitude toward presentation shaped my understanding of scientists. Their always humble, patient and considerate manners towards others also hugely influence me.

My sincere thanks also go to Dr. Vinh Truong who helped in the synthesis of BDNF mimetic and advice on chemistry related work.

I would also like to thank Mr. Silvio Mattievich for his technical support. Without his help and valuable advice, the experiments had not been possible to conduct.

I gratefully acknowledge Dr. Andrew Rooda for modifying the code for the  $\text{Ca}^{2+}$  transients, Ms. Karla Contreras for assisting with cell assays, Dr. Kun Zhou and Mr. Fanyi Li for their assistance in cell imaging.

I am very fortunate to work and spend most of my time with my group mates: Mr. Jason Marroquin, Miss. Sepideh Motamed, Ms. Patcharin Chen, Mr. Richard Fernando, Mr. Andrew Hong, Mr. Fnayi Li, Mr. Kelly Tsang, Mr. Julian Ratcliffe and Miss. Yue Shi. I would also like to thank the fellow PhD students and postdocs in our department for their help and supports.

I am indebted to my roommates Ms. Yue Hua for her support during the thesis writing.

Thanks for the great food she cooked.

Finally, I want to thank my family for their love and support. Without my parents' firm support, I would not finish my PhD project



## Table of Contents

Copyright notice .....	i
Abstract .....	ii
Declaration .....	i
Publication during the enrolment .....	ii
Acknowledgements .....	i
Table of Contents .....	iii
List of Figures.....	vii
List of Tables.....	xi
List of abbreviations and acronyms.....	xii
1 Introduction.....	14
Background of myocardial infarction and biomaterial based therapies.....	15
Objectives of the project .....	18
Structure of the thesis.....	18
2 Literature Review .....	21
2.1 Biomaterials used for cardiac tissue engineering.....	22
2.1.1 Synthetic thermoplastics .....	28
2.1.2 Synthetic elastomers .....	32
2.1.3 Naturally derived polymers .....	37
2.1.4 Summary.....	44
2.2 Methods applied for aligned cardiomyocytes.....	45
2.2.1 Physical cues .....	45
2.2.2 Mechanical cues .....	47
2.2.3 Electrical cues .....	48
3 Developing elastomeric biomaterials from P34HB and PGS for soft tissue engineering	50
3.1 Introduction.....	52
3.2 Material and methods .....	54
3.2.1 Materials.....	54
3.2.2 Synthesis of P34HB/PGS blends .....	54

3.2.3	X-Ray Diffraction (XRD).....	54
3.2.4	Differential scanning calorimetry (DSC) .....	55
3.2.5	Visual examination .....	55
3.2.6	Mechanical characterization .....	55
3.2.7	Percentage of esterification characterization .....	56
3.2.8	Degradation .....	57
3.2.9	Cytocompatibility.....	58
3.2.10	Cardiomyocyte culture .....	59
3.2.11	Immunocytochemistry.....	59
3.3	Results and discussion.....	60
3.3.1	Crystallinity of P34HB blends.....	60
3.3.2	Thermal analysis of P34HB/PGS blends.....	62
3.3.3	Transparency of P34HB/PGS blends.....	63
3.3.4	Mechanical properties.....	65
3.3.5	Titration results .....	67
3.3.6	Degradation Tests.....	68
3.3.7	Cytotoxicity Assessment.....	70
3.3.8	Cardiomyocytes cell culture .....	72
3.4	Conclusions.....	74
4	Micropatterning of PGS.....	76
4.1	Introduction .....	77
4.2	Materials and methods.....	78
4.2.1	Fabrication of the master .....	78
4.2.2	PDMS stamp fabrication .....	79
4.2.3	PGS substrate fabrication .....	79
4.2.4	Micropattern characterization .....	80
4.2.5	Contact angle tests .....	80
4.3	Results and Discussion.....	81
4.4	Conclusion .....	86
5	Micropatterned tissue-like bioelastomers improve cardiomyocyte alignment and beating homogeneity .....	87
5.1	Introduction.....	89

5.2	Materials and Methods .....	90
5.2.1	Mechanical and morphology characterization.....	90
5.2.2	PGS film pretreatment.....	91
5.2.3	Cardiomyocytes cell culture .....	91
5.2.4	Video imaging and quantification.....	92
5.2.5	Immunocytochemistry.....	92
5.2.6	Nuclei alignment analysis .....	92
5.2.7	Calcium imaging.....	93
5.2.8	Statistical Analysis .....	93
5.3	Results and Discussion.....	94
5.3.1	Mechanical properties of PGS .....	94
5.3.2	Cell alignment and immunochemical analysis.....	95
5.3.3	Beating and intracellular calcium transient characterization.....	100
5.4	Conclusion .....	103
6	Incorporation of BDNF mimetic in PGS and effect on cardiomyocytes cell culturing...	105
6.1	Introduction.....	107
6.2	Material and methods .....	110
6.2.1	Synthesis of PGS and BDNF incorporated PGS (PGSB) .....	110
6.2.2	Mechanical characterization of PGSB.....	110
6.2.3	Thermal characterization.....	111
6.2.4	Degradation characterization of PGSB .....	111
6.2.5	UV-vis spectroscopy characterization .....	112
6.2.6	Nuclear Magnetic Resonance (NMR) characterization .....	112
6.2.7	HPLC characterization.....	112
6.2.8	BDNF treatment and calcium transient imaging .....	113
6.2.9	Viability assay .....	113
6.2.10	Cardiacmyocyte hypertrophy assay .....	114
6.2.11	Statistical analysis.....	115
6.3	Results and Discussion.....	115
6.3.1	Mechanical properties of PGSB .....	115
6.3.2	Thermal properties of PGSB .....	116
6.3.3	Degradation of PGSB and UV-Vis spectroscopy .....	117

6.3.4	Analysis of degradation products of PGSB by HPLC .....	120
6.3.5	<sup>1</sup> H NMR of degradation products .....	123
6.3.6	Calcium transients in cardiomyocytes in presence of BDNF full protein or BDNF mimetic .....	125
6.3.7	Cardiac cellular viability and cardiomyocyte hypertrophy .....	130
6.4	Conclusion .....	131
7	Conclusions and future work.....	133
7.1	Conclusions.....	134
7.2	Limitations of the study and future work.....	136
	Reference .....	139

## List of Figures

Figure 1-1 The injury and healing of myocardium tissue at different stages (a) healthy myocardium tissue (b) protein loss of cardiomyocytes due to leaky membranes (c) the replacement of cardiac fibroblasts and (d) scar developed in the infarcted area. ....	16
Figure 1-2 Cardiomyocyte suspension is directly injected into the defective tissue or into the systemic circulation (left branch). The cells are expected to home to the site of interest or stay at the site of injection. However, little guidance is provided to the cells by the transplant system. Cardiomyocytes may also be delivered through a biomaterial carrier (right branch), typically a biodegradable polymer. More robust cardiomyocytes are adhered to the biomaterial carrier. Reproduced with permission from American Chemical Society (2001) .....	17
Figure 2-1 Synthetic thermoplastic scaffolds exhibit good biocompatibility with cardiomyocytes. Muscle-specific features of engineered cardiac tissue were found on these biomaterials. (a) Transmission electron micrograph showing myofibrils, sarcomeres with Z lines (z), abundant mitochondria (mit) on PGA. Scalebar = 500 nm. (b) Immunohistochemical staining for F-actin which covers the entire surface of the PCL scaffold. Scalebar = 50 $\mu$ m (c) SEM micrograph of the PCL surface. The mesh is covered with multilayers of cells. Scalebar = 100 $\mu$ m. a) Reproduced with permission from The American Physiological Society Copyright (2001) b) Reproduced with permission from Elsevier (2005) c) Reproduced with permission from Elsevier (2005). ....	32
Figure 2-2 (a) Phase contrast images of monolayer aligned cells cultured on PU films (left), additional cells cultured on the aligned cells (middle) and the additional cells labeled with cell tracker green (right). (b) The structure of accordion-like PGS scaffold (monolayer and bilayer) and cardiomyocytes cultured on the bilayer scaffold (c) $\alpha$ -actin (red), connexin 43 (green) and nuclei (blue) of cardiomyocytes cultured within PEGylated fibrinogen hydrogels. a,b&c) reproduced with permission from Elsevier .....	37
Figure 2-3 (a) Filaments (green) and connexin 43 (red) were found on cardiomyocytes cultured on a tubular collagen scaffold. (b) More aligned cardiomyocytes were found on carbon nanotube (CNT) incorporated gelatin compared with the control group. (c) Vascularization with alginate scaffold C and without B. a) Reproduced with permission from American Chemical Society Copyright. b) Reproduced with permission from Elsevier Copyright (2002). c) Reproduced with permission from American Heart Association Copyright.....	44
Figure 2-4 The diffusion spectrum MRI tractography of visualized fibers in the normal heart (a) and infarcted heart (b). The difference in colour indicates the fibres at different depths. Reproduced with permission from Wolters Kluwer Health, Inc. ....	47

Figure 2-5 The significant improvement in cell alignment by physical cues (a), mechanical cues (b) and appreciable improvement by electrical cues (arrow indicates the electrical field direction) (c). Reproduced with permission from Elsevier.....	49
Figure 3-1 Examples of XRD scans (10° to 60°) of (a) pure PGS and blends (b) pure P34HB and (c) crystallinity as a function of P34HB weight percentage. ....	62
Figure 3-2 Non-isothermal DSC curves of pure PGS and P34HB/PGS blends (30% & 50%). ....	63
Figure 3-3 (a) Visual observation to show the single transparent phase at low content (≤50 wt%). (b) The ROIs with the same pixels were labelled in different samples and the standard ROI is shown separately at the bottom of the figure. (c) The light intensity of ROI in different samples. ....	65
Figure 3-4 Examples of stress strain curves of P34HB (a), PGS (b), P34HB/PGS blends (c) after curing .....	66
Figure 3-5 (a) Percent esterification of pure PGS and P34HB/PGS blends and (b) The unreacted sebacic acid(g) in 100g blends.....	68
Figure 3-6 (a) Weight loss of PGS and P34HB/PGS blends over time; (b) pH change of PGS and P34HB/PGS over time.....	69
Figure 3-7 Images of SNL cells in extracts prepared with different samples in the first day (left image) and the second day (right image) (a) PGS; (b) 30% P34HB/PGS; (c) 50%P34HB. (d) summary of percentage of living cells after incubation. ....	72
Figure 3-8 (a) Elongated cardiomyocytes were found on the PGS film. Hypertrophic cardiomyocytes were found on 30% P34HB/PGS (b) and 50% P34HB/PGS (c) Round cardiomyocytes were found on the P34HB films; (d) Comparison between cardiomyocytes cultured on different samples.....	74
Figure 4-1 Schematic diagram showing the steps in the fabrication of micropatterned PGS .....	80
Figure 4-2 Examples of PGS micopatterns with 1.5 μm (a), 3 μm (b) and 7 μm (c) depth and the examples of measurements in crest width(d) and chanel depth (e) .....	82
Figure 4-3 Insufficient exposure time leads to the shallow groove depth (a) compared with designs (b) .....	83
Figure 4-4 Insufficient UV exposure led to detachment of the photoresist patterns (a). Corresponding patterns on the solid silicon wafer (b). Scale bar = 100 μm. ....	83
Figure 4-5 The PGS peeled from silicon wafer with damage (a) and the PDMS replica peeled from silicon wafer (b).....	84
Figure 4-6 PGS peeled from PDMS and exhibited damaged features (a) and limited damage with a sucrose coating (b) .....	84
Figure 4-7 Quantification of groove width, channel width and channel depth (μm) of micropatterned PGS films.....	85

Figure 5-1 (a) Stress-strain curves of PGS synthesized at 160 °C under vacuum conditions for 8 hr (b) 50-cyclic-stress-strain curve of PGS synthesized under the same conditions. ....	95
Figure 5-2 Phase contrast images of cardiomyocytes cultured on PGS films with different patterns showing alignment with channels of nominal width (a) 10 $\mu$ m, (b) 20 $\mu$ m, (c) 50 $\mu$ m patterns and (d) for unpatterned PGS. The alignment of cardiomyocytes was confirmed by fluorescent images stained with troponin I antibody which is a specific marker of myofilaments of cardiomyocytes (green) (e) 10 $\mu$ m, (f) 20 $\mu$ m, (g) 50 $\mu$ m patterns and (h) unpatterned PGS. The inserted images in (e) - (h) show elongation of nuclei towards the channel directions in micropatterned PGS. (i) The degree of angles between the orientation of the nuclei and channel direction summarized in 10°, and (j) quantification of the proportion of aligned nuclei (degree of angles below 20°) on different pattern features. ....	98
Figure 5-3 Fluorescent images comparing the effects of different PGS micropatterns on cardiomyocytes alignment. (a-h) show confocal images of cardiomyocytes (day 7) fixed and stained with DAPI (blue), connexin (green) and sarcomeric $\alpha$ -actinin (red) that stains for the striated Z-lines of myotubes in cardiac muscle. The arrows indicate the alignment direction of the cardiomyocytes. (a-d) were taken at 10x magnification while (e-i) were taken at 40x magnification following the order of 10 $\mu$ m, 20 $\mu$ m, 50 $\mu$ m and unpatterned PGS. ....	100
Figure 5-4 (a) Representative traces showing beating characteristics of cardiomyocytes at day 4 on 10 $\mu$ m, 20 $\mu$ m, 50 $\mu$ m and unpatterned substrates by monitoring pixel intensity in regions of interest over a period of 20s. (b) Comparison of the average time between beats and beat homogeneity (indicated by standard deviation) between different patterned PGS and unpatterned PGS.....	102
Figure 5-5 Amplitude histograms of $\text{Ca}^{2+}$ transients measured using Fluo-4 (a) and peak amplitude scattergrams (b) from over 100 cells for PGS films with of 10 $\mu$ m, 20 $\mu$ m, 50 $\mu$ m micropattern size and unpatterned films. (c) The number of activated cells involved in a $\text{Ca}^{2+}$ transient. ....	103
Figure 6-1 (a) BDNF effects on synaptogenesis through TrkB receptor and downstream pathways. (b) Activation of truncated TrkB has the potential to modulate glial $\text{Ca}^{2+}$ signaling. A) Reproduced with permission from Nature Publishing Group (2013) B) Reproduced with permission from Taylor and Francis Group (2004) .....	107
Figure 6-2 Chemical structures of (a) glycerol (b) sebacate and (c) BDNF mimetic (LM224-A) .....	109
Figure 6-3 (a) Stress-strain curves of PGS and PGSB. (b) The Young's modulus of PGS and PGSB. No significant difference in moduli was observed with incorporation of the BDNF mimetic (the percentage indicates the molar ratio of BDNF mimetic in the copolymer) .....	116
Figure 6-4 DSC results of BDNF mimetic, PGS and PGSB. ....	117

Figure 6-5 UV-vis spectra of the BDNF mimetic and PGSB degradation products shown in (a). The typical BDNF mimetic absorption peak was at 202 nm. The concentration of the BDNF mimetic released was calculated based on the calibration curve (b). The peak of BDNF mimetic was not obvious for PGSB soaked for a week in MQ water (c).....	119
Figure 6-6 Visual inspection of the PGSB degradation DMEM solutions with or without enzyme at different time points. ....	120
Figure 6-7 (a) BDNF mimetic HPLC peak at 15.1 min at different concentrations (mAu = milliabsorbance units). (b) The peak (circled) was found in PGSB degraded in 1mol/L hydrochloric acid. (c) The released BDNF mimetic concentration in DEME with and without porcine liver esterase enzyme at different time points.....	122
Figure 6-8 The <sup>1</sup> H-NMR spectra showing the proton peaks of amide and aromatic ring in the degradation product (a) and in pure BDNF mimetic (b). ....	124
Figure 6-9 Scattergrams of calcium transients of cardiomyocytes cultured on unpatterned substrates (a) PGS without any treatment (b) PGS treated with 20 nM BDNF full protein (c) PGS treated with 60 nM BDNF mimetic (d) 5% PGSB. ....	126
Figure 6-10 Scattergrams of calcium transients of cardiomyocytes cultured on 20 μm patterned substrates (a) PGS without any treatment (b) PGS treated with 20 nM BDNF full protein (c) PGS treated with 60 nM BDNF mimetic (d) 5% PGSB ....	127
Figure 6-11 Histogram of cardiomyocytes calcium transients amplitudes cultured on unpatterned substrates (a) PGS without any treatment (b) PGS treated with 20 nM BDNF full protein (c) PGS treated with 60 nM BDNF mimetic (d) 5% PGSB. ....	128
Figure 6-12 Histogram of cardiomyocytes calcium transients amplitudes cultured on 20 μm patterned substrates (a) PGS without any treatment (b) PGS treated with 20 nM BDNF full protein (c) PGS treated with 60 nM BDNF mimetic (d) 5% PGSB.....	129
Figure 6-13 The calcium transient amplitude comparasion between the drug treated and control groups of unpatterned (e) and 20 μm patterned (f) samples. ....	129
Figure 6-14 The 100 nmol/L BDNF mimetic did not affect the viability of cardiomyocytes (a) BDNF mimetic or BDNF full protein at different concentrations did not clearly reveal any inhibition effects to Ang II(b) (* indicates significant difference from control group). ....	131



## List of Tables

Table 2-1 Selected synthetic thermoplastics, elastomers and naturally occurring polymers investigated as scaffold materials .....	24
Table 3-1 Crystallinity of blends, pure PGS and pure P34HB .....	62
Table 3-2 Summary of P34HB/PGS blends thermal properties (* indicates significant difference from PGS with $p < 0.05$ ) .....	63
Table 3-3 Summary of mechanical properties of P34HB/PGS blends (* indicates significant difference from PGS with $p < 0.05$ ).....	67

## List of abbreviations and acronyms

3D	Three dimensional
ACE	Angiotensin converting enzyme
ADSC	Adipose tissue-derived stem cells
BDNF	Brain derived neurotrophic factor
BrdU	Bromodeoxyuridine
BMC	Bone marrow cells
DAPI	4',6-diamidino-2-phenylindole
DEME	Dulbecco's modified eagle medium
DSC	Differential scanning calorimetry
ECM	Extracellular matrixes
EDV	End-diastolic volume
EHT	Engineered heart tissue
ESC	Embryonic stem cells
ESV	End-systolic volume
FDA	Food and Drug Administration
FEG	Field emission gun
GelMA	Gelatin mechacrylate
HA	Hyaluronic acid
HF	Heart failure
HPLC	High performance liquid chromatography
JoVE	Journal of Visualized Experiments
LV	Left ventricle
LVEDD	Left ventricular end-diastolic diameter
LVEF	Left ventricular ejection fraction
MAGNUM	Myocardial assistance by grafting a new bioartificial upgraded myocardium
MEM	Minimal essential medium
MI	Myocardial infarction
MQ	Milli Q
MSC	Mesenchymal stem cells
NBCS	New born cow serum
NGS	Normal goat serum
NMR	Nuclear Magnetic Resonance
PEG	Polyethylene glycol
PCL	Polycaprolactone
PDLA	Poly-D-lactide
PDMS	Polydimethylsiloxane
PBS	Phosphate buffered saline
PGA	Poly (glycolic acid)
PGS	Poly (glycerol sebacate)
PGSB	BDNF mimetic incorporated PGS
PLA	Polylactide
PLLA	Poly-L-Lactide

PU	Polyurethane
RASS	Renin-angiotensin-aldosterone system
RGD	Arginylglycylaspartic acid
ROI	Region of interest
ROS	Reflective oxygen species
SD	Standard deviation
SEM	Scanning electron microscope
SMC	Smooth muscle cells
TEM	Transmission electron microscopy
TIPS	Thermally induced phase separation
TrkB	Tropomyosin receptor kinase B
UBM	Urinary bladder matrix
XRD	X-Ray Diffraction

# 1 Introduction

## Declaration for Thesis Chapter [1]

### Declaration by candidate

In the case of Chapter [1], the nature and extent of my contribution to the work was the following:

Nature of contribution	Extent of contribution (%)
Major research and writing	90

The following staff/students contributed to the work.

Name	Nature of contribution	Extent of contribution (%) for student co-authors only
Wayne Cook	Provided corrections	N/A
John Forsythe	Provided corrections	N/A

The undersigned hereby certify that the above declaration correctly reflects the nature and extent of the candidate's and co-authors' contributions to this work\*.

**Candidate's  
Signature**

	<b>Date</b> 26 <sup>th</sup> /08/2016
---	--

**Main  
Supervisor's  
Signature**

	<b>Date</b> 26 <sup>th</sup> /08/2016
---	--

## **Background of myocardial infarction and biomaterial based therapies**

Myocardial infarction (MI), also commonly known as heart attack, is the cause of about 12.8 % of all deaths globally, making it the leading cause of death [1]. The most common reason for MI is the atherosclerotic plaque build-up in coronary arteries, which compromises the blood flow to myocardial tissue [2]. In some cases, the narrowing of artery results in an increased blood flow speed and removal of the plaque. However, if the plaque does not rupture, a thrombus will develop in this position. The myocardial tissue is deprived of oxygen when a clot is developed in the upstream in coronary artery, which serves the area of myocardium. Irreversible damage is formed in this area 20 mins after the formation of the clot. First, the membranes of cardiomyocytes become leaky due to the deprivation of oxygen. Then, the invasion of enzymes through leaky membranes results in the loss of proteins in cardiomyocytes and the invasion further leads to the cardiomyocytes death. Dead cardiomyocytes are removed by neutrophils and macrophages. As the adult heart has limited regeneration capacity, the dead cardiomyocytes are replaced by cardiac fibroblasts. Finally, a scar is formed in this area by type I collagen synthesized by cardiac fibroblasts (Fig. 1-1).

## 1. Introduction

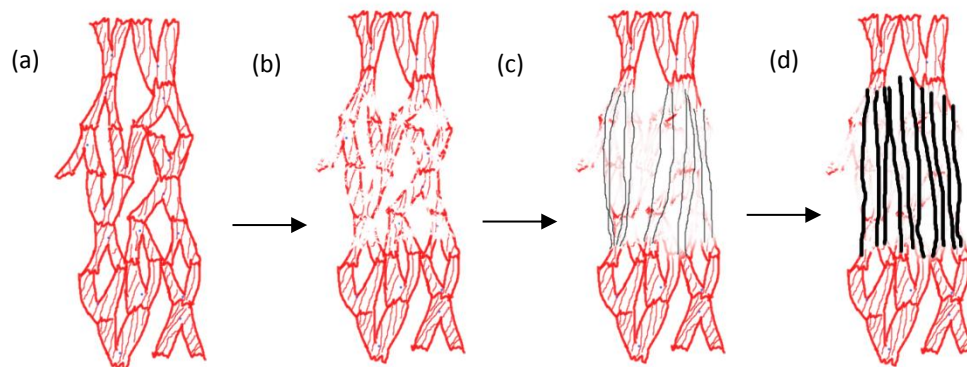


**Figure 1-1 The injury and healing of myocardium tissue at different stages (a) healthy myocardium tissue (b) protein loss of cardiomyocytes due to leaky membranes (c) the replacement of cardiac fibroblasts and (d) scar developed in the infarcted area.**

Compared with healthy myocardial tissue, the scar tissue lacks contractile function. But to maintain the cardiac output at an acceptable level, hypertension is developed in the heart which leads to an increase in the size of left ventricle. The extra burden on other myocardial tissue over time will finally lead to heart failure [3].

Blood flow can be restored by thrombolysis without myocardial tissue damage if the clot is detected in the early stages. However, this is not always the case. Medications need to be given to a patient if MI is advanced to reduce the risk of other complications, the risk of another MI and mortality. Such drugs include  $\beta$ -blockers which reduce the force of heart beat and the beat rate, nitrates which dilate the blood vessels to improve blood flow and angiotensin converting enzyme (ACE) inhibitor to reduce blood pressure and negative structural changes [4]. Though the drug treatments relieve symptoms and prevent

## 1. Introduction

deterioration of the MI, they do not address the underlying cause of cardiomyocytes death and lack of regeneration. A straightforward way is to introduce cardiomyocytes to the infarcted myocardial tissue. Early studies showed that introducing these cells into the infarcted myocardium by injection of cells in a suspension either into the circulating blood or directly into the myocardium was not efficient, with substantial cell loss [5-7]. Dramatic improvement in cell attachment and accuracy of cells localization can be achieved by the use of biomaterial carriers [8, 9]. The specially designed biomaterials can also be used as a template for the formation of new tissue masses from the combination of transplanted cells and interfacing host cells [10] (Fig .1-2).

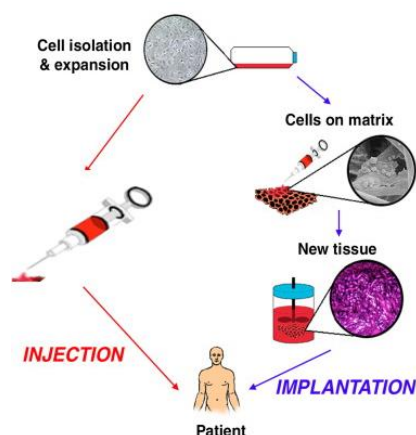


**Figure 1-2 Cardiomyocyte suspension is directly injected into the defective tissue or into the systemic circulation (left branch). The cells are expected to home to the site of interest or stay at the site of injection. However, little guidance is provided to the cells by the transplant system. Cardiomyocytes may also be delivered through a biomaterial carrier (right branch), typically a biodegradable polymer. More robust cardiomyocytes are adhered to the biomaterial carrier. Reproduced with permission from American Chemical Society (2001)**

Mechanical support protects the thinning area of myocardial tissue with an elastic modulus less than 50 kPa [11] from rupture when cardiomyocytes are lost. The modulus

## 1. Introduction

of myocardial differs at different pathological processes. After fibrosis, the myocardial tissue partially loses elasticity with a modulus up to 900 kPa with an extension of 20% [12] which is much larger than the modulus of normal myocardial with a modulus of 160kPa [13]. The use of an elastic patch that attaches to the external surface has been suggested. When the left ventricle expands, energy is loaded into the patch and is released to the heart during the contraction [14].

### **Objectives of the project**

The drawbacks relating to the PGS application as myocardial tissue such as such as the unfavourable to adhesion of MSCs, hESCs and cardiomyocytes [5, 15] and the incapability to simultaneously adjust the stiffness and degradation rate [16]. Additionally, due to the unique features of myocardial tissue like alignment in cardiomyocytes arrangement [17], modifications need to be applied on PGS to fit the working environment and assist the normal function of myocardial tissue. In this project, PGS based scaffolds were designed and fabricated i) to address the fast degradation rate of PGS compared with the long healing period of myocardial tissue, ii) to improve the alignment and beating behaviour of cardiomyocytes cultured on the scaffold and iii) to deliver potential therapeutic drugs to maintain normal function of cardiomyocytes.

### **Structure of the thesis**



## 1. Introduction

Chapter 1. This chapter introduces the general pathophysiology of MI and the mechanisms of the heart's self-healing after MI. It describes the negative aspects of self-healing due to the lack of regenerative ability of cardiomyocytes and the formation of fibrosis. The potential therapies of MI are introduced and the prospect of biomaterial-based therapies are discussed. The chapter also includes the aims and motivations for the project.

Chapter 2. In this chapter, the requirements of biomaterials in myocardial tissue engineering are discussed. The biomaterials used in this area are summarized and the advantages and limitations of different biomaterials are discussed. The methods that have been previously used to form aligned cardiomyocytes structures are briefly summarized. Hypotheses and approaches taken in the project based on literature trends and conclusions are introduced in this chapter as well.

Chapter 3. Blending is a convenient and low-cost way to make new materials with tunable properties. In this chapter, the P34HB/PGS blend system was explored. The mechanical, thermal properties and crystallinity of these materials were characterized. The mechanism of their reduced degradation rate was discussed in terms of greater hydrolysis resistance of P34HB. The cytocompatibility of the blends was demonstrated by culturing SNL cells in media extracts and by studying their effect on mouse cardiomyocytes. Although the cardiomyocytes cultured on the blends did not show ideal cell morphology, there was no significant difference of cell density compared with the negative control group.

## 1. Introduction

Chapter 4. The technique of micro-contact patterning was applied to fabricate PGS with various topologies. The relationships between the photoresist compositions, fabrication methods and the PGS topology are discussed. The optimization of protocols for micro-contact patterning of PGS is given.

Chapter 5. The optimal features were determined for cardiomyocytes alignment. The relationship between the degree of alignment and the beating behavior is discussed.

Chapter 6. In this chapter poly (glycerol sebacate) (PGS) was used as a substrate to study cardiomyocyte's  $\text{Ca}^{2+}$  transients in the presence or absence of BDNF mimetic. To maintain the BDNF mimetic at a potentially therapeutic level for a long period, the BDNF mimetic was polymerised into the PGS network. The release of BDNF mimetic was studied in the presence or absence of pork liver esterase. The concentration of BDNF mimetic was measured as a function of degradation time.

Chapter 7. A summary of the work carried out and likely future directions have been discussed in the final chapter

## 2 Literature Review

### Declaration for Thesis Chapter [2]

#### Declaration by candidate

In the case of Chapter [2], the nature and extent of my contribution to the work was the following:

Nature of contribution	Extent of contribution (%)
Major research and writing	90

The following staff/students contributed to the work.

Name	Nature of contribution	Extent of contribution (%) for student co-authors only
Wayne Cook	Provided corrections	N/A
John Forsythe	Provided corrections	N/A
Binghui Wang	Provided corrections	N/A

The undersigned hereby certify that the above declaration correctly reflects the nature and extent of the candidate's and co-authors' contributions to this work\*.

**Candidate's  
Signature**

	<b>Date</b> 26 <sup>th</sup> /08/2016
---	--

**Main  
Supervisor's  
Signature**

	<b>Date</b> 26 <sup>th</sup> /08/2016
---	--

### **2.1 Biomaterials used for cardiac tissue engineering**

Myocardial infarction (MI) is the damage of myocardium caused by ischemia or hypoxia. The infarcted tissue does not contribute to tension generation and after weeks, a collagen scar forms at the infarct site. Long term consequences include cardiac remodelling and possible progression to heart failure (HF) [18, 19]. There are several treatments to alleviate the symptoms. To compensate for the loss in cardiac output and a drop in blood pressure, renin-angiotensin-aldosterone system (RAAS) is excessively activated. However, chronic overactivity of the RAAS leads to collagen formation and cardiomyocytes hypertrophy, which plays a fundamental role in HF. Therefore HF related symptoms could be alleviated by pharmacological therapy to cut off the pathways between the RAAS such as angiotensin receptor blockers, angiotensin-converting enzyme inhibitors and aldosterone blockers [20]. Another treatment is the implantation of pacing devices to control electrical/mechanical asynchrony which are used for patients with marked symptoms [21]. However, neither therapy can control the inevitable progression to heart failure [22].

Several strategies have been studied as alternative therapies. Passive mechanical constraints by a muscle wrap can possibly halt or even reverse the remodelling of the dilated heart [23, 24]. The key issue is to find a biomaterial that provides the desired

## 2. Literature Review

mechanical properties such as high elasticity and Young's modulus less than 1Mpa [25].

Another promising strategy is cell transplantation. Replacement cells are injected into the infarcted area via the pericardium [26], [27] coronary arteries [7, 28] and endocardium.

To possibly improve cell engraftment and site accuracy, it has been proposed that cells can be transplanted using a cardiac patch [29]. Cell attachment is a basic requirement for the cardiac patch and it must also provide mechanical support to the myocardium.

Therefore, the choice of biomaterial is critical. Here, biomaterials used for myocardial tissue engineering and the effects in treatment are summarized (Tab. 2-1) and discussed.

Generally, they are divided into three groups: synthetic thermoplastics, synthetic elastomers and naturally occurring polymers. The advantages and disadvantages of the three types biomaterials are discussed. Multicomponent blends and copolymers are categorized by the major component. Despite differences in the fabrication method, the biomaterials are reviewed in the following sequence: i) without any cells, ii) with non-cardiac cells, iii) with cardiac cells, iv) with stem cells and v) used for human trials.

Proper alignment of cardiomyocytes with neighbouring cells provides optimal coupling for electrical signal propagation, synchronous cell contractions, and effective force production required for normal cardiac function [30]. Achieving the parallel organization cardiomyocytes is an important objective in cardiac tissue engineering. The strategies to achieving parallel cardiomyocytes are also divided into three groups by the cues they provide: physical cues, mechanical cues and electrical cues.

## 2. Literature Review

**Table 2-1 Selected synthetic thermoplastics, elastomers and naturally occurring polymers investigated as scaffold materials**

Biomaterial	Type of scaffold	Cell type	Major findings	Reference
<b>Synthetic thermoplastics based material</b>				
PLLA, PLGA, PLGA/PEG	Electrospun fiber meshes	Cardiomyocytes	Elongated cell morphology mostly found on PLLA due to the hydrophobicity	[31]
PGA	Electrospun fiber meshes	Cardiomyocytes	Thick scaffold up to 2mm could be achieved by perfusion	[32]
PLGA /Collagen	Gas forming porous scaffolds functionalis with collagen	Cardiomyocytes	Increased characteristic cardiac markers and stronger contractile properties of cardiomyocytes	[33]
Polymerized 1,3-trimethylene carbonate with PDLLA	Salt leaching porous scaffold polymerized with	Cardiomyocytes	Reduced compression modulus with good biocompatibility	[34]
PLLA/PLGA	Salt leaching porous scaffold	Multi cardiac cells	Vascularization found in the scaffold	[35]
PGA	Cloths	Bone marrow cells	Increased capillary densities and reduced systolic pressure	[36]
	Films	Embryonic stem cells	Improved blood pressure and ventricular function	[37]
PCLA	Films	Smooth muscle cells	Improved ventricle systolic function	[38]

## 2. Literature Review

PCL	Electrospun fiber meshes	Cardiomyocytes	Up to 5 layers formed on the fiber meshes	[39]
PCLA	Particle leaching scaffolds	Mesenchymal stem cells	Reduced left ventricular end-diastolic diameter	[40]
PEUU	Films	-	Smaller end-diastolic areas	[41, 42]
<b>Synthetic elastomers based material</b>				
PU	Films	Myoblasts	Increased left ventricular ejection fraction	[43]
	Films	Cardiomyocytes	Multilayers cells	[44]
	Electrospun fiber meshes & thermally induced phase separation	Embryonic stem cells	The bulk of the cells were found within 200 µm from the surface	[34]
PGS	Microablated films	Cardiomyocytes	Anisotropic mechanical properties and improved alignment	[45]
	Microablated films	C <sub>2</sub> C <sub>12</sub> muscle cells	Improved alignment	[46]
	Electrospun fiber meshes	Cardiomyocytes	Anisotropic mechanical properties	[47-50]
	Films		Male Wistar Rats	[51]
	Porogen leaching porous scaffolds	Cardiac fibroblasts and cardiomyocytes	Formation of vessels on the scaffold	[52]
	Films	Embryonic stem cells	No significant infarcts or necrosis by suturing patches on healthy hearts	[5]
PEG	Gel		Prevention of wall thinning at 4 weeks	[53]

## 2. Literature Review

	Gel		Reduced adhesion of marker proteins and pro-inflammatory cells	[54, 55]
	Gel functionalized with fibrinogen	Embryonic stem cells	Maturation of cardiomyocytes at day 10-14 with beating behavior	[56]
<b>Naturally derived based polymers</b>				
Porcine urinary bladder matrix	Gel		More functional cardiomyocytes	[57]
Porcine myocardial matrix	Gel	Cardiomyocytes	Favorable for endothelial cells and cardiomyocytes attachment	[58]
Porcine small intestinal matrix	Gel		Smaller LV end-diastolic volume and end-systolic volume	[59]
Collagen	Foam disks		Reduced infarct fibrosis	[60]
	Fiber meshes	Bone marrow cells	No readmission of patients	[61]
	Tubular scaffolds	Cardiomyocytes	Aligned cardiomyocytes	[62]
	Gel foam	Cardiomyocytes	Spatially uniform distribution of cardiomyocytes	[63]
Gelatin	Meshes	Cardiomyocytes	Migrated to the surface of the matrix and formed 300-500 $\mu\text{m}$ thick cell layer	[64]
Gelatin/CNT	Gel	Cardiomyocytes	Aligned cardiomyocytes with electrical stimulation	[65]
Fibrin	Gel	Cardiomyocytes	8 mm thick structure by perfusion	[66]
	Gel		Large amounts of muscle tissue situated around the vessels found in the gel	[67]
Alginate	Gel	Cardiomyocytes	<i>in situ</i> gelation in the presence of viable myocytes	[68]



## 2. Literature Review

	Gel		Degradation in 9 weeks	[69]
	Gel	Cardiomyocytes	Cardiomyocytes with high metabolic activity	[70]
	Gel		Reduction of LV volume and the improvement in LV function	[71]
Chitosan	Gel		Scavenge reflective oxygen species and improve cell graftment	[72]
	Electrospun fiber meshes	Cardiomyocytes	No obvious cell alignment	[73]
	Gel with collagen and petide	Cardiomyocytes	Improved cardiomyocyte morphology and viability	[74]
	Lyophilized porous scaffolds with carbon nanofibers	Cardiomyocytes	Increased metabolic activity	[75]
Hyaluronic acid	Concentrated viscous solution	Cardiomyocytes	Improved cell migration and wound healing	[76]
Hyaluronic acid benzyl ester	Non-woven meshes	Cardiomyocytes	Infiltration of lymphocytes, giant cells and new blood cells into the implants	[77]

### 2.1.1 Synthetic thermoplastics

Many synthetic thermoplastics have been approved by the Federal Food and Drug Administration (FDA) for certain medical applications such as poly(lactic acid) (PLA), poly(glycolic acid) (PGA) and poly(methyl methacrylate) (PMMA) [78]. Another advantage of synthetic thermoplastics is the tunable physical properties. By changing the molecular weight and the ratio between monomers, the glass transition temperature, crystallinity and mechanical properties can be easily adjusted, however, the change is within a certain range.

#### **Poly( $\alpha$ -hydroxyesters): PLA/PGA/PLGA**

PLA, PGA, and their copolymers are linear aliphatic polyesters derived from glycolic acid and lactic acid monomers. They have been used in the development of several commercially available medical products, such as sutures, tissue screws and tacks, guided tissue regeneration membranes for dentistry, and internal bone fixation devices [79]. Their application as cardiac scaffolds has also been studied.

PLGA, poly-L-lactide (PLLA) and PLGA/poly (ethylene glycerol) (PEG) have been electrospun into fibrous meshes for cardiac tissue engineering [31]. In this study, cardiomyocytes preferred to grow on a relatively hydrophobic surface displaying more elongated cell morphologies on the PLLA meshes. However the hydrophobicity preference of cardiomyocytes is controversial as Papadaki et al. showed that surface modified PGA scaffolds with increased wettability improved cardiomyocyte attachment due to higher protein absorption rate [80]. Though there is still debate on cardiomyocytes preference to hydrophilicity, myocardial tissue could be developed within both scaffolds (Fig. 2-1a).

To better mimic the transport conditions within myocardial tissue, perfusion is used to improve the spatial uniformity of cardiomyocyte distribution within PGA electrospun scaffolds [32]. The system

## 2. Literature Review

provides relatively higher oxygen concentration and lower carbon dioxide concentration in the deep layer of the scaffolds. The improvement in local microenvironments is in favour of cardiomyocytes growth. By mimicking the conditions within native cardiac muscle, *in vitro* tissue engineering of cardiac constructs with useful thickness (2 mm) was achieved. Perfusion is also applied on type I collagen incorporated PGLA sponge scaffolds. As shown previous study, high and spatially uniform cell density is found in the scaffolds. Compared with collagen I and PGLA used only scaffolds, the composite scaffolds showed improved structural stability and hydrophilicity respectively. , the Increased characteristic cardiac markers and stronger contractile properties of cardiomyocytes compared to PLGA or collagen sponges [33].

Though PLA, PGA and PGLA have been studied as biodegradable medical implants within the human body, the stiffness is in the magnitude of GPa, which is much higher than myocardial tissue even at fibrosis stage with a Young's modulus of approximately 1 MPa [81, 82]. In an attempt at providing a better mechanical match to cardiac tissue, 1,3-trimethylene carbonate was polymerized in poly-d-lactide (PDLA), which reduced the compression modulus by reducing the glass transition temperature [34]. The biocompatibility was maintained and cardiomyocytes attached and proliferated on the copolymer.

It has been proved that rapid vascularisation is crucial for cell survival, integration and function of the engineered cardiac constructs[14]. To achieve this goal, porous 50% poly-L-lactic acid and 50% poly (lactic glycolic acid) (PLLA/PLGA) blend scaffolds were used in conjunction with cardiac cells, comprised of human embryonic stem cell derived cardiomyocytes, endothelial cells and embryonic fibroblasts. They were implanted in a rat heart as cardiac tissue grafts [35]. The multicellular scaffold supported the vascularization and incorporation of pre-existing human vessels, anastomosing with the host rat vascular network. The condense vessel network was not found in scaffolds incorporating with cardiomyocytes alone. I The formation of a vascular system was found in endothelial cells and embryonic fibroblast co-culture system in another study [83]. It is a trend to fabricate a scaffold in conjunction with multi cells for cell transplantation therapy.

## 2. Literature Review

Other types of stem cells in conjunction with poly( $\alpha$ -hydroxyesters) have also been used to improve cardiac performance. PGA cloths have also been sutured over an infarct area with or without bone marrow cells (BMCs) [36]. The BMCs increased capillary densities and reduced the systolic pressure. The BMCs helped angiogenesis by releasing angiogenic factors but not by cellular migration or vasculogenesis. However, the BMCs differentiation fate was not outlined in this study. An *in vivo* study showed that ESCs seeded on PGA patches significantly improved blood pressure and ventricular function [37]. Such improvement was correlated to cardiomyocytes derived from ESCs differentiation. Compared with MI mice and MI + ESCs free patch groups, the survival rate of MI mice with ESCs-seeded patches was higher [84].

### **Polycaprolactone (PCL)**

PCL is a biodegradable polyester that is commonly used in sutures, drug delivery devices, dental splints, and is also used extensively for rapid prototyping [85]. The glass transition temperature of PCL is around  $-60^{\circ}\text{C}$  which gives the material a softer and more flexible properties compared with poly( $\alpha$ -hydroxyesters) [86]. Knitted PLLA fabric reinforced poly( $\epsilon$ -caprolactone-co-L-lactic acid) (PCLA) promoted aortic smooth muscle cells (SMCs) growth (analysed using anti- $\alpha$ -smooth muscle actin staining) in comparison with gelatin and PGA. The left ventricle (LV) volumes were smaller in both poly( $\epsilon$ -caprolactone-co-L-lactide) scaffolds with or without smooth muscle cells (SMCs) 8 weeks after implantation. However prominent elastic tissue formation was only found in seeded patches attributed to the SMCs. Compared with unseeded and control groups, left ventricle systolic function were significantly improved with  $p < 0.002$  and  $p < 0.0001$  respectively by echocardiography [39]. However, there is no comparison in stiffness or elasticity between different scaffolds in this article, making it difficult to measure the contribution of mechanical properties to cell seeding and cardiac performance.

## 2. Literature Review

PCL based biomaterial also shows biocompatibility to other cells. Cardiomyocytes cultured in electropun poly( $\epsilon$ -caprolactone) (PCL) scaffolds were engineered to form constructs of up to 5 layers and individual layers adhered intimately [87, 88] (Fig. 2-1b, 2-1c). Contractions were observed at an early stage and became stronger and more synchronized with time.

PCLA patches permitted mesenchymal stem cells (MSCs) penetration and growth into the scaffold layers [40]. The scaffold demonstrated retention of the physical dimensions after 2 months *in vivo* which was attributed to its robust physical properties. The MSCs differentiated to cardiomyocytes and 4 weeks after implantation an echocardiography showed the PCLA scaffolds with MSCs significantly reduced the left ventricular end-diastolic diameter (LVEDD) and increased left ventricular ejection fraction (LVEF) compared with the saline injection control. However, cell-free PCLA scaffolds did not show significant improvement in LVEDD, left ventricular ejection fraction (LVEF) and infarct area. Their finding is contrary to another study [89] which showed cell free PCLA scaffolds could prevent LV remodelling and preserve anterior wall thickness. A possible reason for these contrasting results might be caused by the difference between the mechanical properties, scaffold architecture and material purity.

### **Other thermoplastics**

Porous poly(ester urethane) urea (PEUU) synthesized from polycaprolactone and 1,4-diisocyanatobutane have been used as patches to replace the epicardium [41, 42]. Following implantation in animal models, smaller end-diastolic areas were found in the MI+PEUU group compared with the control group. The results corresponded with a thicker infarcted ventricular wall in the MI+PEUU group.

## 2. Literature Review

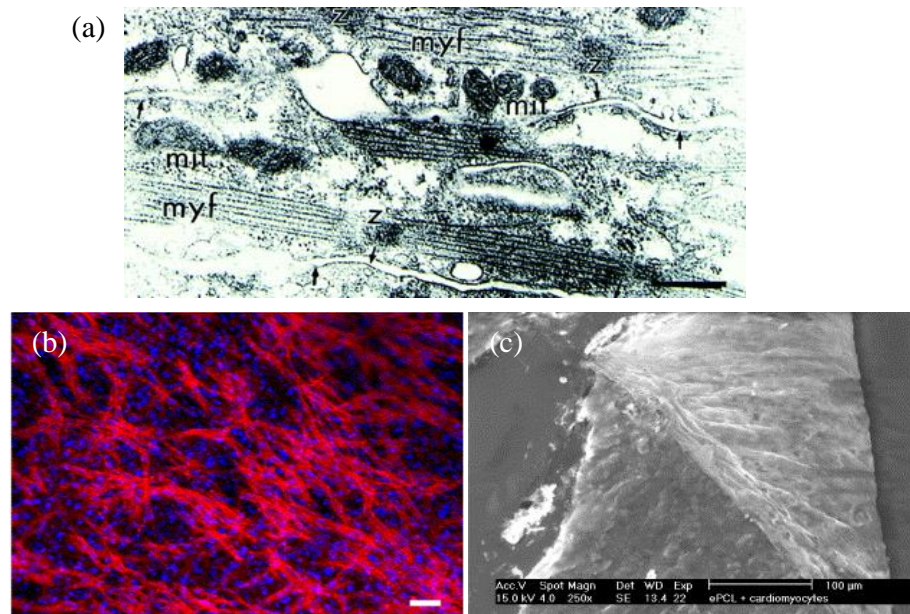


**Figure 2-1 Synthetic thermoplastic scaffolds exhibit good biocompatibility with cardiomyocytes. Muscle-specific features of engineered cardiac tissue were found on these biomaterials. (a) Transmission electron micrograph showing myofibrils, sarcomeres with Z lines (z), abundant mitochondria (mit) on PGA. Scalebar = 500 nm. (b) Immunohistochemical staining for F-actin which covers the entire surface of the PCL scaffold. Scalebar = 50 μm (c) SEM micrograph of the PCL surface. The mesh is covered with multilayers of cells. Scalebar = 100 μm. a) Reproduced with permission from The American Physiological Society Copyright (2001) b) Reproduced with permission from Elsevier (2005) c) Reproduced with permission from Elsevier (2005).**

### 2.1.2 Synthetic elastomers

Although synthetic thermoplastics show good biocompatibility and biodegradability, the high stiffness limits its use in cardiac tissue engineering. In addition, plastic deformation is not conducive to the dynamic environment of cardiac tissue. On the other hand, synthetic elastomers are usually softer yet still keep the predictable and reproducible mechanical and physical properties. Moreover, stable elasticity enables their applications in cardiac tissue.

#### Polydimethylsiloxane (PDMS)

## 2. Literature Review

PDMS is a silicon based polymer widely used in medical devices due to its good biocompatibility. However, there have been only a limited number of studies using PDMS as a cardiac biomaterial because it is non-degradable [90]. For this reason, secondary surgery is required to remove the material. However PDMS is extensively used as a mould for soft lithography to fabricate biomaterials with micro or nano structures [91].

### **Polyurethanes (PU)**

PU represents a large family of polymers composed of organic units linked by carbamate (urethane) functionality. It can be synthesized to be either thermoplastic or elastomeric. Here, only PU elastomers are discussed. To test the functional outcomes of implantation of myoblast based scaffolds, PU patches synthesized from hydroxytelechelic polyester (from adipic acid and di(ethylene glycol)) and 4,4'-diphenylmethane diisocyanate (MDI) were implanted at the site of infarction with and without myoblasts [43]. The introduction of ester groups in PU enables polymer degradability. PU patches with myoblasts increased LVEF, but it is more likely that the improvement is caused by the myoblasts because such improvements were also found in myoblasts injection and not with the non-seeded PU implantation. Besides incorporating the degradable part in polyisocyanate or polyol, the degradability of PU can also be obtained by using a degradable chain extender. Segmented PU can be synthesized by two-step condensation reaction with diisocyanate, PCL and chain extender (by L-phenylalanine and 1,4 cyclohexane dimethanol) [44]. Laminin lanes were coated on PU mentioned above. Primary aligned cardiomyocytes were found on the surface of the PU film (Fig. 2-2a). A second population of cardiomyocytes integrated with the original patterned cells. By repeating the procedure, multilayers of cardiomyocytes could be achieved. To test the effect of material macro-architecture on the adhesion and viability, electrospinning and thermally induced phase separation (TIPS) were applied on PU synthesized from polycaprolactone, lysine-based diisocyanate and degradable chain extender to fabricate porous 3D scaffolds [92]. A morphology difference was found in embryonic stem cells (ESCs) derived cardiomyocytes between the two scaffolds. Elongated cardiomyocytes were mainly found on

## 2. Literature Review

electrospun fibers and exhibited contractile activity. However, round cardiomyocytes within the TIPS scaffolds also showed contractile activity. It is interesting as round cardiomyocytes are usually regarded as unattached or dead cells. The bulk of the cells were found within 200  $\mu\text{m}$  from the surface. The percentage of dead cells increased in the interior of the TIPS scaffolds indicating oxygen diffusion was not sufficient.

### **Poly (glycerol sebacate) (PGS)**

PGS is a crosslinked elastomer designed especially for soft tissue engineering. PGS is usually synthesized in two steps, (1) pre polycondensation step and (2) crosslinking. The PGS mechanical properties can be tuned by changing heating time, heating temperature and the ratio between glycerol and sebacate [16]. The degradability and biocompatibility of PGS as a cardiac tissue has been proved *in vivo*. Magnetic resonance imaging studies showed that the PGS cardiac patch size decreased from  $36 \pm 8 \text{ mm}^3$  to  $3 \pm 2 \text{ mm}^3$ , 6 weeks after implantation while the  $\text{TiO}_2$  reinforced poly(ethyleneterephthalate)/dimer fatty acid remained unchanged [51]. PGS patches sutured on adult rat hearts did not result in significant infarcts or necrosis, but there was only minor adhesion to the chest wall and there was no significant change in cardiac function produced by the patches [5].

The anisotropic mechanical properties which more closely match myocardial tissue can be achieved by applying laser microablation on crosslinked PGS with a preferred stiffness and orthogonal preferred stiffness of 83 kPa and 31 kPa [45]. (Fig. 2-2b). Aligned cardiomyocytes were found on the microablated rectangular and honeycomb films. Bilaminar honeycomb scaffolds with 3D interconnected pore networks were fabricated by overlaying one lamina over a second lamina which also increased the stiffness from 220kPa to 700kPa due the elevation in temperature for effective crosslinking [93].  $\text{C}_2\text{C}_{12}$  muscle cells were also cultured on these patches and exhibited alignment on the patches [46].



## 2. Literature Review

. anisotropic mechanical properties of PGS can also be achieved by electrospinning. However, the traditional way of electrospinning does not work for PGS, because the PGS prepolymer flows and permanently deforms during the crosslinking reaction because of the high temperatures. Therefore, to maintain the nanofiber structure, a protective shell is required to restrict flow during the high temperature reaction to fabricate 3D PGS nanofiber meshes [47-50]. Different materials have been used as the shell such as PCL [49], gelatin [50] and poly(vinyl alcohol) [94]. Aligned PGS fibres exhibits slightly non-linear J-shaped curvature (stress tracks or rises relatively horizontally along the strain, but its values at some point begin to rise sharply) which is a feature of the myocardium [94]. The aligned structure of the fibres also facilitates cardiomyocyte alignment however the stiffness had minimal effect on alignment [50]. In attempt to improve the thickness of the fibre meshes, PGS/ poly(3-hydroxybutyrate-co-3-hydroxyvalerate) (PHBV) electrospinning fibres were rolled up [95]. However, it is difficult to determine whether the low concentration of PGS (2%) in PHBV could significantly improve the elasticity of the scaffolds.

Co-cultures of cardiac fibroblasts and cardiomyocytes have also been used to enhance cardiac physiological function [52]. Porous PGS layers induced parallel alignment of myocytes over layers of collagen-producing fibroblasts. Formation of vessels was found on the scaffold that had been sutured on the infarct area after two weeks.

### **Polyethylene glycol (PEG) hydrogels**

PEG has excellent biocompatibility and has been approved by the FDA in a number of drug formulations due to its low fouling (low protein adsorption) properties [96]. PEG gels are also widely used as a supporting matrix in cardiac tissue engineering as it provide proximate Young's modulus with tens of kPa [97]. The early study showed that cardiac function could be improved solely by injecting poly (ethylene glycol) (PEG) into an infarct region and crosslinked *in situ* [53]. The LVEDD was reduced with complete prevention of wall thinning at 4 weeks. At 13 weeks, the LVEDD of PEG injected hearts were

## 2. Literature Review

similar to the saline injected groups. Passive structural reinforcement which prevented post-MI remodelling by the PEG based gel injections was also shown by others [54, 55]. The improvement is attributed to the anti-fouling properties of PEG which can reduce adhesion of marker proteins and pro-inflammatory cells onto the hydrogel surface and decrease the extent of capsule formation and immune response [98]. However, the low-fouling properties also prevents or delays the adsorption of bioactive molecules such as extracellular matrix proteins that support the growth and function of encapsulated cells. A common approach to circumvent this is either to adopt co-polymerization of PEG with other macromolecules with cell binding sites, or introduce multiple functional groups to graft biologically relevant ligands and sequences [99]. Blends of biofunctional molecules with the hydrogel network is another strategy [100]. The most representative example of such a signal would be the integrin binding peptide Arg-Gly-Asp, also known as RGD. RGD has a significant and dose-dependent influence on HL-1 cardiomyocyte viability with PEG hydrogels [101]. Microspheres of PEG have been fabricated by phase separation from dextran solutions and were modified with arginine-glycine-aspartic acid (RGD) peptide after pre-gelation [102]. The HL-1 cardiomyocytes cultured in the scaffolds proliferated, expressed cardiomyocyte markers, and retained electrical activity over a month. Fibrinogen incorporated PEGylated hydrogels were used to culture human embryonic stem cells and rat neonatal cardiomyocytes [56]. The human ESCs derived cardiomyocytes matured between 10-14 days in culture and exhibited contraction amplitude, although this was not as synchronized compared to rat neonatal cardiomyocytes due to the mixed population of cells used. Maturation of both cell types within the hydrogels was confirmed by cardiac-specific biomolecular markers, including alpha-sarcomeric actin, actinin, and connexin-43 (Fig. 2-2c). The cardiomyocytes also responded to agonists such as isoproterenol, carbamylcholine and heptanol indicating such hydrogels could be used for drug delivery.

## 2. Literature Review

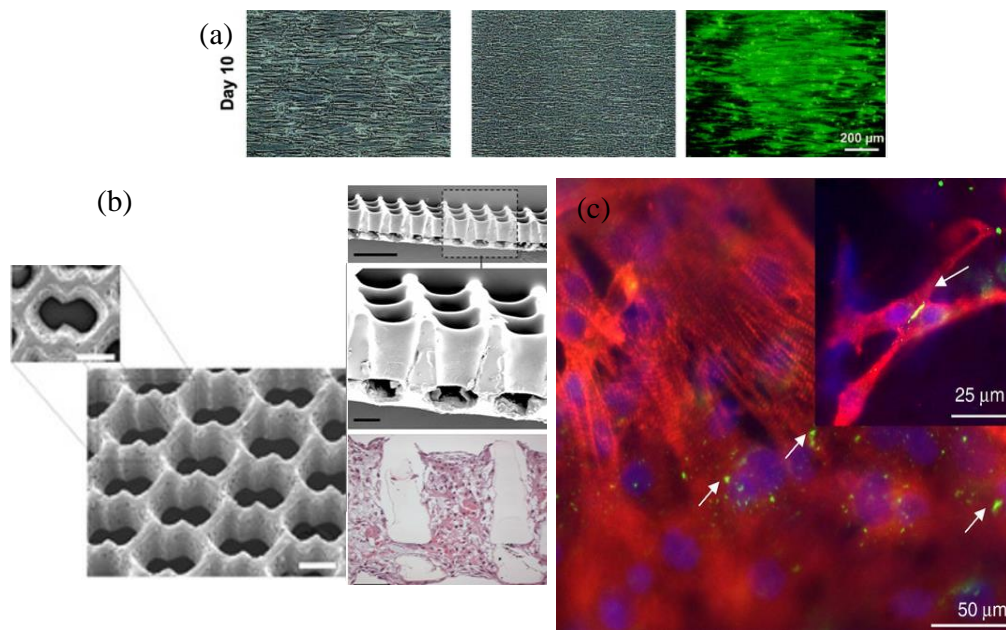


**Figure 2-2 (a) Phase contrast images of monolayer aligned cells cultured on PU films (left), additional cells cultured on the aligned cells (middle) and the additional cells labeled with cell tracker green (right). (b) The structure of accordion-like PGS scaffold (monolayer and bilayer) and cardiomyocytes cultured on the bilayer scaffold (c)  $\alpha$ -actin (red), connexin 43 (green) and nuclei (blue) of cardiomyocytes cultured within PEGylated fibrinogen hydrogels. a,b&c) reproduced with permission from Elsevier**

### 2.1.3 Naturally derived polymers

Naturally occurring polymers can provide a conducive substrate for cellular attachment, proliferation, and differentiation in its native state and have therefore been used for cardiac tissue engineering [103]. Advantages of using fibrin also include extraction from the patient's blood, an easy readjustment and implantation procedure, increase in viability and early proliferation of delivered cells, and benefits even with the patch alone [104]. Though most naturally occurring polymers are composed of the structural and functional molecules that characterize the native tissue extracellular matrix (ECM), their poor mechanical properties and variable physical properties with different sources is a common problem. It's also difficult to identify the exact composition of some naturally occurring polymers from organisms.

#### Matrix based gels

## 2. Literature Review

The matrix based gels, as a multi-component material, has shown great potential for cardiac tissue engineering, though the effective parts in the gel are seldom mentioned. Decellularized urinary bladder matrix (UBM) has been studied for reconstruction in many tissue engineering studies, such as laryngeal tissue and esophageal tissue. UBM gel has been used as cardiac tissue scaffold, leading to a significant improvement in  $\alpha$ -smooth muscle actin-positive cells, which is consistent with functional cardiomyocytes.[105] Porcine myocardial matrix based gels have been used for cardiac tissue engineering. The nanofibrous structure of the glycosaminoglycan present in the matrix makes it favorable for endothelial cells and smooth muscle cell attachment [57]. Myocardial matrix also enhanced cardiac muscle and reduced infarct fibrosis without affecting peripheral tissue, cardiac rhythm and blood chemistry. The protective effect was also found in CorMatrix ECMs made from decellularized porcine small intestinal submucosa [59]. Patch repair based on the CorMatrix ECMs was applied to 11 patients. In the follow-up analysis, there was no readmission showing that the CorMatrix ECMs are a safe alternative for ventricular patch repair.

### Collagen

Mechanical strength in tissues is largely provided by collagen [97]. Among the 28 types of collagens, type I collagen is intensively studied due to its excellent biocompatibility and ubiquitous distribution in the body. Cardiomyocytes with liquid collagen type I, matrigel and serum-containing culture media were thoroughly mixed to form engineered heart tissue (EHT). Such EHT could retain the contractile function of the uninjured heart and develop thicker muscle structures without inducing arrhythmia. Following 14 days implantation, the tissue was invaded by nerve fibres. However, a homogenous tissue construct with thin cardiomyocyte strands could not be achieved by the EHT and only compact cardiomyocytes were found [61]. In another *in vivo* study, a circular collagen type I foam prepared from porcine skin was sutured on the injured myocardium [60]. The scaffold induced neo-angiogenesis and enhanced the thickness of the vessel. The large vessel formation retarded the LV remodeling. Bone marrow stem cells were also transplanted with or without collagen matrix onto the scar area [61, 106]. Combined therapy

## 2. Literature Review

showed an additional beneficial effect on LV remodeling compared to cell therapy alone. The additional collagen scaffolds provided structural integrity within the body and normalized cardiac wall stress in injured regions. For the purpose of cell alignment, oriented type I collagen tubular scaffolds manufactured using a counter rotating cone extrusion device guided cardiomyocyte phenotype (Fig. 2-3a) [62]. Rat heart ventricle cell fractions containing many cardiac cells were cultured on 3D type I collagen scaffolds to study the effect of multicellular competitive environment [107]. Cardiac fibroblasts present in the scaffold did not overgrow the cardiomyocytes and synchronized beating behavior was observed. Multilayer connected cardiomyocytes structures were revealed by transmission electron microscopy (TEM). More complex constructs could be achieved by collagen gel-cell inoculation followed by culture medium perfusion [108]. High yield, high rate and spatially uniform distribution of cardiomyocytes could be achieved in the collagen gel scaffold. Due to the good biocompatibility to cardiomyocytes, collagen based scaffolds have been used as *in vitro* models for the effects of chemical, mechanical and electrical signals change on cardiomyocytes beating behavior [109-111]. Tissue engineered constructs could be achieved

### **Gelatin**

Gelatin is the denatured form of collagen, and is a key biomaterial that has seen many applications across the food, pharmaceutical capsule and biomaterials industries. The majority of gelatin used for hydrogel formation comes from pigskin or cowhide [112]. In the denaturation process, only the hydrogen bonds and hydrophobic bonds that stabilize the collagen helix are broken. The chains are disentangled and dissociate into their components with a random coil configuration [113].

Gelatin based scaffolds are inherently bioactive and promote the proliferation of human atrial cardiomyocytes [64]. Although the cells were injected in the center of the gelatin matrix, they preferentially migrated to the surface of the matrix and formed 300-500  $\mu\text{m}$  thick cell layer. Methacryloyl groups are commonly introduced onto the gelatin backbone via the reaction between

## 2. Literature Review

gelatin amines and methacrylic anhydride to synthesize gelatin methacrylate (GelMA). This allows crosslinking of the gelatin via free radical polymerization [114] or via Michael addition reactions [115]. Carbon nanotubes (CNTs) can be incorporated into GelMA hydrogels to render the hydrogel electroactive [65] thereby facilitating electrical coupling between cardiomyocytes or even electrical stimulation. Aligned cardiomyocyte structures were achieved by electrical stimulation through the whole matrix (Fig. 2-3b). CNT-GelMA showed 3-times higher spontaneous beating rates and 85% lower excitation threshold. These results can be attributed to better electrical cell–cell coupling enabled by more homogeneously distributed cell–cell junctions and the conductive CNT network.

Despite the advantages in gelatin and GelMA based hydrogels, they are difficult to modify chemically as it is highly insoluble in organic solvents. It also has limited solubility in water, and generally will reach its solubility limit at around 15 % (w/v) which will ultimately restrict the range of mechanical properties. Recently gelatin hydrogels have been made photodegradable by incorporating photolabile o-nitrobenzyl esters [63] into the crosslinks. Micropatterned hydrogels were fabricated by exposure with ultraviolet (UV) light at 360-480 nm and a photomask. Cardiomyocytes cultured on the micropatterned substrates showed improved alignment identified by nuclei and  $\alpha$ -actin. Electrical stimulation of aligned cardiomyocytes-seeded gels showed lower excitation threshold. Cell proliferation and distribution of cardiomyocytes on gelatin-matrices can also be increased by cyclic mechanical stretching [116].

### **Fibrin**

Fibrin gel is a biodegradable and nontoxic biomaterial formed by fibrinogen and thrombin during hemostatic coagulation [117]. Using perfusion, a solid 8 mm thick structure could be formed by mixing rat cardiomyocytes with fibrin glue [66]. Fibrin gels filled with cardiomyocyte suspensions were surgically placed around the femoral artery and vein of adult rats [67]. After 3 weeks, the gels were filled with living tissue with large amounts of muscle tissue situated around the vessels.

### **Alginate**

## 2. Literature Review

Alginate is found in a wide variety of brown seaweeds as a structural polysaccharide. Alginate has been widely used in biomedical science and engineering due to its biocompatibility [118]. However, like gelatin, physical or chemical modifications are usually applied on alginate to improve cell attachment. Cardiomyocytes cultured in pure alginate remained round with no sign of attachment due to the lack of cell adhesion motifs in alginate. The attachment of cardiomyocytes could be improved by surface modification or incorporation with hydrophilic material. For example, the cardiomyocytes cultured in alginate/collagen beads were evenly distributed by comparing the cell density between the edge and the centre of a bead. The beating behavior could be observed at day 60 with no significant change in rate compared with day 14 [119]. Alginate is negatively charged and readily forms hydrogels, by the addition of divalent cations such as  $\text{Ca}^{2+}$ . Functionalized alginate and hyaluronic acid gelled *in situ* in the presence of viable myocytes [68]. *In situ* crosslinking did not impair cardiomyocyte viability, however the gel was only stable for 3 days. Although alginate is inherently non-degradable in mammals, ionically crosslinked alginate gels can be dissolved by release of the divalent ions into the surrounding media due to exchange reactions with monovalent cations such as sodium ions [69]. The disappearance of ionically crosslinked alginate scaffolds was also reported by Leor et al. after implantation in rats, following 9 weeks [120]. Isolated cardiomyocytes were seeded on porous alginate hydrogels and cultured for 4 days before implantation. Intensive neovascularization from the neighboring coronary network were found on the scar area (Fig. 2-3c). Histological examination revealed the presence of myofibers embedded in the collagen fibers. The deterioration in LV contractility in control groups was not found in alginate biograft treated groups. A similar *in situ* study of gelated alginate based injectable gel was reported by Landa et al. and the crosslinking was triggered by perturbing the calcium ion concentration [70]. The biomaterial was replaced by connective tissue within 6 weeks. Both recent and old infarct area thickness were improved by injection of the matrix. Porous alginate scaffolds could be synthesized by incorporating guluronic acid [121]. Cardiomyocytes viability on the scaffolds was 60-90% and aggregated within the pores with high metabolic activity. The cardiomyocytes exhibited  $23 \pm 10$  beats/min at an initial cell seeding density of  $2.6 \times 10^7$  cells/cm<sup>3</sup>. In clinical study, the self-gelling alginate hydrogel was

## 2. Literature Review

implanted in 11 patients with dilated cardiomyopathy [71]. The reduction of LV volume and the improvement in LV function occurred immediately after implantation. Such advantages were sustained for 3 months and attributed to the reduction of wall stress and improved regional cardiomyocyte function.

### **Chitosan**

Like alginate, chitosan is also a polysaccharide, but is positively charged which facilitates cell adhesion. It is synthesized by deacetylation of chitin. Injectable, thermally responsive chitosan hydrogels can be formed by mixing with  $\beta$ -glycerol phosphate solution [72]. *In vitro* and *in vivo* studies showed that chitosan hydrogels can scavenge reactive oxygen species (ROS) which lead to graft cell death by impairing adhesion-related molecules. Hence chitosan hydrogels could improve the MI microenvironment and engraftment of ADSCs (adipose tissue-derived stem cells). Cardiomyocytes cultured on electrospun chitosan nanofibres did not show polarized cell structures and coherent contractions although this was improved by co-culturing with fibroblasts [73]. The expression of sarcomeric actin and connexin-43 was higher under this condition. Conjugation of chitosan-collagen hydrogels with angioprotein-1 derived peptide improved cardiomyocyte morphology and viability [74]. Carbon nanofibres have been used to induce conductivity within chitosan based scaffolds [75] which increased the metabolic activity indicated by higher cardiac specific genes involved in muscle contraction and electrical coupling.

### **Peptide amphiphiles**

Peptide amphiphiles are a class of molecules that combine the structural features of amphiphilic surfactants with the functions of bioactive peptides and are known to assemble into a variety of nanostructures that form self-supporting hydrogels. Self-assembling peptide (RAD16-II peptide) nanofibres can increase cardiomyocytes retention and promote capillary density in the peri-infarct area



## 2. Literature Review

[122]. Intramyocardial injections of peptide nanofibres alone could also prevent left ventricle remodeling but was not as efficient as with cardiomyocytes in scar length and necrotic area ratio[123].

### **Hyaluronic acid**

Hyaluronic acid (HA) is an anionic, nonsulfated glycosaminoglycan distributed widely throughout connective, epithelial and neural tissues [124]. HA contributes significantly to cell proliferation and migration and HA based biomaterials have been intensively studied in tissue engineering [125]. A non-woven mesh was fabricated from HA benzyl ester microfilaments and used as a cardiac patch [77]. Although the stiffness of the matrix is as high as the myocardial tissue, after 1-week static culture, it dropped to the half level of myocardial tissue, with a stiffness of 40kPa. An *in vivo* study showed infiltration of lymphocytes, giant cells and new blood cells into the implants. Cardiomyocytes were treated with H<sub>2</sub>O<sub>2</sub> as a heart ischemia, and then incubated in hyaluronic acid gel of different molecular weights [76]. High molecular weight HA (1000 kDa) improved cell migration and wound healing via cytoskeletal rearrangement of cardiomyocytes.

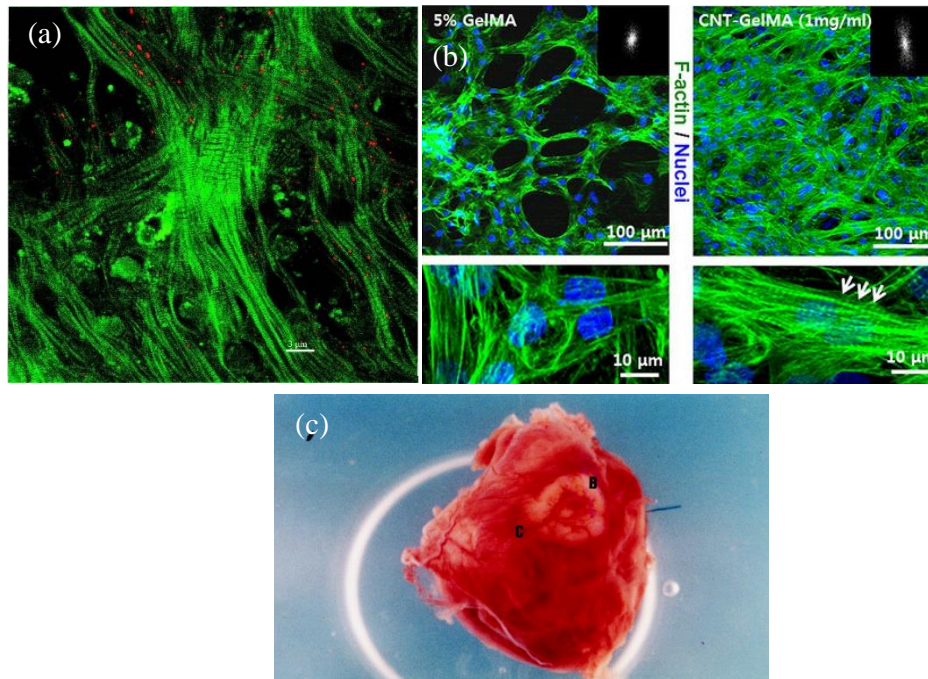


**Figure 2-3 (a) Filaments (green) and connexin 43 (red) were found on cardiomyocytes cultured on a tubular collagen scaffold. (b) More aligned cardiomyocytes were found on carbon nanotube (CNT) incorporated gelatin compared with the control group. (c) Vascularization with alginate scaffold C and without B. a) Reproduced with permission from American Chemical Society Copyright. b) Reproduced with permission from Elsevier Copyright (2002). c) Reproduced with permission from American Heart Association Copyright.**

### 2.1.4 Summary

Despite intensive studies on myocardial tissue engineering, challenges remain in the area. Although some scaffold/matrices' mechanical properties match that of the myocardium quite well, there is still a lack of understanding the ideal mechanical properties of the infarct region. Tough biomaterials might prevent the remodeling of the heart but also decrease the output of the heart [126]. The choice of cells is another critical issue. Compared with smooth muscle cells which do not have spontaneous beating behavior, cardiomyocytes are more suitable for regeneration. Recently, reprogramming strategies showed that cardiac fibroblasts could be converted directly to cardiomyocytes [127]. Cardiomyocytes derived from induced pluripotent stem cells offer many advantages such as a potential unlimited supply of autologous cells and elimination of immune rejection but such techniques have not been applied in

## 2. Literature Review

conjunction with scaffolds. A combinatory approach, which uses proper cells, signalling molecules and engineered scaffolds to enhance cell growth, proliferation, vascularization and to support the damaged heart is still required.

### 2.2 Methods for aligning cardiomyocytes

Alignment of cardiomyocytes contributes to the anisotropic tissue structure of the heart, and facilitates efficient electrical and mechanical activation of the ventricles [128]. Thus, to develop functional cardiac patches, it is critical to maintain an appropriate structural organization of cardiomyocytes. In general, three types of methods have been applied to provide physical, mechanical and electrical cues to generate aligned cardiomyocytes.

#### 2.2.1 Physical cues

As the structural organization of the myocardium correlates with aligned matrix fibres (Fig. 2-4), scaffolds which provide a similar morphology can align the cells cultured on them [129] (Fig. 2-4). Aligned nanofibres produced using electrospinning have been applied using synthetic thermoplastics [31, 128, 130-133] but also elastomers [50, 131] and naturally occurring polymers [134]. The alignment of the nanofibres is introduced by a rotating disk/drum. Aligned electrospun fibres are suitable for aligned cardiomyocytes culture, and also favours cardiomyocyte maturation[135]. The *Nppa* gene, which regulates the levels of immunoreactivity atrial natriuretic peptide (ANP) level and ANP itself, were significantly lower than the cardiomyocytes cultured on isotropic meshes and TCPs. Decrease in ANP indicates more mature cardiomyocytes because ANP plays a role in cardiac development and potentially acts as a modulator for apoptosis *in vivo*. The study showed evidence that physical cues provided by electrospinning can induce phenotypic changes in cardiomyocytes.

## 2. Literature Review

The physical cues for cardiomyocyte alignment can also be achieved by micropatterning. The general procedures contain 3 steps: First, photolithography creates micropatterns on a substrate by selectively exposing areas of a photoactive polymer. Second, the exposed material is then removed chemically or thermally to produce a mould [136]. Last, the patterns are transferred onto the biomaterial surface by casting the biomaterial solution or melt on the mould. Compared with electrospinning, thicker and tougher scaffolds can be fabricated by patterning. However, such techniques are usually used to control 2D cell alignment on the surface. In attempt to solve this problem, many types of cells (human umbilical vein endothelial cells, cardiac side population cells (with the ability to differentiate to cardiac cells) and immortalized rodent myoblasts) were encapsulated in gelatin methacrylate and cast on PDMS molds mentioned above [137]. Multi-layer cells are difficult to fabricate directly via 2D cell culture, however aligned and elongated cells were found through the gelatin constructs at different layers. However, this method only works for materials which is suitable for internal cell growth. Two-photo laser scanning (TPLS) was also applied to ablate the inner part of a peptide modified PEG hydrogel [138]. Fibrin clusters with fibroblasts were encapsulated within the hydrogel and underwent guided migration in the micropatterned regions. However only fibroblast alignment in PEG hydrogel is reported using TPLS and it is unknown whether cardiomyocytes will align using this technique.

The principle for cardiomyocytes alignment on micropatterned substrates are also studied. It is generally suggested that focal adhesions and actin filaments are confined on the nanostructures, and thus limit the orientation of the long axis of focal contacts and induce their alignment, which induces cell alignment [139, 140]. Patterning in micro size could also provide confinement of cardiomyocytes for alignment but uses a different mechanism. Substrates with pattern sizes comparable to the cell size [63, 141, 142] (Fig. 2-5a) provide the highest alignment of cardiomyocytes. Cardiomyocytes orientation was confined by the micropattern structure, which induces cell alignment.

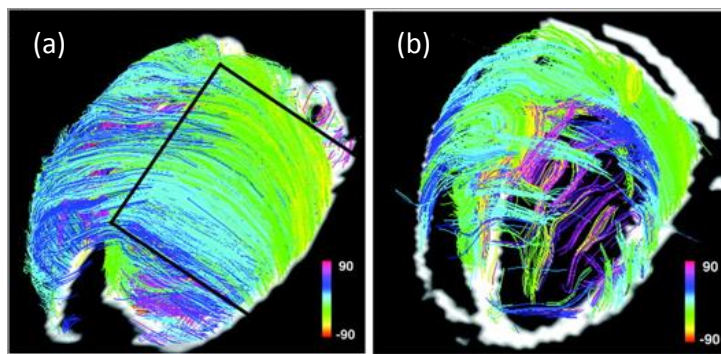


**Figure 2-4 The diffusion spectrum MRI tractography of visualized fibers in the normal heart (a) and infarcted heart (b). The difference in colour indicates the fibres at different depths. Reproduced with permission from Wolters Kluwer Health, Inc.**

### 2.2.2 Mechanical cues

Mechanical stretch has been implicated as the growth stimuli in the heart. Physiologically, mechanical stretch is reported to contribute to the orientation of cardiomyocytes. Unidirectional mechanical stresses placed on cardiomyocytes has been implicated as a major regulator in the heart [143]. Cardiomyocytes repetitively stretched and relaxed 5-10% at 10-30 Hz for 3-4 days showed significant improvement in alignment cultured on silicon rubber [143]. Similar results with improved alignment were also found for cardiomyocytes cultured on collagen [144] (Fig. 2-5b). The alignment change is regulated by N-cadherin which is caused by mechanical stretch [145]. Another protein Rac1 was activated by stretch stimulation and the Rac1 activation was essential for the stretch-induced cell alignment [146]. Blocking this protein in cardiomyocytes showed no preference in orientation after 24hrs stretch. However, Rac1 is also a hypertrophy signal in cardiomyocytes and overexpress this protein might lead to hypertrophy in cardiomyocytes. The stress conditions need to be taken into consideration as well, because High stress is likely to exist in situations of cardiac remodelling which leads to heart failure by activating protein kinases. Hypertrophy and apoptosis can be seen in cardiomyocytes by the stress activated protein kinases. Recent studies showed that mechanical cues can be transmitted by

## 2. Literature Review

material [147]. Cardiomyocytes can adjust their alignment in response to mechanical deformations caused by their neighbours, even though the cells are not necessarily connected to each other.

### 2.2.3 Electrical cues

Electrical stimulation of cardiomyocytes preserves contractility [148], maintains calcium transients [149] and increases protein synthesis [150]. Electrical stimulation promotes cardiomyocyte orientation although it is much weaker compared with physical cues [151] (Fig. 2-5c). The orientation and elongation response of cardiomyocytes was completely abolished by inhibition of actin polymerization (Cytochalasin D) and only partially by inhibition of phosphatidylinositol 3 kinase (PI3K) pathway. To transform uniform electrical signals across the whole scaffold, a conductive material such as carbon carbonnanofibres[152, 153], graphene[154] or polyaniline[155] is blended with the biomaterial especially when cardiomyocytes are not confluent.

The electrical stimulation also directs mesenchymal stem cells (MSCs) differentiation towards a cardiomyocyte lineage [156]. The cells reoriented perpendicular to the direction of the current and adopted an elongated morphology. Using qPCR, an upregulation in a range of cardiac markers was detected, the greatest of which was observed for cardiac myosin heavy chain with a 40-fold increase on carbonnanotubes (CNTs) incorporated PLA scaffolds. In 10 days. On the non-conductive PLA scaffolds without CNTs, a 12-fold increase was observed during the same period. The upregulation in cardiac proteins was also found by electrical stimulation.

## 2. Literature Review

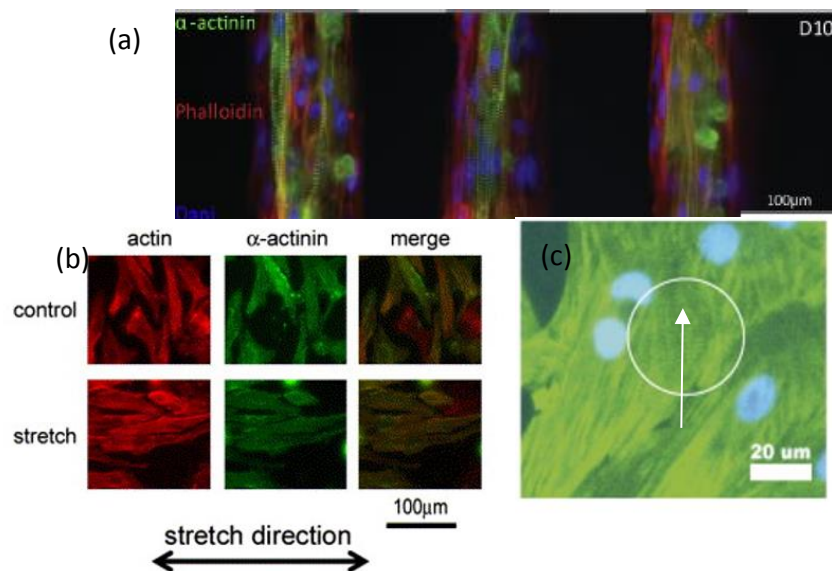


**Figure 2-5** The significant improvement in cell alignment by physical cues (a), mechanical cues (b) and appreciable improvement by electrical cues (arrow indicates the electrical field direction) (c). Reproduced with permission from Elsevier

Though many studies showed that efficient alignment of cardiomyocytes could be achieved by providing physical, mechanical or electrical cues, little is known about the change in the biological pathways. The relations between these cues and the cell behaviours worth further digging.

# 3 Developing elastomeric biomaterials from P34HB and PGS for soft tissue engineering

## Declaration for Thesis Chapter [3]

### Declaration by candidate

In the case of Chapter [3], the nature and extent of my contribution to the work was the following:

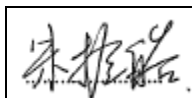
Nature of contribution	Extent of contribution (%)
Major research and writing	85

The following staff/students contributed to the work.

Name	Nature of contribution	Extent of contribution (%) for student co-authors only
Tulio Fernandez	SNL cells cytocompatibility images taking	5
Bing Xu	Tensile test program setting	5
Qizhi Chen	Provided corrections and assisted in research planning	N/A
Wayne Cook	Provided corrections and assisted in research planning	
John Forsythe	Provided corrections and assisted in research planning	N/A

The undersigned hereby certify that the above declaration correctly reflects the nature and extent of the candidate's and co-authors' contributions to this work\*.

Candidate's  
Signature



Date

26<sup>th</sup>/08/2016



3. Developing elastomeric biomaterials from P34HB and PGS for soft tissue engineering

<b>Main Supervisor's Signature</b>		<b>Date</b> <b>26<sup>th</sup>/08/2016</b>
--	---	---

### 3.1 Introduction

Bacterially synthesized polyhydroxyalkanoate (PHA) has attracted attention because most of these polyesters are biodegradable and biocompatible. A polyhydroxyalkanoate is the polymer formed from a hydroxyl-alkanoic acid (i.e. carboxylic acid), which can be defined as any acid with the structure  $\text{HO-R-COOH}$ , where R is an alkyl unit having the composition of  $\text{C}_n\text{H}_{2n}$ . However, in the biomaterials field, PHA is usually restricted to those sources which are derived from bacteria [157-160]. Hence, poly(lactic acid) (PLA), which is formed by conventional synthesis from bio-derived monomers, and polycaprolactone (PCL), which is derived from synthetic monomers, are usually excluded from the PHA class [161].

Among over 150 types of PHAs which has been synthesized, the most intensively investigated polymer is poly(3-hydroxybutyrate) (P3HB). Naturally occurring P3HB has been found as a ubiquitous component of cellular membranes of animals [162]. The presence of relatively large amounts of low molecular weight P3HB (monomer or oligomer with repeating units less than 10) in human blood, as well as the fact that the degradation product, 3-hydroxybutyric acid (3HB) is a natural human metabolite present in the brain, heart, lung, liver, kidney, and muscle tissue [163]. However, PHB is hard and brittle, which significantly hampers its practical use due to difficulties encountered during plastic processing techniques. Recently, a copolymer poly(3-hydroxybutyrate-4-hydroxybutyrate) (P34HB) has been studied as a candidate biomaterial. The second monomer 4-hydroxybutyric acid (4HB) can reduce the polymer crystallinity and improve the stretchability to some extent compared with P3HB without losing biocompatibility. Actually, 4HB oligomers and monomers can be used in the therapeutic treatment of patients, for example, in the treatment of patients with narcolepsy, chronic schizophrenia, catatonic schizophrenia, neurosis, alcoholism and drug addiction [164]. Degradable scaffolds made from P34HB have been reported to be successfully applied as a tissue engineering tri-leaflet heart valve in a sheep animal model [165]. However, despite a certain improvement compared with P3HB, P34HB has a

### 3. Developing elastomeric biomaterials from P34HB and PGS for soft tissue engineering

number of disadvantages, including being mechanically rigid due to crystallization, thermoplastic behaviour (lack of elastic stretchability), a narrow processing window and poor hydrophilicity [166].

Blending is a convenient and low-cost way to make new materials with tunable properties and P34HB based blends have been studied with many materials, such as poly(3-hydroxybutyrate), poly(3-hydroxybutyrate-co-3-hydroxyvalerate) (PHBV), poly(butylene succinate) (PBS), poly(lactic acid) (PLA), vitamin E and collagen [167-172]. However, most studies only focused on the miscibility, mechanical properties, thermal stability and crystallinity of the blends but neglected the potential application as biomaterials. The degradability and biocompatibility of the blends are rarely mentioned in the literature which is exclusively based on P34HB thermoplastics with no disclosure of crosslinked thermosets containing P34HB.

PGS, on the other hand, though elastic, but undergoes rapid degradation (several weeks), which has limited its application for tissue engineering of softest types, which typically have healing rates of several months or even years. The blend of PHA and PGS could be a potential approach to maximise the advantages and minimise the disadvantages of these two polymers, achieve a satisfactory combination of the desired mechanical properties of elastomeric polymers and slow degradation kinetics of PHA.

## **3.2 Material and methods**

### **3.2.1 Materials**

Poly (3-hydroxybutyrate-4-hydroxybutyrate) (P34HB) with an average molecular weight  $M_n=8.9 \times 10^4$  and molecular ration of repeating monomer 4HB=9% was purchased from GreenBio Materials Co., Ltd (Binhai, Tianjin, China). Glycerol (99% by wt%) and sebacic acid (99% by wt%) were obtained from Sigma-Aldrich Castle Hill, NSW, AU.

### **3.2.2 Synthesis of P34HB/PGS blends**

The synthesis included three steps. First, glycerol and sebacic acid were thoroughly mixed in a molar ratio of 1:1 in a glass breaker. The mixture was then heat treated at 130 °C under nitrogen for 24 hr to obtain the PGS prepolymer [173]. The PGS pre-polymer and P34HB of various weight fractions (10-90 wt% of P34HB) were melted by Kugelrohr apparatus under 170 °C for 30 min under nitrogen atmosphere (Pure P34HB was heated at the same environment). The melt blend was cast onto glass slides evenly and smoothly. The resultant casts were heated for further reaction (crosslinking and copolymerisation) at 170 °C under vacuum for 12 hr and then cooled to room temperature under vacuum. These polymer sheets were peeled off after soaking in water overnight. After peeling off, these sheets (< 1 mm in thickness) were thoroughly dried under vacuum at room temperature for 24 hr.

### **3.2.3 X-Ray Diffraction (XRD)**

The crystallinity and the crystal structure of P34HB/PGS blends with P34HB content from 0% to 50% were analysed by wide-angle x-ray diffraction at 40 kV (Scintag Pad5 generator) with the Cu  $K\alpha$  radiation as the x-ray source. Measurements were performed in the  $2\theta$  range of 2 to 60° at a scanning speed of 5°/min. All the samples were prepared to 1.5cm×1.5cm square films for the tests. The percent

### 3. Developing elastomeric biomaterials from P34HB and PGS for soft tissue engineering

crystallinity of the samples was calculated by Jade 5.0. Each experiment was conducted with three specimens.

#### **3.2.4 Differential scanning calorimetry (DSC)**

The thermal behaviour of pure P34HB, PGS and P34HB/PGS was characterized using a Perkin Elmer Pyris1 Differential Scanning Calorimeter (DSC) under a nitrogen atmosphere. The nitrogen flow rate was 20 ml/min. All the specimens were crimp sealed in aluminium crucibles and had a typical mass of about 6 mg. Then the specimens were cooled to -50 °C at a cooling rate of 40 °C/min. After reaching thermal equilibrium, the specimens were further heated from -40 to 170 °C at a heating rate of 20 °C/min to study the thermal behaviour. Each experiment was conducted with three specimens.

#### **3.2.5 Visual examination**

Visual examination was performed on the P34HB/PGS blends from 0% to 90%. All the samples covered a letter under the same light condition. The transparency of the materials was compared by the light intensities of the regions of interest with 117 pixels under each material using ImageJ.

#### **3.2.6 Mechanical characterization**

Tensile test samples were punched out using a standard dumbbell shaped mould, with the gauge length and width being 12.5 and 3.25 mm, respectively. The thickness of each sample was measured by a calliper. Cyclic and tensile testing were conducted for each specimen at room temperature by an Instron 5860 mechanical tester equipped with a 100 N load cell. The crosshead speed was 25 (for cyclic tests) and 10 (for tensile tests) mm/min. Under normal physiological conditions, the maximum strain of dynamic loading required of soft tissues such as cardiac muscle is typically around 15% [174]. Therefore, the cyclic test specimens were stretched to a maximum tensile strain of 15% at a rate of 1 Hz. The

### 3. Developing elastomeric biomaterials from P34HB and PGS for soft tissue engineering

Young's modulus ( $E$ ) of each specimen was determined by  $\sigma(\text{Stress})/\epsilon(\text{Strain})$  over the range of strain of 0-10%. The ultimate strength and the elongation at the break values were read directly at the breaking point of the tensile test. The Young's modulus  $E$  is calculated using Hooke's Law:

$$E = \frac{\sigma}{\epsilon}$$

(1)

Resilience, which describes the ability of a material to reversibly deform without the loss of energy [175], was calculated from the cyclic stress-strain data. The resilience is the ratio of the area under the unloading curve to the area under the loading curve at a strain of 15%, as follows [176]:

$$\text{Resilience} = 1 - \frac{\text{area under loading curve} - \text{area under unloading curve}}{\text{area under loading curve}}$$

(2)

For tensile test and tensile test, each group contains six sample.

#### 3.2.7 Percentage of esterification characterization

The degree of esterification of PGS was determined by acid group titration of the remaining carboxyl groups in the PGS and remaining P34HB and by weight loss of the water condensation by-product. In the acid group titration method, 1 g of sample was swelled (crosslinked polymer) in 50 ml chloroform in a flask sealed with Parafilm™ film. The polymers were soaked in the solvent mixture for 24 h to achieve high degrees of swelling. The carboxyl groups were then titrated with a standardized 0.1 mol L<sup>-1</sup> solution of potassium hydroxide in ethanol, keeping the flask sealed from atmospheric CO<sub>2</sub> when standing. Bromothymol blue solution (10 drops) was used as a pH indicator and the end-point of the titration was taken when the solution changed from yellow to bluish green [177]. For all the samples, the end point was taken to have been reached when the colour of the indicator colour remained bluish green for 1 h. The percentage of esterification was calculated by Eq. (3)

### 3. Developing elastomeric biomaterials from P34HB and PGS for soft tissue engineering

$$\text{Percentage Reaction (\%)} = \left( 1 - \frac{\text{Moles unreacted carboxylic acid groups}}{\text{Moles original carboxylic acid groups}} \right) \times 100$$

$$= \frac{(V_1 - V_0) \times C / m_o}{\frac{2 \times m_o \times (1 - p)}{(M_{SA} + M_{Gly})} + \frac{m_o \times p}{M_{P34HB}}}$$

(3)

where  $V_1$  is the volume in litres of 0.1 mol L<sup>-1</sup> KOH used for the sample titration,  $V_0$  is the volume for the blank test (without sample),  $C$  is the concentration of KOH (0.1 mol L<sup>-1</sup>),  $m_o$  is the mass of the sample,  $M_{SA}$ ,  $M_{Gly}$  and  $M_{P34HB}$  are the molecular weights of sebacic acid, glycerol and of poly(3-hydroxybutyrate-co-4-hydroxybutyrate), respectively, and  $p$  is the weight percentage of P34HB in the blends. Each experiment was conducted with three specimens. Unreacted sebacic acid in 100g sample =  $(1 - \text{Percentage Reaction of sebacic acid}) \times (1 - p) \times 100 \times M_{SA}$

(4)

Where  $p$  is the weight percentage of P34HB in the blends and  $M_{SA}$  is the molecular weight of sebacic acid

### 3.2.8 Degradation

Samples of ~50 mg (~50 mm<sup>2</sup> of surface area) P34HB/PGS blends (from 0% to 50%) were weighed and sterilised with 70% ethanol for 15 min followed by drying in a tissue culture hood overnight. Each specimen was then soaked in a well of a 6-well tissue culture plate filled with 2.0 ml culture medium. These culture plates were placed in a tissue culture incubator at 37 °C. The buffer solution and culture medium were changed every second day, while 8µl esterase (1366 units/ ml) (Sigma) was added every day. After incubation for 6, 12, 18, 24, 30 and 36 days, specimens were removed, washed with water and dried in a vacuum oven at room temperature until no further change in weight was detected and the percentage of weight change was calculated by Eq. (4). Each experiment was conducted with three specimens.

### 3. Developing elastomeric biomaterials from P34HB and PGS for soft tissue engineering

$$\text{Weight change (\%)} = \frac{m_t - m_0}{m_t} \times 100$$

(4)

#### 3.2.9 Cytocompatibility

The cytocompatibility study was performed according to the standard cytotoxicity assessment set by International Standardization Organization (ISO 10993). Extracts for tissue culture were prepared by placing 0.5 g of each material in 2.5 ml samples of cell culture medium (DMEM supplemented with 10% Fetal Calf Serum (FCS), 1% l-glutamine and 0.5% penicillin/streptomycin) for 24 h at 37 °C/5% CO<sub>2</sub> in culture incubator. Prior to exposure of cells to these extracts, SNL mouse fibroblasts (Mutant Mouse Regional Resource Centres, University of California Davies, USA) were seeded in standard media at a density of approximately 5000 cells/well in 96 well tissue culture treated plates (Falcon, BD Bioscience, North Ryde, Australia), under standard incubation conditions (37 °C and 5% CO<sub>2</sub>). When the cell monolayers had reached 75% confluence (around day 2), the medium in each well was entirely replaced with 0.2 ml of extract media samples (medium pre-exposed to material) or control media (positive control = medium without pre-exposed to any material; negative control = medium without cells). All cultures were then allowed to proceed for 2 days.

At the end of the incubation period, spent culture media were collected and the degree of cell death was determined by measurement of lactate dehydrogenase (LDH) levels, as released into the culture media ("RELEASED LDH"), using a commercial kit (Sigma–Aldrich TOX-7) as described previously [178]. Finally, each well containing living cells was filled with 0.2 ml fresh cell culture medium and cells were lysed using the solution TOX-7. These lysates were then used to determine the cellular LDH content, which equates to the number of living cells per well ("TOTAL LDH"). The overall LDH level was determined by measuring the absorbance of the supernatant from the centrifuged medium at 490 nm



### 3. Developing elastomeric biomaterials from P34HB and PGS for soft tissue engineering

(after subtraction for background absorbance at 690 nm) using a multiwell plate format UV–vis spectrophotometer (Thermo Scientific). The absorbance results of LDH were converted to the number of cells according to a linear standard curve (not shown). Hence, cytotoxicity can be expressed as Eq. (4)

$$\text{Percentage of living cells} = 1 - \frac{\text{LDH of extract medium}}{\text{Total medium}}$$

(5)

Each experiment was conducted with three specimens.

#### 3.2.10 Cardiomyocyte culture

Neonatal cardiomyocytes (NCMs) were isolated from 1-2 day old rat pups by enzymatic digestion as described previously [179, 180]. NCMs were seeded at  $2.2 \times 10^5$  cells per well in 48 well-plates on blends and incubated in minimal essential medium (MEM) containing 10% new born cow serum (NBCS) and 0.1 mM bromodeoxyuridine (BrdU) at 37 °C in humidified air with 5% CO<sub>2</sub>. 24 hr after seeding, the media was changed to Dulbecco's modified eagle medium (DEME) with 0.1mM BrdU, 10 µg/ml human transferrin (Sigma) and 2.5 U/ml human, insulin (Sigma). Thereafter, NCMs were maintained in DMEM with 10 µg/ml apo-transferrin and 2.5 U/ml insulin without serum or BrdU and culture media was changed every 72 hr, as described previously [180].

#### 3.2.11 Immunocytochemistry

After 4 days of culture, cells were fixed using 4 % paraformaldehyde (PFA), permeated by 0.3 % (w/v) Triton-X. Cardiomyocytes were then blocked with 10 % normal goat serum (NGS) in phosphate buffered saline (PBS) and incubated with anti-troponin I (mouse) in 10 % NGS respectively overnight at 4 °C. The cardiomyocytes were incubated in diluted secondary antibodies (Goat-anti-mouse 568) in PBS at 1:1000 for 1 hr at 37 °C. The samples were rinsed and incubated with 1:5000 4',6-diamidino-2-phenylindole (DAPI) for 5 min and were then sealed with mounting medium on glass slides. Stained samples were

### 3. Developing elastomeric biomaterials from P34HB and PGS for soft tissue engineering

imaged using a microscope (Nikon Eclipse TS 100). Troponin and nuclei were visualized under green (568nm) and UV light (435nm) respectively. The images were analyzed using ImageJ software. The cardiomyocytes size was analyzed by ImageJ with 12 cells in each group.

#### **3.2.12 Statistical Analysis**

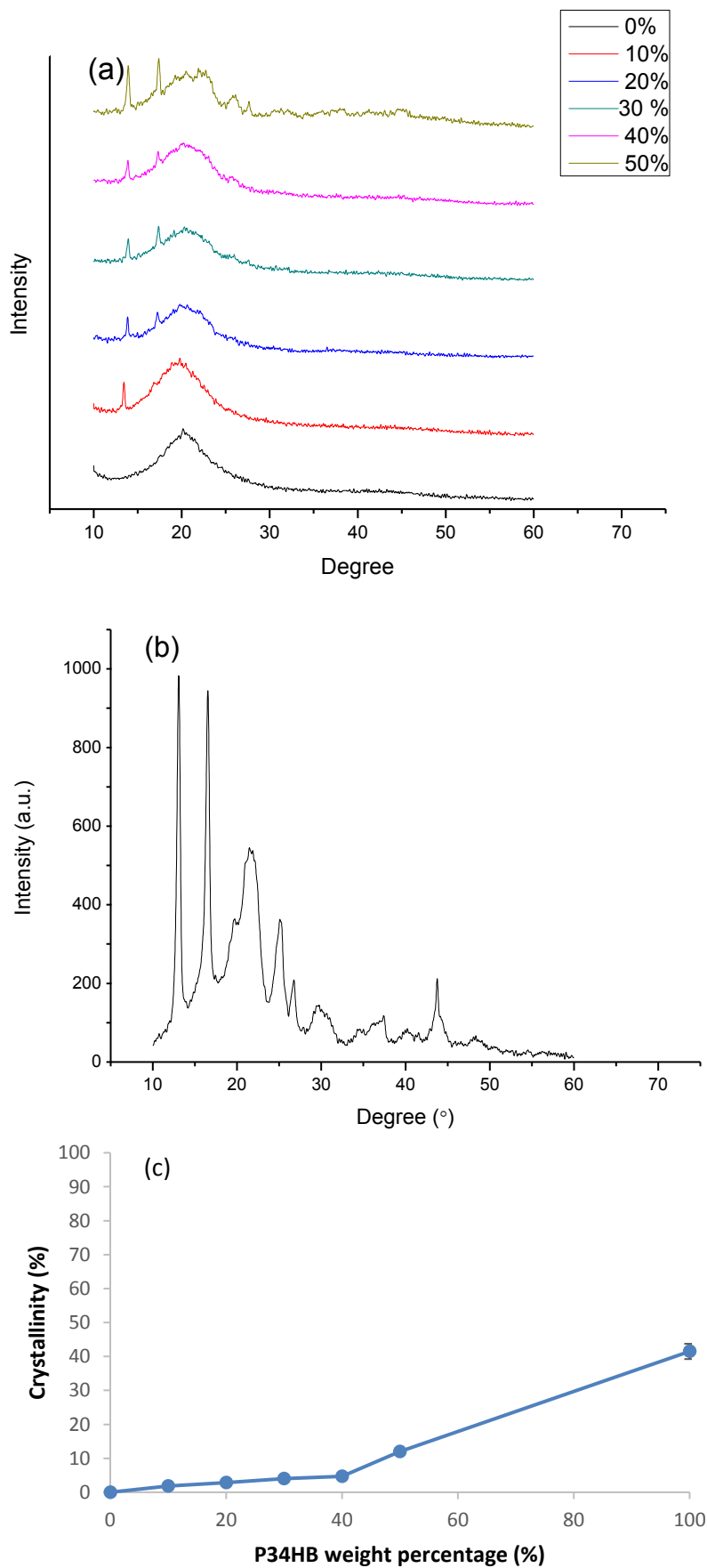
Statistical analysis was performed using GraphPad Prism 6 software package. All data were analyzed using one-way analysis of variance followed by Tukey's post-hoc test. Results are presented by the mean  $\pm$  standard deviation (SD) and a p value less than 0.05 was considered as significant.

## **3.3 Results and discussion**

### **3.3.1 Crystallinity of P34HB blends**

The pure PGS was amorphous at room temperature. The crystal structure was observed in the blends and the crystallinity was proportional to the weight percentage of P34HB when the P34HB weight percentage was below 50%. The crystallization peaks found in the blends were the same as pure P34HB indicating the crystallization was all attributed to P34HB (Fig. 3-1a ,3-1b). However, phase separation was found when the P34HB weight percentage reached 50% with a large increase in crystallinity ( $11.9 \pm 0.3$  %) (Fig. 3-1c, Tab. 3-1). The crystallinity of separated P34HB in 50% P34HB/PGS was even higher than that of pure P34HB (49.9 % vs. 41.5 %). The P34HB crystal structure was refined during the continuous heat treatment for PGS curing and slow natural cooling after that.

3. Developing elastomeric biomaterials from P34HB and PGS for soft tissue engineering



### 3. Developing elastomeric biomaterials from P34HB and PGS for soft tissue engineering

**Figure 3-1 Examples of XRD scans (10° to 60°) of (a) pure PGS and blends (b) pure P34HB and (c) crystallinity as a function of P34HB weight percentage.**

**Table 3-1 Crystallinity of blends, pure PGS and pure P34HB**

Composition of P34HB/PGS (%/%)	Crystallinity (%)
0/100	0
10/90	1.9 ± 0.3
20/80	2.8 ± 0.2
30/70	4.0 ± 0.2
40/60	4.7 ± 0.1
50/50	11.9 ± 0.3
100/0	41 ± 2

#### 3.3.2 Thermal analysis of P34HB/PGS blends

The glass transition temperature of PGS was measured to be around -30 °C, in good agreement with previous work [181]. The crystallization peaks which were only found in PGS and the 10% P34HB/PGS blend (Fig. 3-2). Only one glass transition temperature was observed in all blends. However, as the glass transition temperature of P34HB and PGS are close (-30 °C vs. -17 °C) with overlapping glass transition regions, it was hard to determine phase separation by the glass transition temperature (Tab.3-2). The P34HB melting peak at around 137 °C was found in blends when the P34HB weight ratio was above 30% with no significant change in melting temperature. According to previous research, there should be a slight depression in the melting temperature of the semi-crystalline component of the amorphous/semi-crystalline blends [182, 183]. The unchanged melting temperature might be due to the counteraction of the crystal refinement during synthesis. An obvious melting peak was observed in the 50/50 blend. The P34HB melting enthalpy increase, from 40/60 to 50/50, was greater than that from 30/70 to 40/60, indicating the addition P34HB did not homogeneously disperse in the blend and formed a continuous phase. The result was consistent with the XRD spectra which showed an increase in crystallinity in the 50/50 blend.

### 3. Developing elastomeric biomaterials from P34HB and PGS for soft tissue engineering

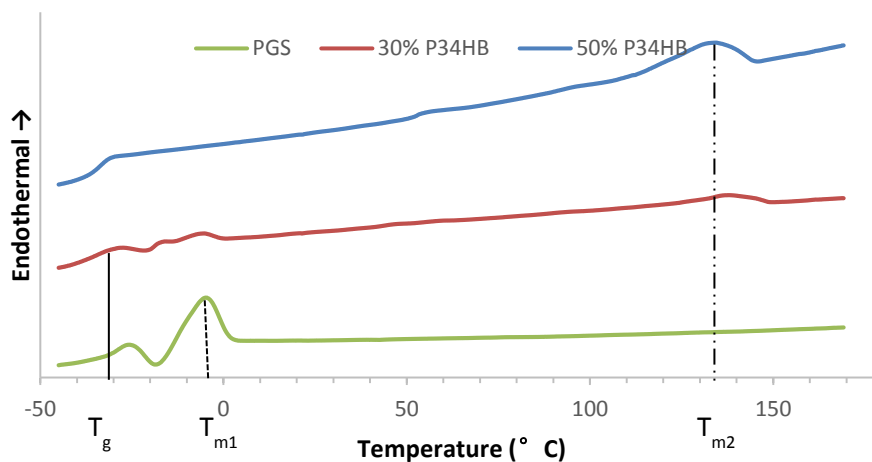


Figure 3-2 Non-isothermal DSC curves of pure PGS and P34HB/PGS blends (30% & 50%).

Table 3-2 Summary of P34HB/PGS blends thermal properties (\* indicates significant difference from PGS with  $p < 0.05$ )

Composition(P34HB/PGS) (%/%)	$T_g(^{\circ}\text{C})$	$T_{m1}(^{\circ}\text{C})$	$T_{m2}(^{\circ}\text{C})$	$\Delta H_{m1}(\text{J/g})$	$\Delta H_{m2}(\text{J/g})$
0/100	$-29.9 \pm 0.3$	$-4.9 \pm 0.8$	-	$12 \pm 1.5$	-
10/90	$-29 \pm 1$	$-2 \pm 1$	-	$9.8 \pm 0.6$	-
20/80	$-27 \pm 2$	-	-	-	-
30/70	$-25 \pm 4$	-	$136 \pm 2$	-	$3.7 \pm 0.4$
40/60	$-24 \pm 2$	-	$132 \pm 2$	-	$4.4 \pm 0.2$
50/50	$-24 \pm 2$	-	$136 \pm 1$	-	$6.6 \pm 0.4$
100/0	$-17 \pm 1$	-	$136.9 \pm 0.5$	-	$34.3 \pm 0.8$

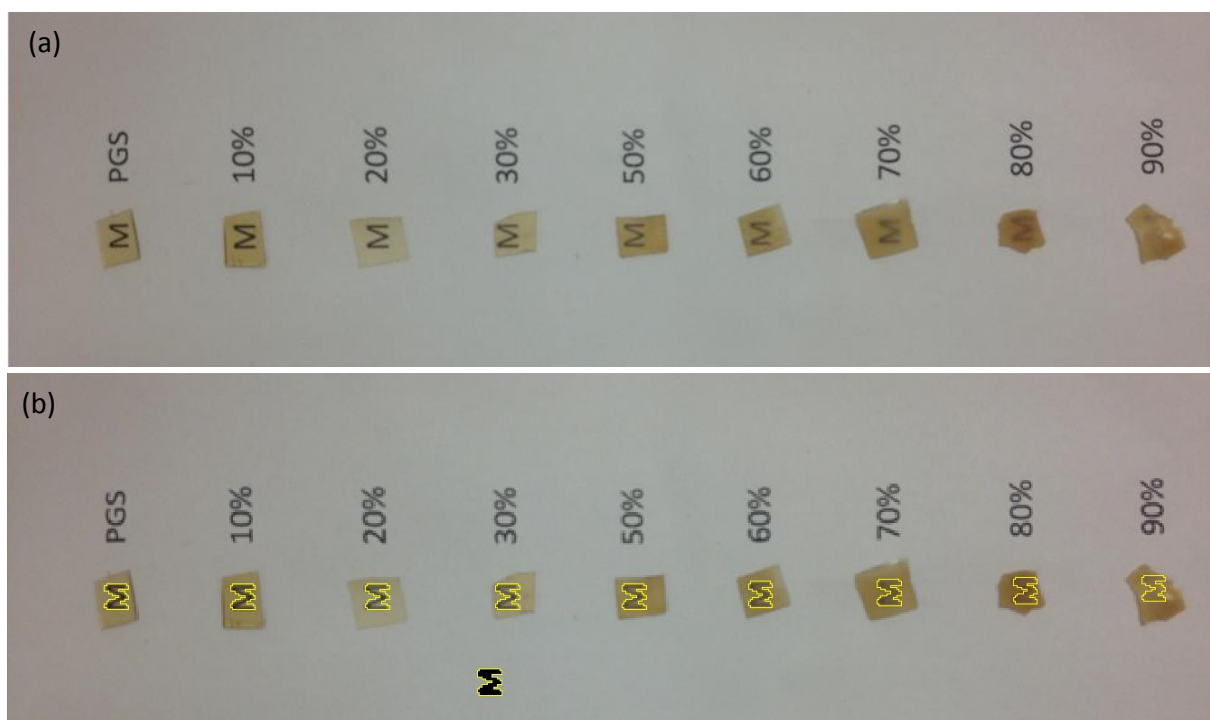
### 3.3.3 Transparency of P34HB/PGS blends

Visual examination (Fig. 3-3) showed that the synthesised P34HB/ had a good transparency when the content of P34HB was 50wt % or below, which means that the material is homogeneous. The blended

### 3. Developing elastomeric biomaterials from P34HB and PGS for soft tissue engineering

polymers with over 50wt % P34HB were more opaque. As amorphous PGS is transparent and crystalized P34HB was opaque, this figure indicates the crystal structure was formed when the P34HB content is high.

The transparency of the materials was compared by the light intensities of the regions of interest under each material. The measuring areas of M with 117 pixels are shown in Fig 3-3(b) and the light intensity was given in in Fig 3-3(c). Significant differences were found between most samples (27 out of 36 were significant). The light intensity, however, could only give a general idea of the transparency differences between different samples due to the difference in sample thickness. The yellowish opaque blends with high content of P34HB also provided a certain light intensity at the ROI, making comparison even harder.



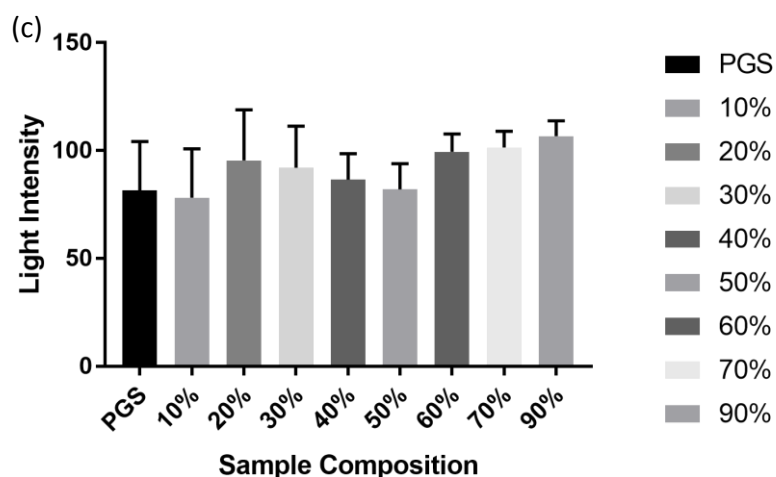
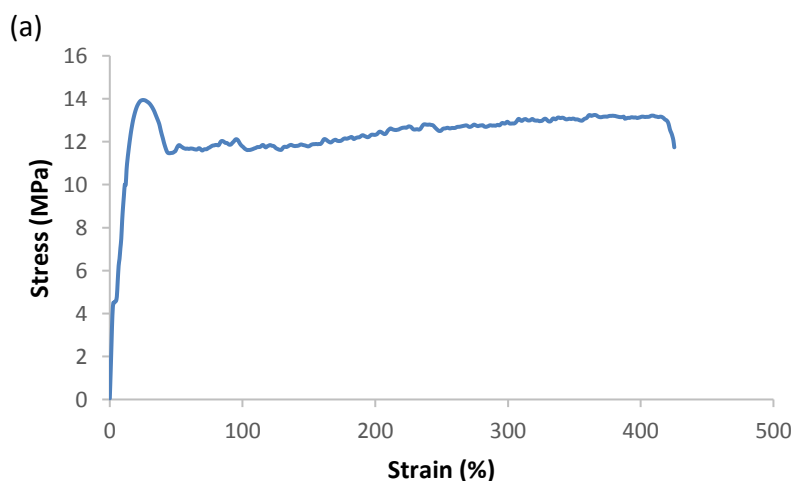


Figure 3-3 (a) Visual observation to show the single transparent phase at low content ( $\leq 50$  wt%). (b) The ROIs with the same pixels were labelled in different samples and the standard ROI is shown separately at the bottom of the figure. (c) The light intensity of ROI in different samples.

### 3.3.4 Mechanical properties

Compared with pure P34HB polymers (Fig. 3-4a), the P34HB/PGS blends of P34HB showed typical elastomeric behaviour of cross-linked elastomers, with trajectory stress-strain curves (Fig. 3-4b). When the content of P34HB reached 50wt%, the stress-strain curves began to bend more severely and the shape of the stress-strain curve was different from PGS. With P34HB content further increasing ( $\geq 60$ wt % P34HB), however, the blends became brittle such that the cast and heat treated sheets could not maintain integrity during peeling from the glass slides.



### 3. Developing elastomeric biomaterials from P34HB and PGS for soft tissue engineering

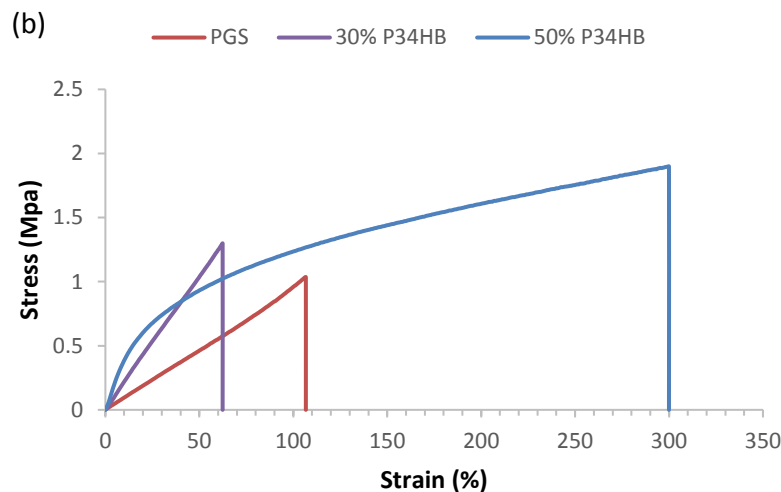


**Figure 3-4 Examples of stress strain curves of P34HB (a), PGS (b), P34HB/PGS blends (c) after curing .**

Compared with the pure PGS, the Young's moduli of P34HB/PGS blends increased concurrently with the increment of P34HB component up to 50 wt.% (Tab. 3-3). The Young's moduli still fell within several MPa and met the stiffness requirements soft tissue like cornea [184] and spinal cord[185] . The increased Young's modulus was attributed to the addition of P34HB, as the Young's modulus of P34HB is much higher than that of PGS. The 50% of P34HB is a critical point of mechanical properties. At this point, the properties of the blend were significantly different from the other blends, with the largest Young's modulus, ultimate stress and elongation at break. The cyclic tests also showed that the resilience of P34HB/PGS blend dropped from  $97.9 \pm 0.7$  to  $81.4 \pm 1.8$  when the P34HB proportion increased to 50 wt. %. Though the resilience of 50% P34HB/PGS was still higher than that of pure P34HB (65%), the blend lost much of its elasticity. The mechanical of blends after degradation is still unknown and need to be further investigated.



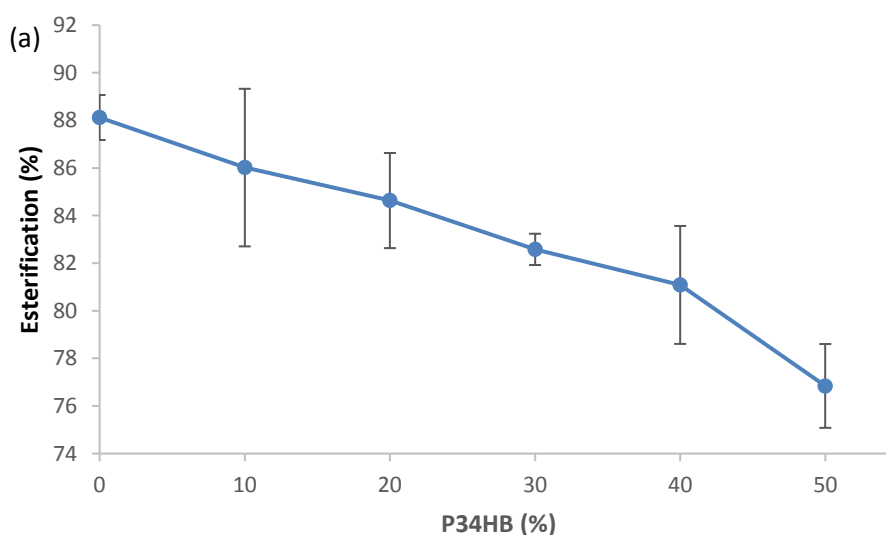
### 3. Developing elastomeric biomaterials from P34HB and PGS for soft tissue engineering

**Table 3-3 Summary of mechanical properties of P34HB/PGS blends (\* indicates significant difference from PGS with  $p < 0.05$ )**

Composition (P34HB/PGS) (%/%)	Young's modulus (MPa)	Ultimate stress (MPa)	Elongation at break (%)	Resilience (%)
0/100	$1.0 \pm 0.1$	$0.95 \pm 0.09$	$99 \pm 7$	$97.9 \pm 0.7$
10/90	$1.4 \pm 0.2$	$1.0 \pm 0.1$	$92 \pm 7$	$95.3 \pm 0.8$
20/80	$2.0 \pm 0.3$	$1.2 \pm 0.1$	$63 \pm 6$	$93.0 \pm 1.0$
30/70	$3.1 \pm 0.3$	$1.2 \pm 0.1$	$62 \pm 7$	$93 \pm 1$
40/60	$3.3 \pm 0.2$ *	$1.5 \pm 0.1$	$60 \pm 10$	$90.4 \pm 0.8$ *
50/50	$3.8 \pm 0.2$ *	$1.2 \pm 0.5$ *	$210 \pm 30$ *	$81 \pm 2$ *
100/0	$91 \pm 2$ *	$12.1 \pm 0.7$ *	$430 \pm 14$ *	$62 \pm 3$ *

### 3.3.5 Titration results

The degree of esterification decreased with the addition of P34HB. The introduction of P34B created a physical barrier and reduced the reaction probability of glycerol and sebacic acid, thus making the percentage of esterification contributed by these two monomers lower. But the effect was not significant. Even for the 50/50 blend, the percentage of esterification is still over 75% (Fig. 3-5 (a)). Though the percentage of esterification varies with samples, the unreacted sebacic acid in each sample was similar (Fig. 3-5 (b)).



### 3. Developing elastomeric biomaterials from P34HB and PGS for soft tissue engineering

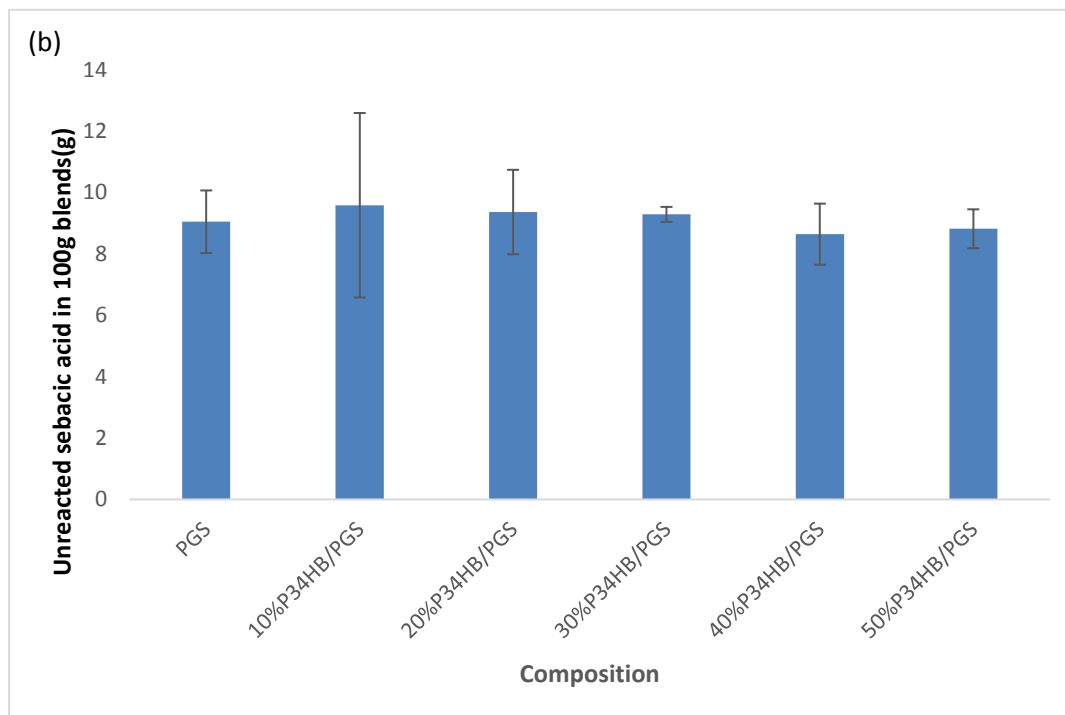


**Figure 3-5 (a) Percent esterification of pure PGS and P34HB/PGS blends and (b)The unreacted sebacic acid(g) in 100g blends.**

#### 3.3.6 Degradation Tests

According to degradation tests, the weight of all samples dropped with an increase in time. But only the degradation rate of pure PGS accelerated especially after 18 days. Even a small amount of P34HB could slow down the degradation rate of PGS. As shown in the XRD results, a part of the P34HB in the blends remained crystallized even in low P34HB content materials. In the first few days, the weight loss of all samples were proportional to the weight percentage of PGS. After 14 days, the degradation rate of PGS was maintained at a similar rate while the rate was slowed down in the blends with a change in gradient (Fig. 3-6a). It had been established that the PGS underwent surface degradation [186]. At the beginning, the weight loss could be attributed to the PGS degradation. After initial degradation, more P34HB was presented in the interfaces of the blends. The degradation rate of P34HB was much slower than that of PGS, so the weight loss was slowed down. The phenomena were found in all blends especially when the weight percentage of P34HB was high (Fig. 3-6b). The pH values of all samples showed similar trends. In

### 3. Developing elastomeric biomaterials from P34HB and PGS for soft tissue engineering

the beginning, the pH values dropped dramatically and remain stable afterwards. As the culture medium were changed every second day, the acidity could not accumulated for a long time. However, with longer soaking times, the pH values raised a little except pure PGS. The trend of pH change was consistent with the weight loss due to the same reason.

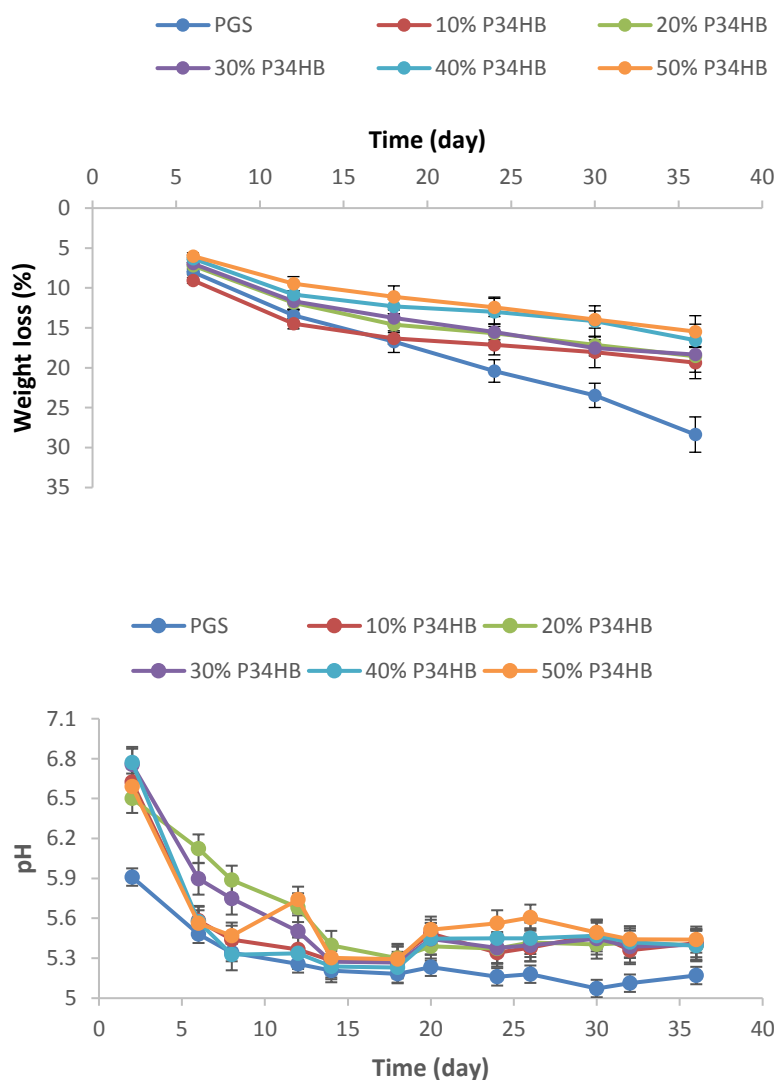


**Figure 3-6 (a) Weight loss of PGS and P34HB/PGS blends over time; (b) pH change of PGS and P34HB/PGS over time.**

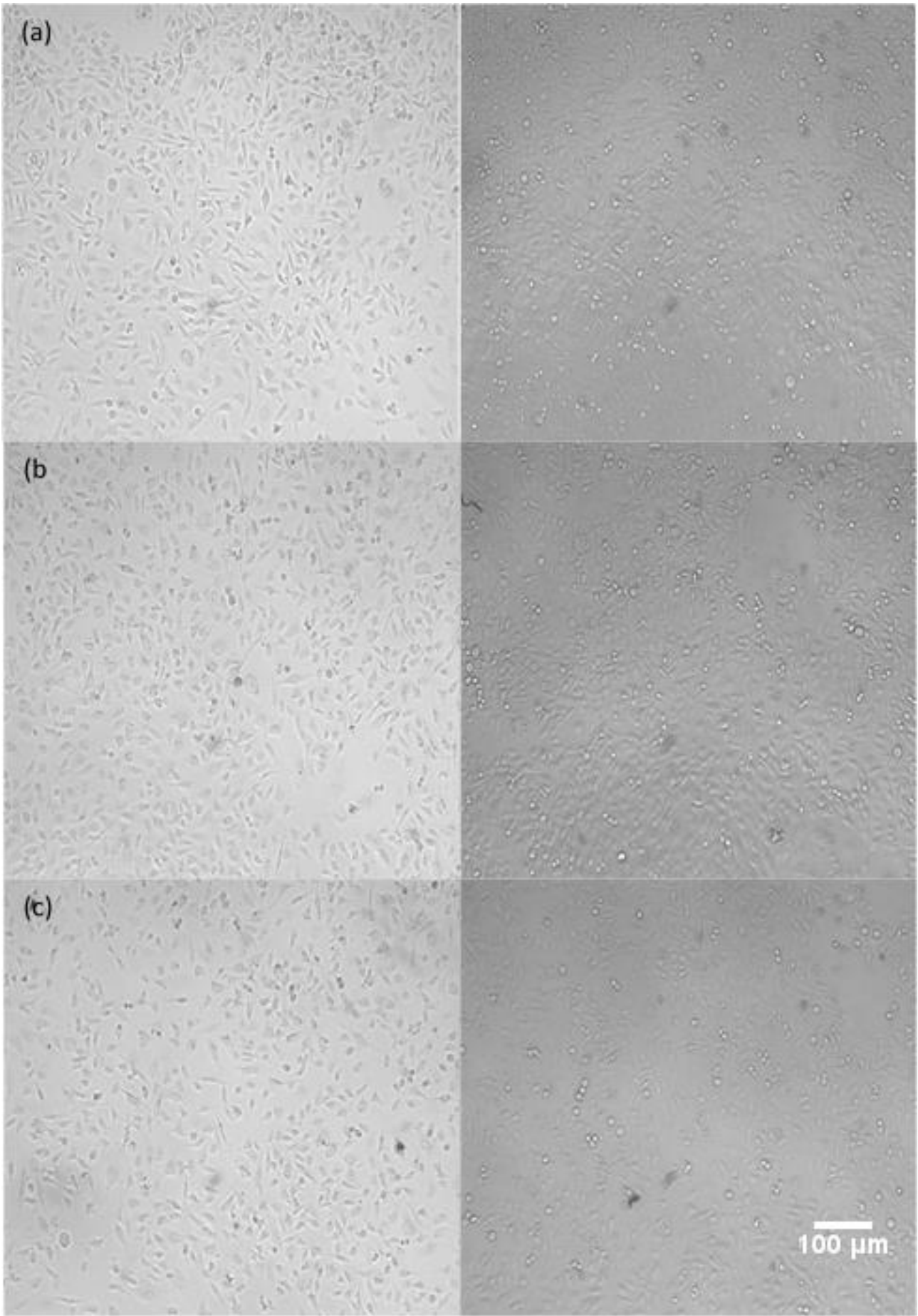
### **3.3.7 Cytotoxicity Assessment**

Although more dead cells floating on the surface with round shape were found in the second day, examples of the cell numbers increased over time in every medium (Fig. 3-7a-3-7c). No significant difference was found between the live cells percentage in all culture media.

All media showed acceptable cytotoxicity with living cells over 80%. It is still lower than the SNL cells cultured on TCPs with over 95% cells alive reported elsewhere [187]. In previous studies, the cytotoxicity of the material was caused by the unreacted sebacic acid [188]. Although a higher proportion of P34HB blends had a relatively lower percentage in esterification, the original sebacic acid was less in the blends. The total amount of unreacted sebacic acid were similar, thus making the cytotoxicity similar.

The cell viability needs to be further studied. Though the acidities in each well with different P34HB/PGS blends are similar, the surface morphology of different samples might differ from one to each other due to the difference in degradation speed between PGS and P34HB. The change in morphology and hydrophilicity might affects cell viability.

3. Developing elastomeric biomaterials from P34HB and PGS for soft tissue engineering



### 3. Developing elastomeric biomaterials from P34HB and PGS for soft tissue engineering

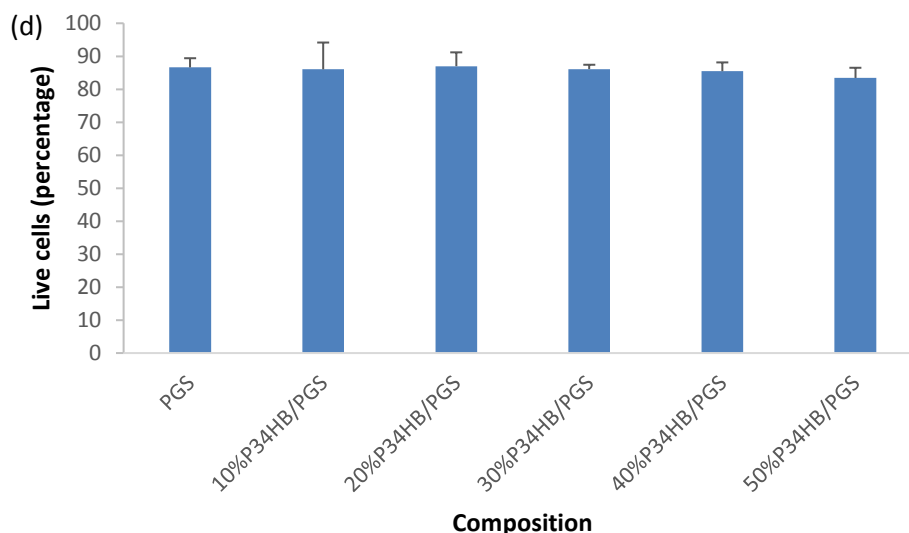


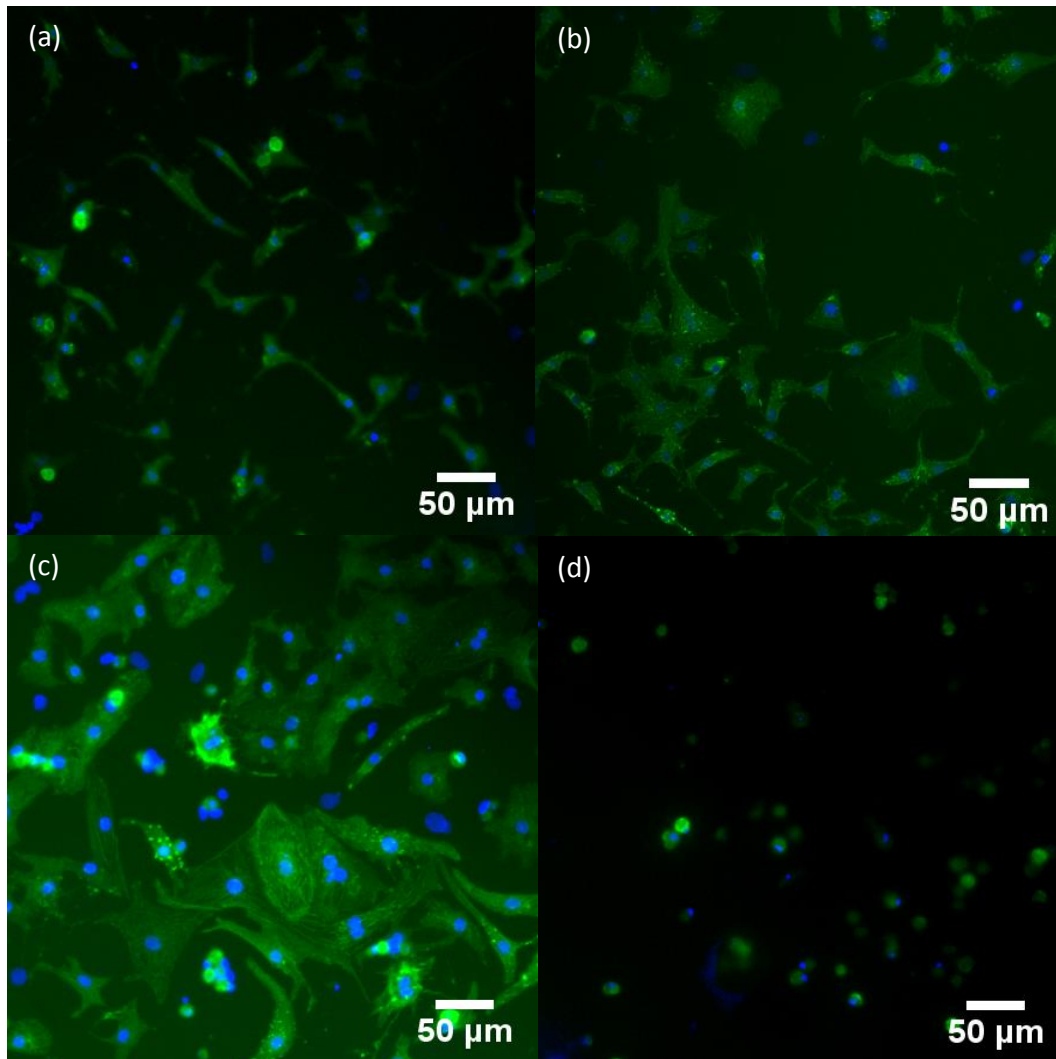
**Figure 3-7 Images of SNL cells in extracts prepared with different samples in the first day (left image) and the second day (right image) (a) PGS; (b) 30% P34HB/PGS; (c) 50%P34HB. (d) summary of percentage of living cells after incubation.**

#### 3.3.8 Cardiomyocytes cell culture

Cardiomyocytes attached and grew on PGS and P34HB/PGS blends (Fig. 3-8a-d). More hypertrophic cardiomyocytes were found on the substrates with higher percentage of P34HB (Fig. 3-8e). The cardiomyocytes cultured on PGS showed normal cell size at approximately  $300\mu\text{m}^2$  [189]. Previous studies showed that collagen synthesis caused an elevation in stiffness resulting in cardiomyocyte hypertrophy [190]. However, cardiomyocytes cultured on stiffer materials such as PGA [191] and PGLA [40] did not show a change in cell morphology. For the similar reason, the difference in hydrophilicity between P34HB and PGS cannot be the reason for the difference in alignment, as more PGA is a more hydrophobic material with a contact angle around  $75^\circ$  [192], which is higher than that of P34HB ( $60^\circ$ ) and PGS ( $32^\circ$ ) [173, 193]. Cardiocytes cultured on P34HB were still round at day 4 indicating poor attachment (Fig. 3-8d). One possible reason might be the degradation products from P34HB might prevent proper attachment of cardiomyocytes. Though the major degradation product, oligo (3-hydroxybutyrate) from P34HB has a positive effect on fibroblast growth [187], the effects of the other degradation product oligo

### 3. Developing elastomeric biomaterials from P34HB and PGS for soft tissue engineering

(3-hydroxybutyrate-4-hydroxybutyrate) on cardiomyocytes is still unknown. Whether these two degradation products would induce cardiomyocyte hypertrophy need to be further studied. Experiments of cardiomyocytes culture need to be carried out with more samples in each group to identify if the results are repeatable.



### 3. Developing elastomeric biomaterials from P34HB and PGS for soft tissue engineering

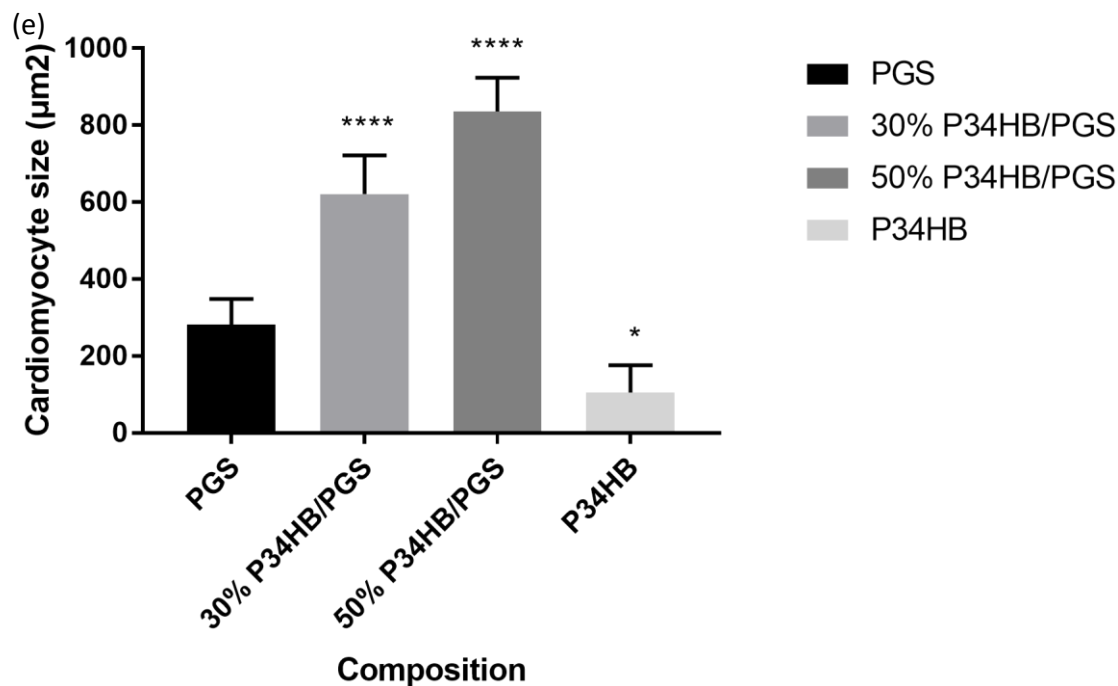


**Figure 3-8 (a) Elongated cardiomyocytes were found on the PGS film. Hypertrophic cardiomyocytes were found on 30% P34HB/PGS (b) and 50% P34HB/PGS (c) Round cardiomyocytes were found on the P34HB films (d); (e) Comparison between cardiomyocytes sizes cultured on different samples.**

## 3.4 Conclusions

To address the fast degradation rate of PGS, P34HB with slower degradation rate was blended with PGS. Even a small amount of P34HB in the blends slowed down degradation. The slow degradation rate was attributed to the crystal structure of P34HB and the surface degradation mechanism of PGS. However, the degradation cannot be controlled by blending P34HB with PGS as the degradation speed differences were not found between groups. The blend showed good elasticity with tunable Young's modulus up to 3.3 Mpa. The lost in elasticity was found when the weight percentage of P34HB reached 50% due to the phase separation.. Despite the change in mechanical properties, all blends showed good cytocompatibility. However, the blends were not ideal biomaterials for cardiomyocyte cell culture as hypertrophic cardiomyocytes were found when cultured on the blends especially when the P34HB



### 3. Developing elastomeric biomaterials from P34HB and PGS for soft tissue engineering

percentage was high. The reason for the hypertrophic cardiomyocytes is still unknown and need further investigation.

# 4 Micropatterning of PGS

## Declaration for Thesis Chapter [4]

### Declaration by candidate

In the case of Chapter [4], the nature and extent of my contribution to the work was the following:

Nature of contribution	Extent of contribution (%)
Major research and writing	80

The following co-authors contributed to the work.

Name	Nature of contribution	Extent of contribution (%) for student co-authors only
Wei Sheng	Air plasma treatment	N/A
Yuanshen Qi	SEM samples coating and images taking	5
John Forsythe	Provided corrections and assisted in research planning	N/A
Wayne Cook	Provided corrections	N/A

The undersigned hereby certify that the above declaration correctly reflects the nature and extent of the candidate's and co-authors' contributions to this work\*.

**Candidate's  
Signature**

	<b>Date</b> 26 <sup>th</sup> /08/2016
---	--

**Main  
Supervisor's  
Signature**

	<b>Date</b> 26 <sup>th</sup> /08/2016
---	--

### 4.1 Introduction

Controlling the interaction between cells and biomaterials is critical for the optimization of cell functions such as proliferation, differentiation, migration and apoptosis [194]. Therefore, identifying chemical and physical microenvironmental cues can help gain a better understanding of cells and enhance the regenerative outcomes of tissue engineered constructs. [195].

The intracellular signalling downstream pathways can be triggered by transmembrane proteins, so the type of proteins [196], the distribution of the proteins [197, 198] and conformation of the proteins [199, 200] on the biomaterial surface are important chemical cues. Physical cues are equally important and potentially allows for long-term activation of cell signalling pathways. Among the physical cues, topography is considered to be one of the most important cues to mimic the host organism [201]. For example, the topography of the scaffold which constrains cell spreading can affect cellular development [202, 203].

Generally, an elastomeric stamp e.g. polydimethylsiloxane (PDMS) can be obtained by casting and curing the prepolymer on the master. By repeating the procedure on the stamp, the substrate with the required structure can be obtained. However, such techniques cannot be applied on all biomaterials. Rigid biomaterials lead to non-conformal contact with the stamp leaving voids created by the natural roughness. Conversely very soft biomaterials are unable to reach a precise geometric structure. Failure to meet the requirements leads to a reduction in resolution and even a collapse in the structure [204].

Poly(glycerol sebacate) (PGS) is a tough, biodegradable elastomer and shows many physical similarities to PDMS. Both polymers are elastic with tunable mechanical properties in the same range, e.g. the Young's modulus can be varied from several hundred kPa to MPa [16, 205]. The crosslinking of both

#### 4. Micropatterning of PGS

polymers is initiated by heating and it is possible for the monomer/prepolymer in the liquid phase to provide intimate contact with the master/stamp. However, most reported studies on micropatterning biomaterial are achieved by dropping material solutions on the PDMS mould followed by drying or using a very soft hydrogel [63, 141, 142, 206]. Tough and resilient crosslinked PGS elastomer can also maintain the precise structure like PDMS. Although PGS has been intensively studied as a biomaterial for soft tissue engineering only a few cases of microcontact printing were studied [207, 208] and the procedures are not well established.

In the chapter, PGS substrates with micopatterned surface structures were fabricated. The change in parameters and fabrication methods are discussed and optimized.

## 4.2 Materials and methods

### 4.2.1 Fabrication of the master

Epoxy-based negative photoresist SU-8 2002, SU-8 2005 and SU-8 2007 (Microchem) was evenly cast on a precut (1 cm × 1 cm) silicon wafer ultrasonically cleaned by ethanol and isopropanol. The silicon wafer with photoresists was spun at 500 rpm for 10 s with an acceleration of 100 rpm/s followed by 200 rpm/s for 30 s with acceleration of 300 rpm/s based on the manufacturer's process to generate film with different thickness [209]. Photomasks with alternating chrome and clear strips of 10, 20 or 50  $\mu\text{m}$  (Bandwidth Foundry International Pty Ltd.) were then placed on the surface of the photoresist film. Exposure of UV light at 365 nm for 15 s at 15  $\text{mW}\cdot\text{cm}^{-2}$  selectively polymerized the photoresist films. A visible mask image could be found after heating the silicon wafer on a hot plate at 95 °C for 2 min. The non-polymerized photoresist under the chrome strip was immersed in SU-8 developer with gentle shaking for 10 s followed by a second wash with isopropanol for another 10 s. The rinse step was

#### 4. Micropatterning of PGS

repeated if a white film was produced during the isopropanol wash, which indicated the presence of residual non-polymerized photoresist.

##### **4.2.2 PDMS stamp fabrication**

A 10:1 mixture of Sylgard 184 (Dow Corning) elastomer base to curing agent was poured onto the patterned photoresist on the silicon wafer described above and heated on a hot plate at 150 °C for 10 min. After removal of the cured PDMS from the silicon wafer, the patterned side of the PDMS mould was then oxidized by air plasma (K1050X plasma asher, Quorum Emitech, U.K.) for 1 min at an intensity of 15 W to create a hydrophilic surface [208]. 5 µl 60% sucrose aqueous solution was coated on the oxidized PDMS mould within 5 min of plasma treatment. The sucrose coated PDMS mould was then transferred on a 150 °C hot plate and heated for 10 min.

##### **4.2.3 PGS substrate fabrication**

PGS was synthesized based on previously established protocols, with minor modifications [45, 210]. Glycerol and sebacate were mixed thoroughly at equal molar ratio at room temperature. The monomers underwent polycondensation at 130 °C under 130 cm<sup>3</sup>min<sup>-1</sup> flow of nitrogen for 24 hr. Approximately 0.3 g of paste-like PGS prepolymer was then cast on the photoresist master, PDMS and sucrose coated PDMS moulds at 150 °C on a hot plate to form a film. The cast PGS sheets were cured at 160 °C under vacuum for 8 hr. After cooling to room temperature, the PGS together with the PDMS mould were removed from the oven and submerged overnight in Milli-Q water. The patterned PGS films were peeled off from the PDMS the next day.

#### 4. Micropatterning of PGS

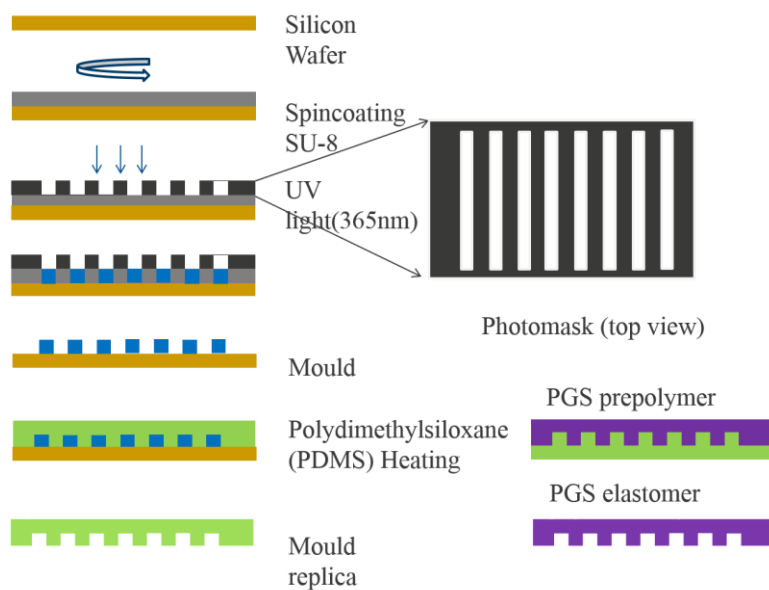


**Figure 4-1 Schematic diagram showing the steps in the fabrication of micropatterned PGS**

#### 4.2.4 Micropattern characterization

The micropatterned structure of the PDMS moulds and PGS films were visualized and quantified using optical profilometry (VeecoWyko NT100) without further surface treatment. The surfaces of the photoresist on silicon wafers were sputter coated with platinum to a thickness of 1 nm and characterised using a JEOL 7001F field emission gun (FEG) scanning electron microscope (SEM), which was operated in the second electron imaging mode.

#### 4.2.5 Contact angle tests

The wettability of the PDMS before and after plasma treatment and sucrose coated PDMS was determined by measuring the water to air contact angle (Dataphysics OCA20 Germany) at room temperature. Water droplets (about 4  $\mu\text{L}$ ) were dropped carefully onto the surface. The average contact angle value was obtained by measuring at 3 different samples.

### 4.3 Results and Discussion

PGS with different pattern width and channel depths were fabricated (Fig. 4-1). The thickness of the features was controlled by the photoresist and spinning speed as per the manufacturer's instructions [209] (Fig. 4-2a-4-2c). However, the recommended UV exposure energy was at a wavelength below 350 nm. For 365 nm UV radiation (which was available in our laboratory), 50% additional exposure time was required according to the following test. The depth of grooves was insufficient compared with designs ( $0.7 \pm 0.2 \mu\text{m}$  vs.  $1.5 \pm 0.2 \mu\text{m}$ ) (Fig. 4-3a, 4-3b) and the patterns were not stable on the surface (Fig. 4-4a, 4-4b). Visible latent images indicated that stable micropatterns were obtained with additional UV exposure time.

#### 4. Micropatterning of PGS

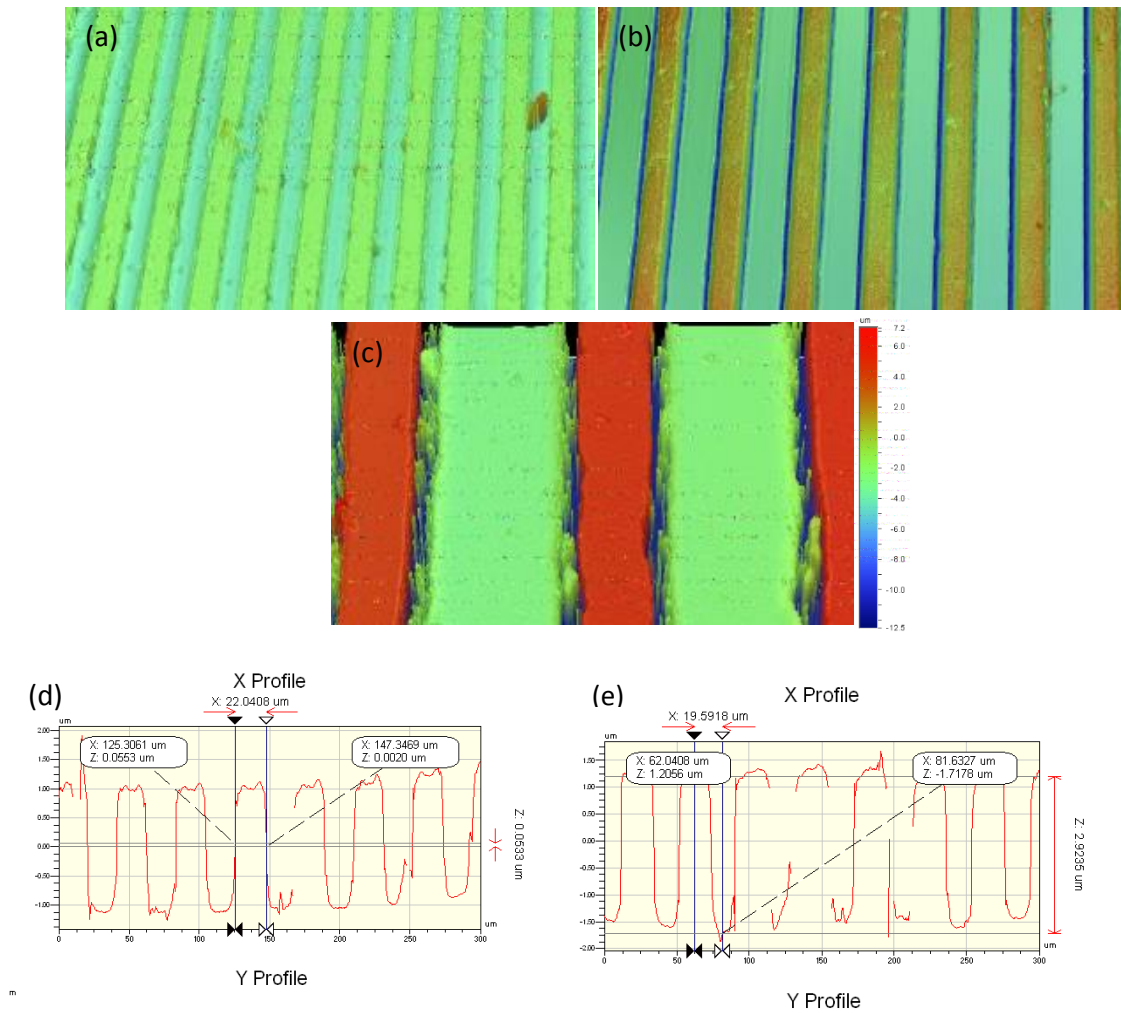


**Figure 4-2 Examples of PGS micropatterns with 1.5 μm (a), 3 μm (b) and 7 μm (c) depth and the examples of measurements in crest width(d) and channel depth (e)**



#### 4. Micropatterning of PGS

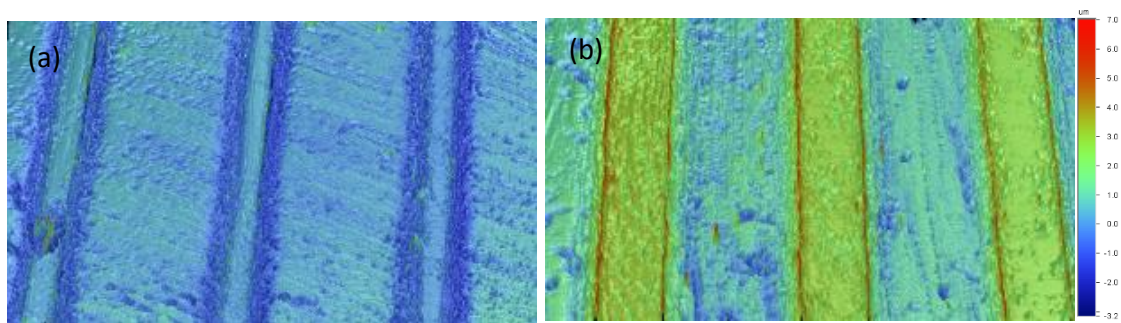


**Figure 4-3** Insufficient exposure time leads to the shallow groove depth (a) compared with designs (b)

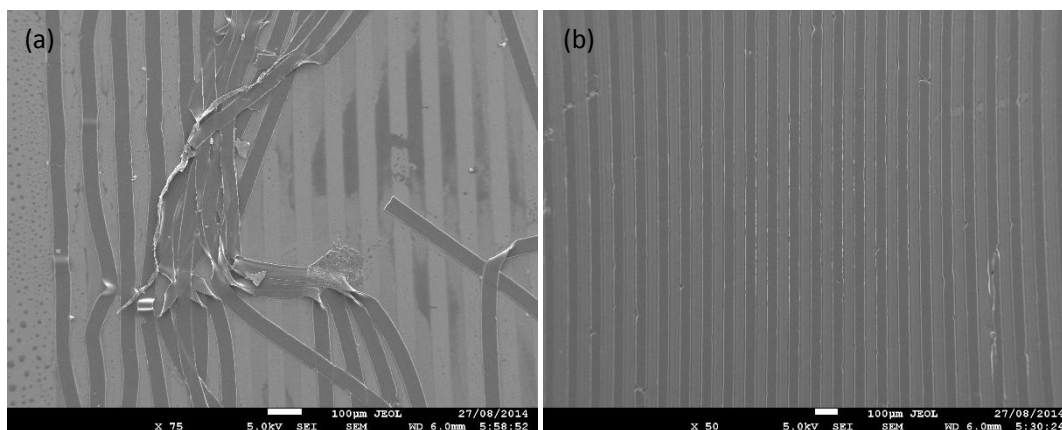


**Figure 4-4** Insufficient UV exposure led to detachment of the photoresist patterns (a). Corresponding patterns on the solid silicon wafer (b). Scale bar = 100  $\mu\text{m}$ .

At first, the PGS prepolymer was directly coated on the silicon wafer. However, after curing, PGS adhered to the silicon wafer. Most surface features on the PGS showed poor resolution (Fig. 4-5a, 4-5b), indicating PGS could not be used as a replacement for PDMS which could replicate structures with a resolution down to 1-2  $\mu\text{m}$  [194]. Solid PDMS presents an external hydrophobic surface with contact an angle of  $120 \pm 4^\circ$ . However, PGS is a hydrophilic material with a contact angle of around  $30^\circ$  [173]. A small amount ( $<0.5$  g) PGS prepolymer did not dispense on the PDMS mould. Only thick PGS (over 0.5 mm) film with curved undersurface could be obtained from the PDMS mould without any treatment. 30 mins after plasma treatment, the water contact angle was  $35.7 \pm 1.7^\circ$  which was similar to PGS. PGS prepolymer dispensed well on the surface. However, after curing, an uneven distribution of PGS was mostly found on the PDMS after plasma treatment. A possible reason is the aging of the air plasma

#### 4. Micropatterning of PGS

treated PDMS surface. As previously reported, the contact angle could return to 50 °, 12 hr after the plasma treatment and finally reaching 100 ° after 350 hr [211]. The improvement was quite limited for plasma treatment if the PDMS was exposed directly to the atmosphere. The PGS could not be freely peeled from the PDMS mould even after soaking overnight. PGS residue was found on the surface of the PDMS mould, which resulted in an accumulation of defects (Fig. 4-6a). The sucrose coating introduced a thin layer between the PDMS and PGS. The thin film retained the hydrophilicity of plasma treated PDMS and could dissolve in water (as the coating was carried out 5 mins after plasma treatment, the average contact angle should be smaller than 35.7°), which facilitated the peeling procedure (Fig. 4-6b). Sucrose aqueous solution direct coating without plasma treatment failed on the PDMS surface due to the surface hydrophobicity.

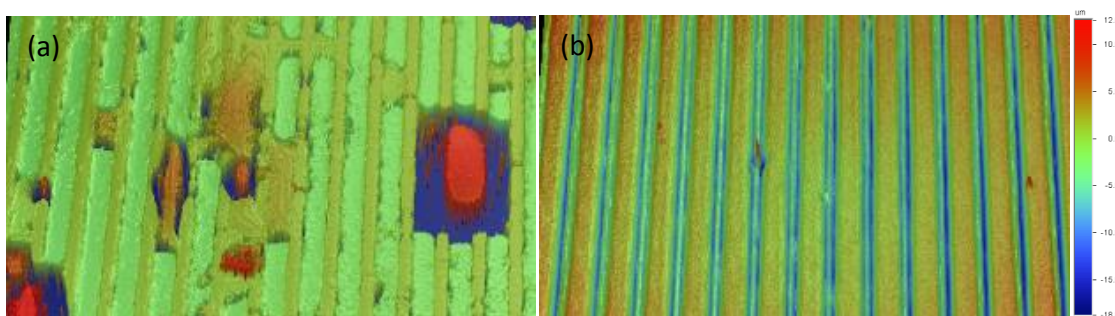


**Figure 4-5 The PGS peeled from silicon wafer with damage (a) and the PDMS replica peeled from silicon wafer (b)**

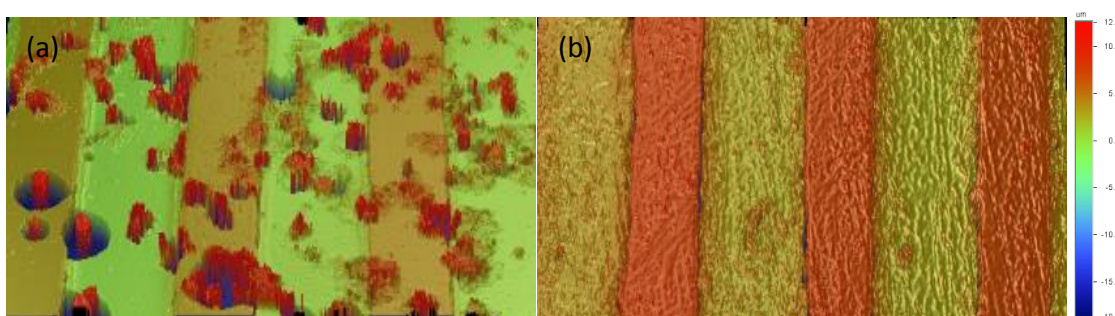


**Figure 4-6 PGS peeled from PDMS and exhibited damaged features (a) and limited damage with a sucrose coating (b)**

The repeating grooves and crests patterned features were designed to improve cell alignment. However previous studies have shown that cell alignment is also influenced by the groove depth [63, 212]. The

#### 4. Micropatterning of PGS

increase in cell alignment is proportional with groove depth, and a groove depth of 2  $\mu\text{m}$  is the threshold for robust alignment [213]. However, deeper grooves might isolate cells grown on the channels and grooves, which weakens cell-cell communication and cell coordination [147]. Taking this into consideration, 3  $\mu\text{m}$  was chosen as the depth of the grooves to increase cell alignment. The widths of the grooves (bottom sections) and channels (top sections) created on the PGS films were stamped from the PDMS mould and measured as well as the channel depth (Fig. 4-7). There was no significant difference between the channel depth of the different patterns. The widths of the channels and grooves were similar to the pattern of the photomask although the groove widths were consistently lower than the channel widths for all 10  $\mu\text{m}$  ( $8.6 \pm 0.8 \mu\text{m}$  vs.  $11.3 \pm 0.4 \mu\text{m}$ ), 20  $\mu\text{m}$  ( $17.2 \pm 1.0 \mu\text{m}$  vs.  $22.2 \pm 0.9 \mu\text{m}$ ) and 50  $\mu\text{m}$  ( $47.7 \pm 0.9 \mu\text{m}$  vs.  $56.7 \pm 1.2 \mu\text{m}$ ) films (Fig. 4-7). This is the same situation in the moulds, so the difference was introduced at the very beginning by UV light diffraction which leads to crosslinking of the photoresist in shaded areas which may have narrowed the groove size, which has also been reported elsewhere [63].

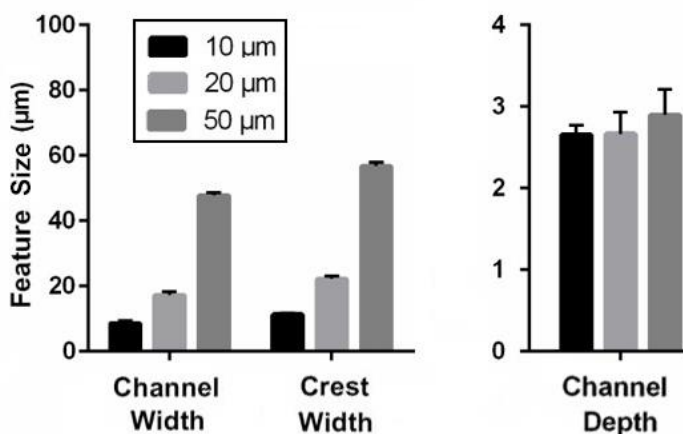


**Figure 4-7 Quantification of groove width, channel width and channel depth ( $\mu\text{m}$ ) of micropatterned PGS films.**

## 4.4 Conclusion

PGS with designed features could be fabricated by microprinting from PDMS. Although PGS and PDMS are both crosslinked elastomers with similar crosslinking procedures, PGS is not a good substitution for PDMS as a replica of pattern. Apart from the long curing time, the hydrophilicity of PGS made it hard to be separated from the silicon wafer. The improvement was limited for casting PGS on the PDMS mould with plasma treatment and the design features could only be achieved with a sucrose coating after plasma treatment. The UV scattering led to reduced resolution of the PGS, however, the error was with 1-2  $\mu\text{m}$  which was reported previously as the resolution of microcontact printing [194]. However, microcontact printing is a convenient way to fabricate microstructures on PGS elastomers.

# 5 Micropatterned tissue-like bioelastomers improve cardiomyocyte alignment and beating homogeneity

**Declaration for Thesis Chapter [5]**

**Declaration by candidate**

In the case of Chapter [5], the nature and extent of my contribution to the work was the following:

Nature of contribution	Extent of contribution (%)
Major research and writing	80

The following co-authors contributed to the work.

Name	Nature of contribution	Extent of contribution (%) for student co-authors only
Kelly Tsang	Provideed $\alpha$ -actinin antibody	N/A
Kun Zhou	Confocal imaging and assistant with beating analysis	N/A
Andre Rodda	Assistant with code analysis	N/A
John Forsythe	Provided corrections and assisted in research planning	N/A
Wayne Cook	Provided corrections	N/A
John Haynes	Provided corrections and assisted in beating analysis	N/A

5. Micropatterned tissue-like bioelastomers improve cardiomyocyte alignment and beating homogeneity

<b>Binghui Wang</b>	Provided corrections and assisted in cell culture	N/A
---------------------	---	-----

The undersigned hereby certify that the above declaration correctly reflects the nature and extent of the candidate's and co-authors' contributions to this work\*.

**Candidate's  
Signature**

	<b>Date</b> <b>26<sup>th</sup>/08/2016</b>
---	---

**Main  
Supervisor's  
Signature**

	<b>Date</b> <b>26<sup>th</sup>/08/2016</b>
---	---

## 5.1 Introduction

Myocardial infarction is the damage of myocardium caused by ischemia or hypoxia. Collagen scarring in the infarcted tissue does not contribute to tension generation. Long-term consequences include cardiac remodeling and possible progression to heart failure. Part of the problem is the lack of ability of cardiac tissue to undergo significant regeneration [18, 19]. To combat this lack of endogenous repair, many studies have attempted to introduce stem cells or cardiomyocytes into dysfunctional areas in the hope that they can replace damaged cells and improve cardiac function [27, 214, 215]. However, introducing cells into the scar area by direct injection into the myocardium or via circulating blood results in poor engraftment [216, 217].

In an effort to improve cardiac engraftment, cardiac tissue engineering strategies now focus on cellular transplantation techniques combined with degradable scaffolds to create viable myocardial replacement tissue [7, 218-221]. The degradable scaffolds must, however, fulfil certain criteria to meet the mechanical demands of cardiac tissue without cracking or disintegrating [222]. Elastomeric materials such as polydimethylsiloxane (PDMS) exhibit good biocompatibility but are non-degradable [90, 223, 224]. Thermoplastic polyurethane and poly (lactic-co-glycolic acid) are biodegradable but undergo plastic deformation and failure when exposed to long-term cyclic strain [194, 225]. Gelatin based hydrogels are elastomeric, but lack dimensional stability due to swelling, and have poor mechanical strength and low extensibility which limits their use [63, 221, 226]. In contrast to these materials, poly (glycerol sebacate) (PGS) appears to be an ideal material for implantation work. It is a biodegradable elastomer designed especially for soft tissue engineering that does not undergo plastic deformation under long-term repeated cyclic strain [16, 210]. The intrinsic elasticity and stiffness of PGS make it compatible with myocardial tissue engineering, since PGS has an adjustable secant modulus which can

5. Micropatterned tissue-like bioelastomers improve cardiomyocyte alignment and beating homogeneity

cover the whole range of heart muscle, possessing a secant modulus of 10-20 kPa at the beginning of diastole and 200-500 kPa at the end [227].

To regenerate functional cardiac tissue, it is important to mimic the natural morphology of the myocardium [151, 228]. Previous studies performed on cardiomyocytes have shown that their cell alignment and intracellular communication can be influenced by the dimensions of the physical features on the surface of the cardiomyocyte culture substrate using either polystyrene, polyurethane [223] or modified gelatin [63]. However, if PGS is chosen to be the substrate, there are limitations to the fabrication methods to produce aligned cardiomyocytes. For example, excimer laser microablation on PGS bilaminar accordion-like honeycomb scaffolds failed to provide good cell alignment [45]. Core/shell electrospinning has also been applied to PGS for this purpose [47, 229], however, the critical limitations of electrospinning was the small pore size and lack of proper cellular infiltration inside the fibres [230].

Here we report the development of mechanically robust elastomeric PGS films patterned using lithography to create microchannels on the surface. We assess how different microchannel dimensions affect the beating behavior of cardiomyocytes.

## **5.2 Materials and Methods**

### **5.2.1 Mechanical and morphology characterization**

PGS specimens with thickness around 300  $\mu\text{m}$  were cut from a cured unpatterned PGS sheet using a dumbbell shaped mould with a gauge length of 12.5 mm and a width of 3.25 mm. The thickness of each specimen was measured using an electronic vernier caliper. The micropatterned structure of the silicon elastomer moulds and PGS films were visualized and quantified using optical profilometry (VeecoWyko NT100) without further surface treatment. Tensile and cyclic tests were performed using an Instron 5860



5. Micropatterned tissue-like bioelastomers improve cardiomyocyte alignment and beating homogeneity

mechanical tester equipped with a 100 N load cell. Extension rates of 10 mm.min<sup>-1</sup> and 25 mm.min<sup>-1</sup> were applied for the tensile and cyclic tests respectively, to be consistent with earlier studies.[48, 187, 231] Specimens for the tensile tests were stretched to failure and those for cyclic tests underwent a strain of 15%, which is typical of the dynamic loading strain of the myocardium under normal physiological conditions [13, 187, 231].

## **5.2.2 PGS film pretreatment**

PGS films were sterilized by soaking in 80% ethanol for 12 hr. To remove any unreacted sebacate in the PGS, the films were soaked in 300 µl of DMEM in a 48 well culture plate placed in an incubator (37 °C in humidified air containing 5% CO<sub>2</sub>) with a culture medium change every 48 hr. The pH value was measured daily by insertion of a pH meter until the pH change was not significant. Porcine skin gelatin (300 µl of 1% solution in MQ water, Sigma) was added to cover the surface of the PGS film. The plate was incubated for 2 hr and then the gelatin solution was thoroughly removed with a Pasteur pipette.

## **5.2.3 Cardiomyocytes cell culture**

Neonatal cardiomyocytes (NCMs) were isolated from 1-2 day old neonatal rat pups by enzymatic digestion as described previously [179, 180]. NCMs were seeded at 2.2×10<sup>5</sup> cells per well in 48 well-plates on pretreated PGS films with different sized micropatterned features and incubated in minimal essential medium (MEM) containing 10% new born cow serum (NBCS) and 0.1 mM bromodeoxyuridine (BrdU) at 37 °C in humidified air with 5% CO<sub>2</sub>. After 24 hr, the media was changed to DMEM with 0.1mM BrdU, 10 µg/ml human transferrin (Sigma) and 2.5 U/ml human, insulin (Sigma). Thereafter, NCMs were maintained in DMEM with the same concentration of apo-transferrin and insulin without serum or BrdU and culture media was changed every 72 hr, as described previously [180].

5. Micropatterned tissue-like bioelastomers improve cardiomyocyte alignment and beating homogeneity

### **5.2.4 Video imaging and quantification**

Cardiomyocyte beating was captured (at 30 frames per second) with a video camera (Sony XCD-X710) attached to a microscope (Nikon Eclipse TS 100). Video frames were used to create an avi computer file for analysis. Beating frequency was calculated by measuring light intensity variation across a region of cells using the Image J plugin, time series analyzer. The beats across different patterns were measured and quantified using a previously described spreadsheet [232] for the comparison between average beat period length.

### **5.2.5 Immunocytochemistry**

After 7 days of culture, cells were fixed using 4 % paraformaldehyde (PFA), permeated by 0.3 % (w/v) Triton-X. Cardiomyocytes were then blocked with 10 % normal goat serum (NGS) in phosphate buffered saline (PBS) and incubated with anti- $\alpha$ -actinin (mouse) (ab9465) (and anti-connexin (rabbit) (ab11370) at 1:200 and 1:1000, respectively, or anti-troponin I (rabbit) (ab47003) at 1:200 in 10 % NGS respectively overnight at 4 °C. The cardiomyocytes were incubated in diluted secondary antibodies (Goat-anti-mouse 568 and goat-anti-rabbit 488) in PBS at 1:1000 for 1 hr at 37 °C. The samples were rinsed and incubated with 4',6-diamidino-2-phenylindole (DAPI) for 5 min and were then sealed with mounting medium on glass slides. Stained samples were imaged using a scanning confocal microscope (Leica SP5 XMP, Germany) with a 40× water immersion objective.

### **5.2.6 Nuclei alignment analysis**

Following a previous reported method [233], images of DAPI-stained nuclei were taken by fluorescence microscopy (Nikon Eclipse TS 100). The images were converted to binary images by Image J and each individual nucleus was fitted to an ellipse. The angle between the nuclei elongation direction and the

5. Micropatterned tissue-like bioelastomers improve cardiomyocyte alignment and beating homogeneity

pattern direction was quantified as the angle of deviation and the angles were grouped in 10° increments.

Differences between nuclei alignment angles less than 20° were considered as aligned [63]. For each pattern, six different sample images from 3 films containing 100-200 cells each were averaged and summarized.

### **5.2.7 Calcium imaging**

Fluo-4 AM (Thermo Scientific™) was dissolved in dimethyl sulfoxide at 10 mM and diluted to a final concentration of 2 µM in DMEM. Cardiomyocytes were incubated in DMEM with Fluo-4 for 30 min at 37 °C. Calcium ion transients were recorded using fluorescence microscopy (Nikon Eclipse TS 100) (excitation at 485 nm, emission at 520 nm). Three different samples were examined for each group, with three randomly selected areas studied per film. Whole-frame images obtained at 1360 × 1024 pixels were continuously recorded to produce image sequences. The image sequences were corrected for darkening over time (likely caused by condensation) using ImageJ's bleach correction tool, and were then analyzed using the ImageJ software plugin LC Pro and previously reported R code [234]. The region of interest was defined as a circle with a diameter of 40 pixels with an area similar to a cardiomyocyte size.

### **5.2.8 Statistical Analysis**

The average time between beats were analyzed using Kruskal-Wallis analysis followed by Dunn's test and the standard deviations were analyzed by F tests between two groups. The other data were analyzed using one-way analysis of variance followed by Tukey's post-hoc test. Results are presented by the mean ± standard deviation (SD) and a value of 0.05 was considered as significant. Significant changes in parameter variance were determined with a Brown-Forsythe test.

5. Micropatterned tissue-like bioelastomers improve cardiomyocyte alignment and beating homogeneity

## **5.3 Results and Discussion**

### **5.3.1 Mechanical properties of PGS**

PGS synthesized at 160 °C under vacuum conditions for 8 hr resulted in a secant modulus of  $625 \pm 30$  kPa at 10% strain (Fig. 5-1a), which is close to the maximum human myocardial stiffness at the end of diastole, which has a secant modulus of 500 kPa [235]. Although the cardiomyocytes cultured on very soft substrates (e.g. those with a Young's modulus of 120 Pa) exhibit more intense spontaneous contractions [236], stiffer materials could provide a greater reduction in myocardium stress and provide a protective effect from ventricular remodelling [126]. For example, previous studies have shown that collagen fibers ( $E = 2\text{--}46$  MPa) are stiffer than the myocardium [16] and could improve myocardial function after infarction with a decrease in left ventricular end-diastolic volume and left ventricular end-diastolic pressure [237]. The elongation at break was greater than that of the myocardium which is typically around 15 % [210], again confirming that the PGS is a suitable substrate for cell growth. For the cyclic test, the resilience, which indicates the elastic recovery ability of the material, was  $98 \pm 1$  %, showing that PGS could deform reversibly with minimal loss of energy. This finding favors a reduced cardiomyocyte workload in contraction while contributing to cardiomyocyte recovery. As the myocardium undergoes numerous beatings during its lifetime, repeated extensions need to be performed on PGS samples to characterize the influence of multiple cyclic tensile deformations. The unchanging elasticity of PGS was confirmed during the 50 deformation cycles of PGS stress-strain curve at different cycles (Fig. 5-1b), indicating that PGS could endure the working environment of the heart [5, 16].

## 5. Micropatterned tissue-like bioelastomers improve cardiomyocyte alignment and beating homogeneity

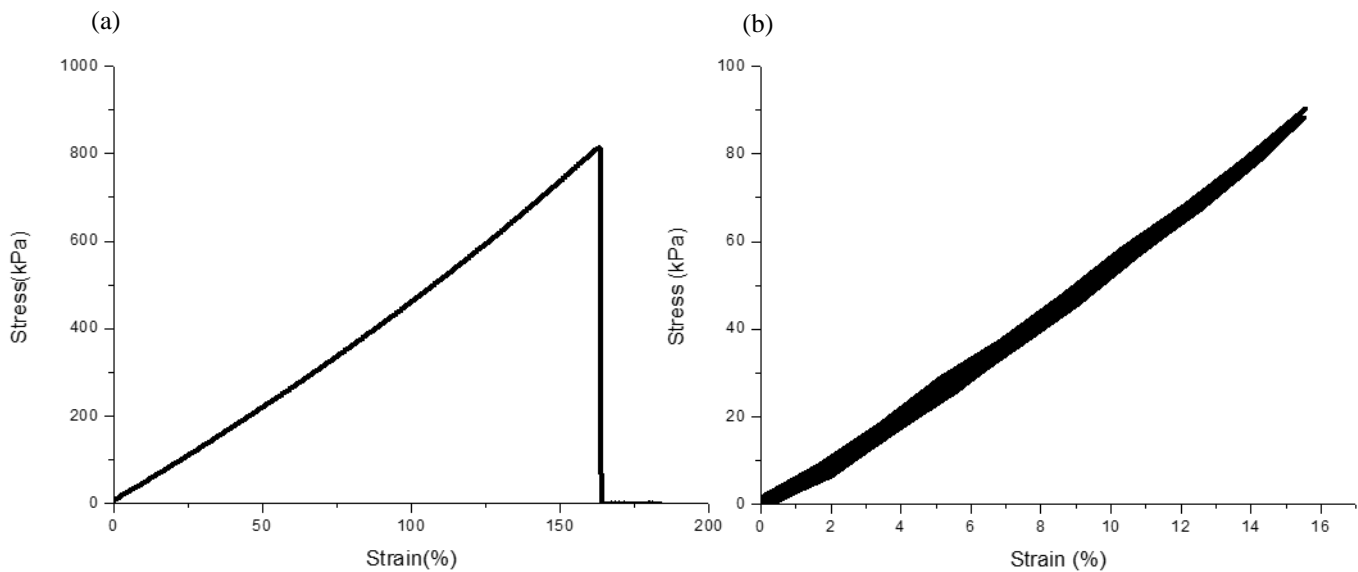


**Figure 5-1 (a) Stress-strain curves of PGS synthesized at 160 °C under vacuum conditions for 8 hr (b) 50-cyclic-stress-strain curve of PGS synthesized under the same conditions.**

### 5.3.2 Cell alignment and immunochemical analysis

Cardiomyocytes grew on both the channels and crests, facilitating physical contact of cells between adjacent channels and ensuring intracellular communications (Fig. 5-2a-5-2c). Overall, the alignment of cardiomyocytes was improved on the patterned PGS (Fig. 5-2a-5-2c) compared with unpatterned films (Fig. 5-2d). This was confirmed by fluorescent images of cardiomyocytes stained on day 7 for actin filaments (troponin I) and nuclei (DAPI). As a cardiac regulatory protein, troponin I regulates the contraction behavior of cardiomyocytes by binding and releasing  $\text{Ca}^{2+}$ . Compared to the isotropic morphology of cardiomyocytes on unpatterned films (Fig. 5-2h), aligned cardiomyocytes showed an elongated cell shape and oval-shaped nuclei along the channel direction of the micropatterned PGS (Fig. 5-2e-5-2g). Cell alignment was most pronounced on the 20  $\mu\text{m}$  micropatterned features. This could be due to the relative size of rat cardiomyocytes which also have a lateral width of approximately 20  $\mu\text{m}$  matching the pattern size [238]. Although previous studies [139, 140, 223] on nanodimensioned channels (approximately 0.45  $\mu\text{m}$  channel width) showed an improvement in cell alignment with the subcellular nanopatterned structures, those cells

## 5. Micropatterned tissue-like bioelastomers improve cardiomyocyte alignment and beating homogeneity

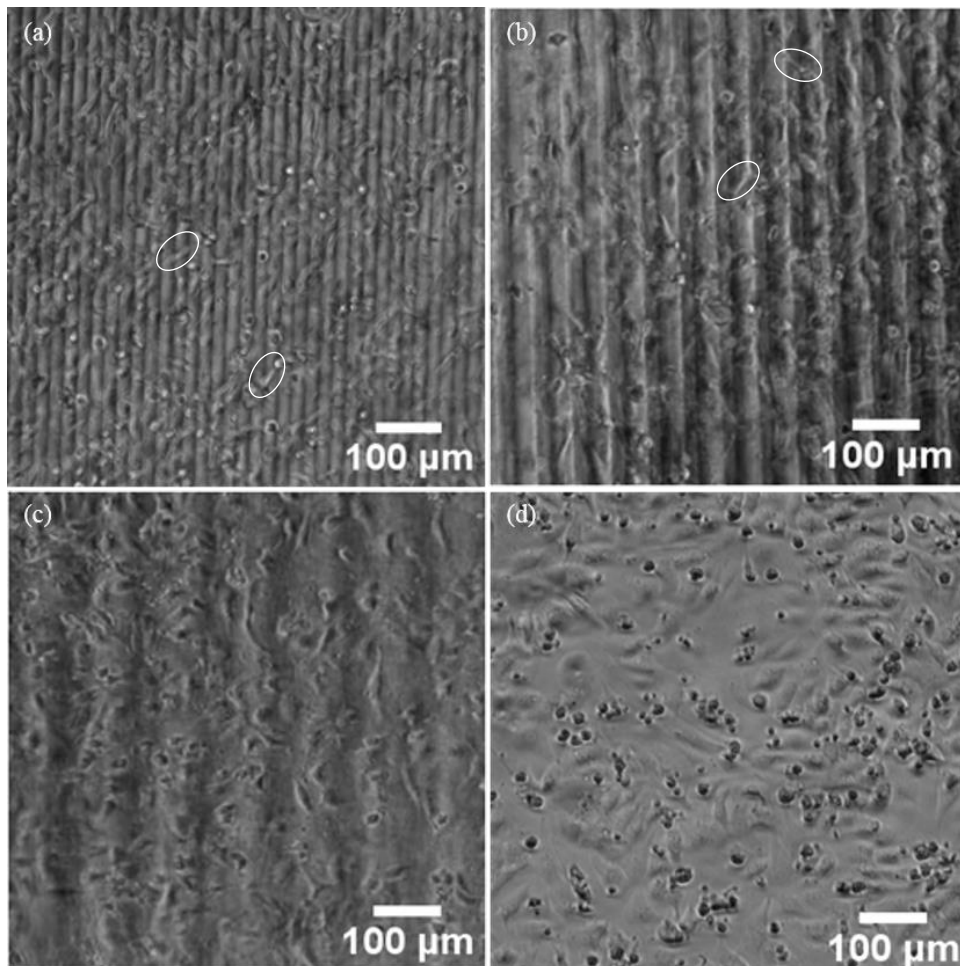
are aligned by the confinements of cell–matrix adhesions and actin filaments in channels. The features shown here are larger and do not correspond with the dimensions of subcellular features. Cardiomyocytes cultured on 10  $\mu\text{m}$  and 20  $\mu\text{m}$  displayed more bridging across the channels (Fig. 5-2a, 5-2b) (examples shown in ellipse). This is in contrast to the 50  $\mu\text{m}$  patterned PGS, where fewer cardiomyocytes bridged across channels (Fig. 5-2c). This could also attributed to the cardiomyocyte size with a longitudinal length around 100  $\mu\text{m}$  [239]. It is more difficult for cardiomyocytes to stretch across 50  $\mu\text{m}$  channels with almost half of the cell hanging over the channel.

As the nuclei showed an elliptical shape in elongated cardiomyocytes [63], the alignment of cardiomyocytes could be quantified based on the elliptical nuclei major axis direction. Due to the strong background emissions of PGS [240], the immunostaining figures are blueish and greenish. Here, we followed a previous study [221] which defined cells to be aligned when the angle between the major axis of elliptical nuclei and the pattern direction was less than 20°. No preference for nuclei orientation was evident on unpatterned films as the nuclei orientation was evenly distributed for all directions (Fig. 5-2i) However, cardiomyocytes cultured on patterned PGS (Fig. 5-2i-5-2j) exhibited a preferential nuclei alignment along the channel direction. Although some cardiomyocytes cultured on the 20  $\mu\text{m}$  channel films bridged across several channels, these films presented the highest proportion of aligned cells with  $61 \pm 7\%$  of the cells having an alignment angle of less than 20° which was statistically ( $p < 0.001$ ) different from the unpatterned films. Lower alignments were found for cardiomyocytes cultured on 10  $\mu\text{m}$  patterned film ( $52 \pm 7\%$  cell alignment) and 50  $\mu\text{m}$  patterned film ( $37 \pm 5\%$  cell alignment) and these percentages were each statistically different from the alignment of non-patterned film with probabilities of  $p < 0.001$  and  $p < 0.005$  respectively.

Confocal microscopy confirmed the cardiomyocytes were elongated with cross-striated sarcomeric structures stained using  $\alpha$ -actinin (red) (Fig. 5-3a-5-3h). Only actinin in cells with contractile phenotypes can be stained as sarcomeric  $\alpha$ -actinin [63], and the cross-striated structures were found in cardiomyocytes cultured both on patterned and unpatterned films. However, on the unpatterned films, there was no preferential cross-striation orientation due to cells spreading in different orientations. The sarcomere

## 5. Micropatterned tissue-like bioelastomers improve cardiomyocyte alignment and beating homogeneity

direction was preferentially aligned on patterned samples perpendicular to the channel direction (Fig. 5-3e-5-3h). In all cases, connexin 43, a gap junction protein that enables rapid electrical conduction, was used to assess the cell-cell conduction (Fig.5-3e-5-3h). A high abundance of gap junctions were not only found on the ends of cardiomyocytes, but also on sides of the cells which, presumably, allows the spread of electrical potential in cardiomyocytes seeded on both channels and crests.



5. Micropatterned tissue-like bioelastomers improve cardiomyocyte alignment and beating homogeneity

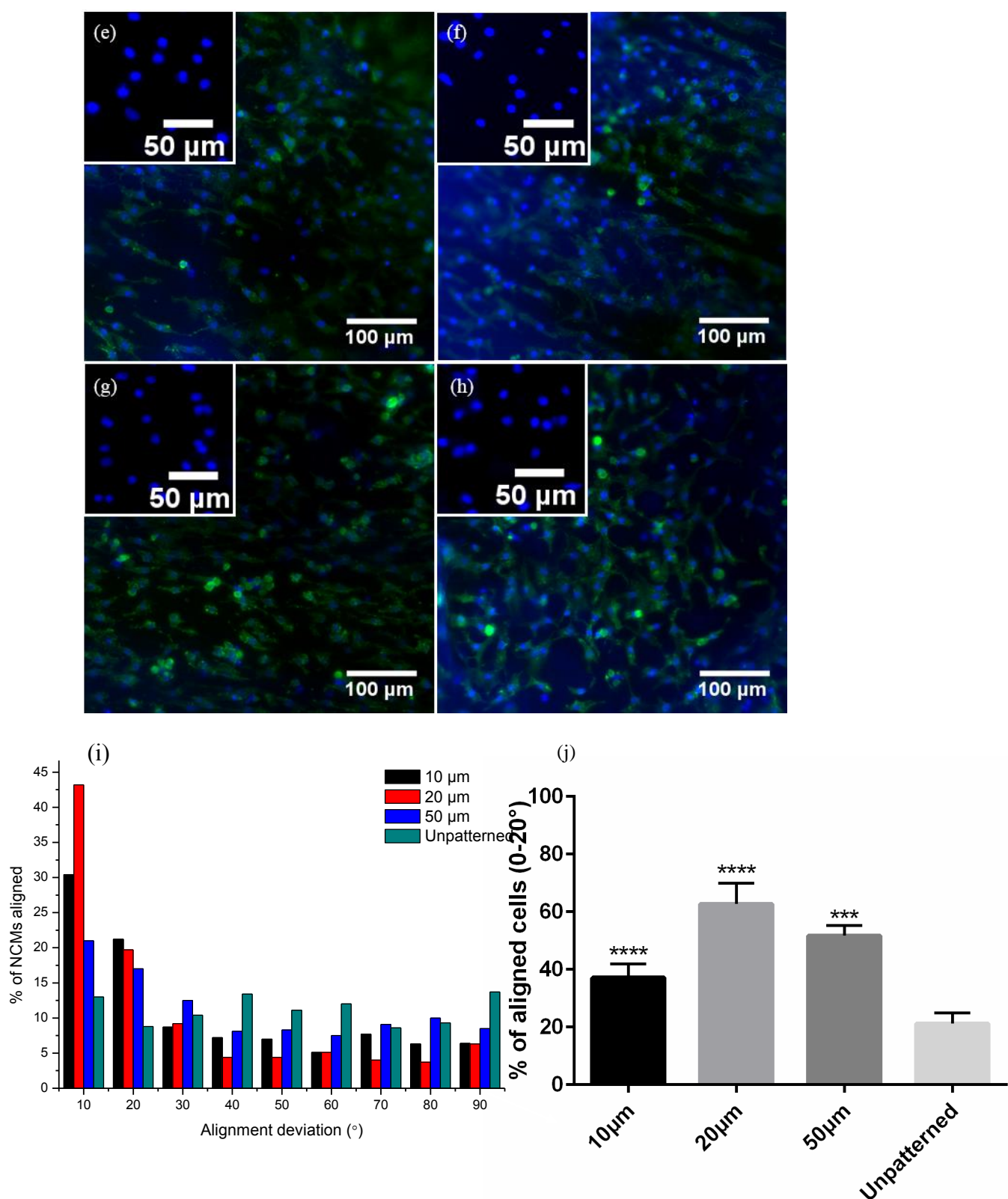
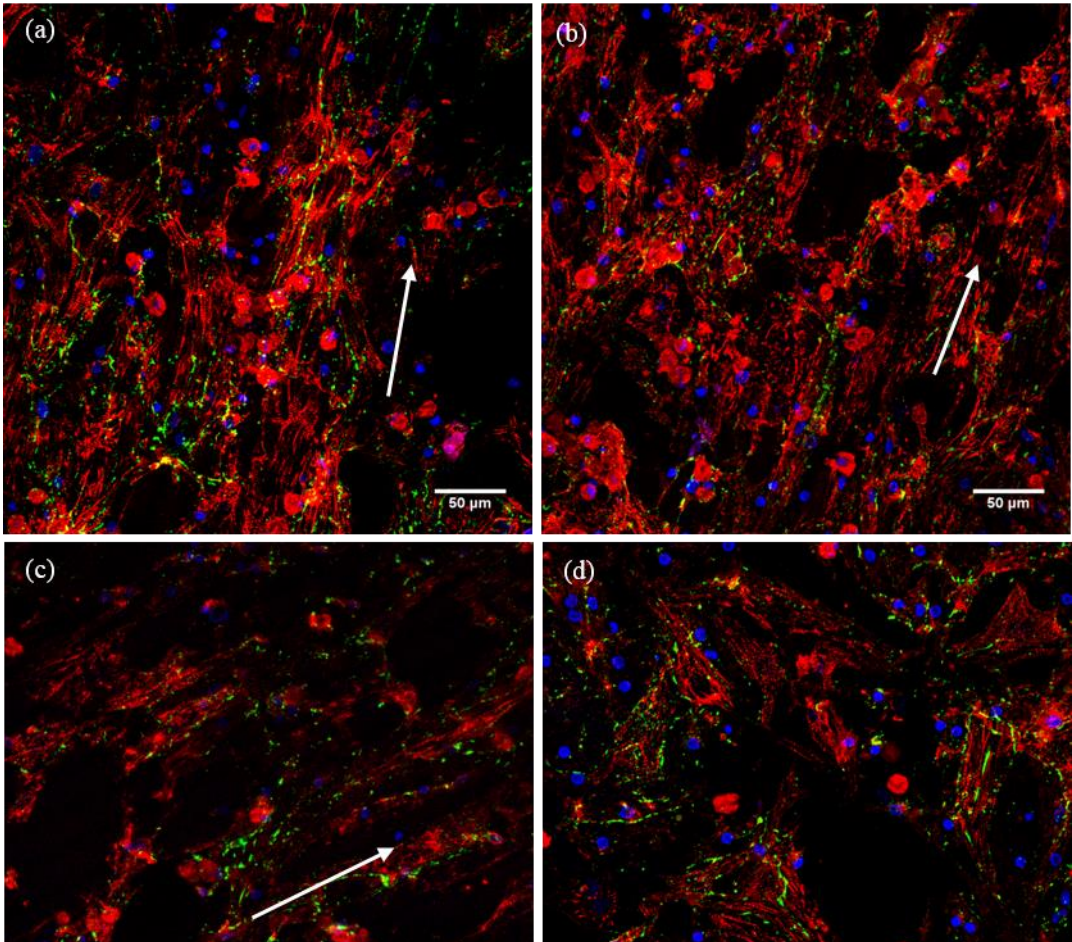


Figure 5-2 Phase contrast images of cardiomyocytes cultured on PGS films with different patterns showing alignment with channels of nominal width (a) 10  $\mu\text{m}$ , (b) 20  $\mu\text{m}$ , (c) 50  $\mu\text{m}$  patterns and (d) for unpatterned PGS. The alignment of cardiomyocytes was confirmed by fluorescent images stained with troponin I antibody which is a specific marker of myofilaments of cardiomyocytes (green) (e) 10  $\mu\text{m}$ , (f) 20  $\mu\text{m}$ , (g) 50  $\mu\text{m}$  patterns and (h) unpatterned PGS. The inserted images in (e) - (h) show elongation of nuclei towards the channel directions in micropatterned PGS. (i) The degree of angles between the orientation of the nuclei and channel direction summarized in 10 $^{\circ}$ , and (j) quantification of the proportion of aligned nuclei (degree of angles below 20 $^{\circ}$ ) on different pattern features.



5. Micropatterned tissue-like bioelastomers improve cardiomyocyte alignment and beating homogeneity



## 5. Micropatterned tissue-like bioelastomers improve cardiomyocyte alignment and beating homogeneity

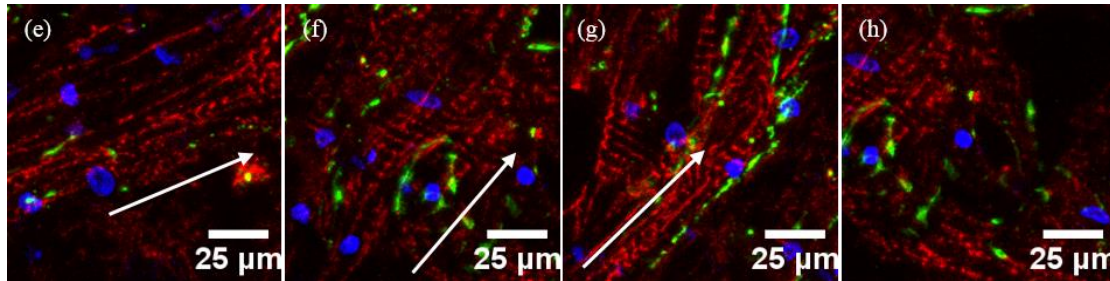


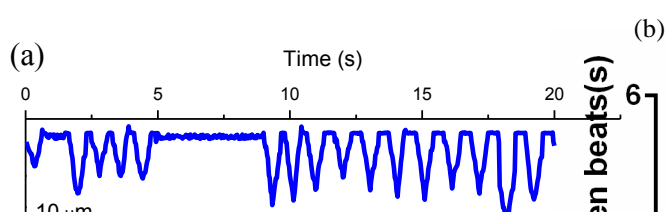
**Figure 5-3** Fluorescent images comparing the effects of different PGS micropatterns on cardiomyocytes alignment. (a-h) show confocal images of cardiomyocytes (day 7) fixed and stained with DAPI (blue), connexin (green) and sarcomeric  $\alpha$ -actinin (red) that stains for the striated Z-lines of myotubes in cardiac muscle. The arrows indicate the alignment direction of the cardiomyocytes. (a-d) were taken at 10x magnification while (e-i) were taken at 40x magnification following the order of 10  $\mu$ m, 20  $\mu$ m, 50  $\mu$ m and unpatterned PGS.

### 5.3.3 Beating and intracellular calcium transient characterization

Spontaneous beating was observed on micropatterned samples seeded with cardiomyocytes as early as 2 days after seeding while weak, heterogenous beating behavior was only observed by day 4 on the unpatterned PGS. Under all conditions the contractile activity of the cells together with PGS substrates was maintained for at least 7 days. Examples of beating behavior at each patterned sample are shown in (Fig. 5-4a). On unpatterned samples, the weak beating might be attributed to the random orientation of the cells (Fig. 5-2d and Fig. 5-2h). Consistent with the nuclei alignment data, significant increases in beating regularity and intensity (Fig. 5-2b) were found on patterned samples compared to unpatterned controls (Fig. 5-2i). Beating homogeneity was characterized by comparing the variance of average beat time between patterned and unpatterned samples. Significant differences were found between 10  $\mu$ m and 20  $\mu$ m patterned samples and the unpatterned sample based on an F test. The weak and imhomogeneous beating behavior of

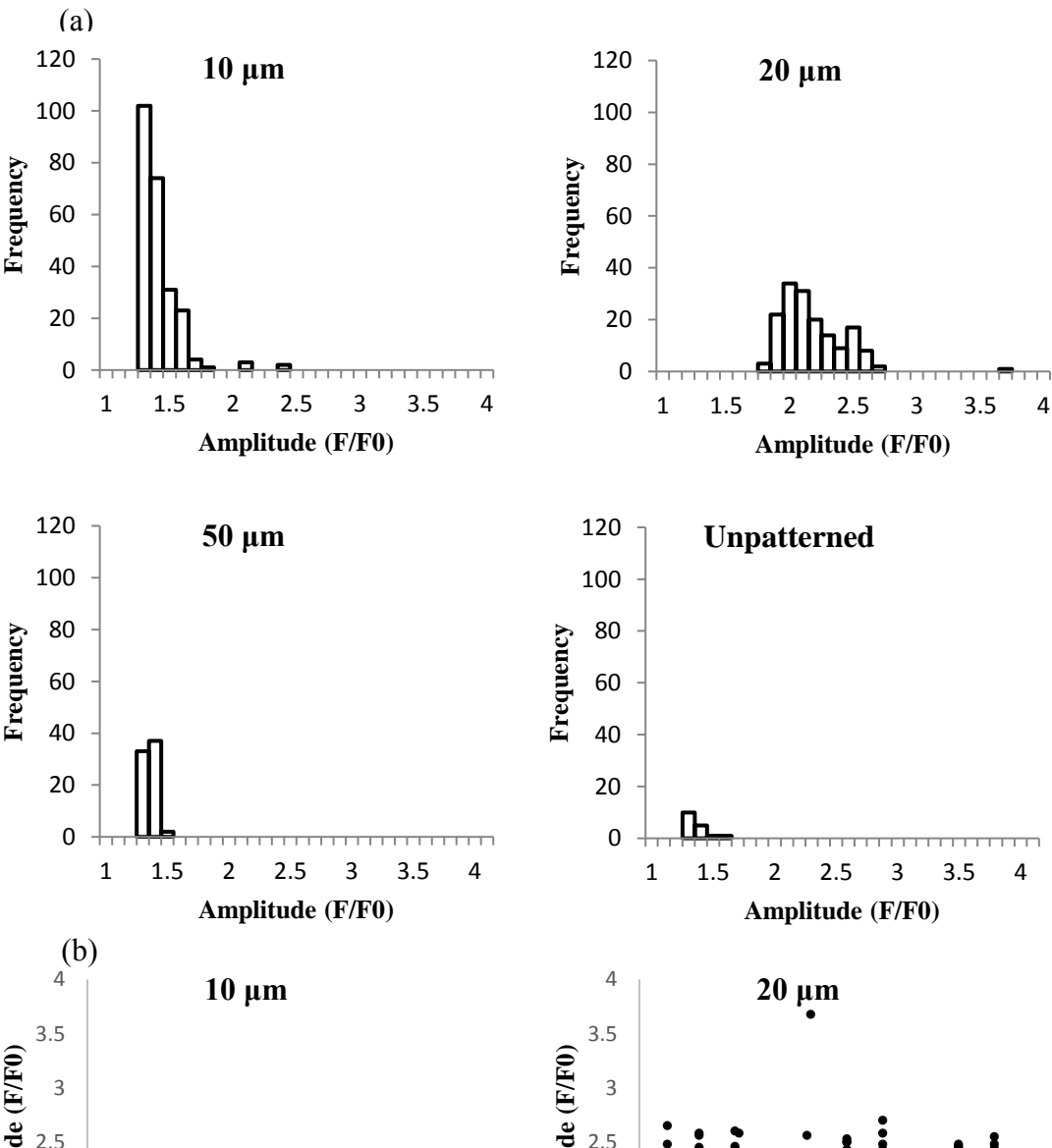
## 5. Micropatterned tissue-like bioelastomers improve cardiomyocyte alignment and beating homogeneity

cardiomyocytes cultured on unpatterned films could not be attributed to the cell density differences between cardiomyocytes (Fig. 5-3a-5-3d) as in a previous study [63]. There is no significant difference in cell density between patterned and unpatterned samples (data not shown here). A recent study showed that cardiomyocytes could adjust their alignment and beating behavior in response to mechanical deformations caused by their neighbours, even though the cells are not necessarily connected to each other [147]. So the random distribution of cardiomyocytes cultured on unpatterned film might lead to a reduced resultant force and deformation in the PGS substrate, making it difficult for these cultures to show spontaneous beating. Cardiomyocyte beating behavior was also characterized by the oscillation of the intracellular  $\text{Ca}^{2+}$  concentration. Cardiomyocytes cultured on unpatterned PGS showed isolated  $\text{Ca}^{2+}$  transients occurring at different frequencies while shorter and more coordinated  $\text{Ca}^{2+}$  transients were found in cardiomyocytes cultured on micropatterned substrates. As  $\text{Ca}^{2+}$  elevation can trigger excitation-contraction coupling which is critical for optimal contractility, the  $\text{Ca}^{2+}$  transient over time reflects the condition of cardiomyocytes. The histograms showed the  $\text{Ca}^{2+}$  transients' intensity distribution of cardiomyocytes cultured on different films (Fig. 5-5a). Stronger intensities were found on the 20  $\mu\text{m}$  patterned film, but the difference was not significant. More regions of interest with significant intensity change were found on the patterned films compared with unpatterned samples, as shown in the frequency increase in the histograms (Fig. 5-5a). Synchronized beating behavior was almost exclusively found on micropatterned samples. Compared with unpatterned samples that showed beating randomly distributed over a period of time, most beats in the micropatterned samples were co-ordinated at certain time points (Fig. 5-5b). This effect was particularly strong on 20  $\mu\text{m}$  patterns, while on 10  $\mu\text{m}$  and 50  $\mu\text{m}$  micropatterned samples, some beats were not co-ordinated i.e. they were found in between the major time points. A previous study has showed that the decreased electrical homogeneity is associated with the less aligned cardiomyocytes [241], which is consistent with the situation for cardiomyocytes cultured on these PGS films. The number of cardiomyocytes involved in the  $\text{Ca}^{2+}$  transients were also significantly increased in micropatterned films (Fig. 5-5c). Better alignment and cell-cell contact with patterned films allow easier  $\text{Ca}^{2+}$  diffusion between cardiomyocytes, resulting in more co-ordinated cardiomyocyte beating behavior.



5. Micropatterned tissue-like bioelastomers improve cardiomyocyte alignment and beating homogeneity

Figure 5-4 (a) Representative traces showing beating characteristics of cardiomyocytes at day 4 on 10  $\mu\text{m}$ , 20  $\mu\text{m}$ , 50  $\mu\text{m}$  and unpatterned substrates by monitoring pixel intensity in regions of interest over a period of 20s. (b) Comparison of the average time between beats and beat homogeneity (indicated by standard deviation) between different patterned PGS and unpatterned PGS.



5. Micropatterned tissue-like bioelastomers improve cardiomyocyte alignment and beating homogeneity

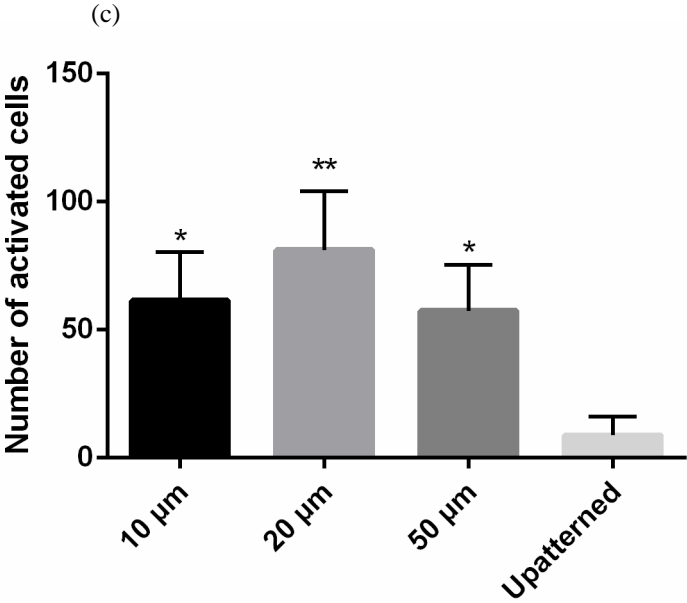


Figure 5-5 Amplitude histograms of  $\text{Ca}^{2+}$  transients measured using Fluo-4 (a) and peak amplitude scattergrams (b) from over 100 cells for PGS films with of 10  $\mu\text{m}$ , 20  $\mu\text{m}$ , 50  $\mu\text{m}$  micropattern size and unpatterned films. (c) The number of activated cells involved in a  $\text{Ca}^{2+}$  transient.

5.4 Conclusion

## 5. Micropatterned tissue-like bioelastomers improve cardiomyocyte alignment and beating homogeneity

Highly elastic PGS substrates were fabricated with different-sized micropatterned channels. Characterization of cardiomyocyte beating behavior showed that promoting cardiomyocyte beating homogeneity requires an extracellular matrix mimicking structure that enables cell attachment and alignment. Compared with unpatterned substrates, cardiomyocytes cultured on the patterned substrates showed increased nuclear alignment and sarcomere alignment and beating regularity, especially for samples patterned with 20  $\mu\text{m}$  channels. An improvement in  $\text{Ca}^{2+}$  transient regularity and increased amplitude were also found in accordance with improvement in cardiomyocyte alignment, indicating that topological modification of substrates can result in rhythmic beating behavior in cardiomyocytes via  $\text{Ca}^{2+}$ -dependent pathways. Further studies may focus on the mechanism of molecular signalling and protein expression change as a result of micropatterning. To sum up, this study established a method of *in vitro* cardiomyocyte culture that is capable of generating “tissue-like” myocytes sheets with potential application *in vivo*. The micropatterned PGS substrates are expected to find applications as tissue engineering substrate materials and in regenerative medicine studies.

# 6 Incorporation of BDNF mimetic in PGS and effect on cardiomyocytes cell culturing

## Declaration for Thesis Chapter [6]

### Declaration by candidate

In the case of Chapter [6], the nature and extent of my contribution to the work was the following:



Nature of contribution	Extent of contribution (%)
Major research and writing	85

The following co-authors contributed to the work.

Name	Nature of contribution	Extent of contribution (%) for student co-authors only
Vinh Truong	BDNF mimetic synthesis	N/A
Yue Shi	HPLC tests	5
Boonlom Thavornnyutikarn	Cryogenic grinding	3
John Forsythe	Provided corrections and assisted in research planning	N/A
Wayne Cook	Provided corrections and assisted in research planning	N/A
Binghui Wang	Provided corrections	

6. Incorporation of BDNF mimetic in PGS and effect on cardiomyocytes cell culturing

The undersigned hereby certify that the above declaration correctly reflects the nature and extent of the candidate's and co-authors' contributions to this work\*.

<b>Candidate's Signature</b>		<b>Date</b> <b>26<sup>th</sup>/08/2016</b>
<b>Main Supervisor's Signature</b>		<b>Date</b> <b>26<sup>th</sup>/08/2016</b>



## 6.1 Introduction

Neurotrophins are a family of proteins that are essential for the development of the vertebrate nervous system [242]. Brain-derived neurotrophic factor (BDNF) is a member of the neurotrophin family which was first discovered in the early 1950s [243]. Like other neurotrophins, BDNF is crucial for supporting the survival of neurons [244]. Except p75<sup>NTR</sup> which all neurotrophins bind to, BDNF also specifically binds to one of the tropomyosinrelated kinase (Trk) receptors, namely, TrkB. The TrkB activation downstream pathways have been intensively studied and are well established for neural cells (Fig. 6-1a). Although TrkB.FL (Full Length) is the predominant TrkB isoform expressed during embryogenesis, truncated TrkB is also expressed in the human brain [245]. Truncated TrkB receptor, which is lacking the kinase domain existing in mammalian brains, is also a receptor of BDNF with high affinity [246]. BDNF-mediated activation of the truncated TrkB controls the release of Ca<sup>2+</sup> from intracellular stores through a G protein and inositol tris-phosphate (IP3)-dependent pathway [247] (Fig. 6-1b).

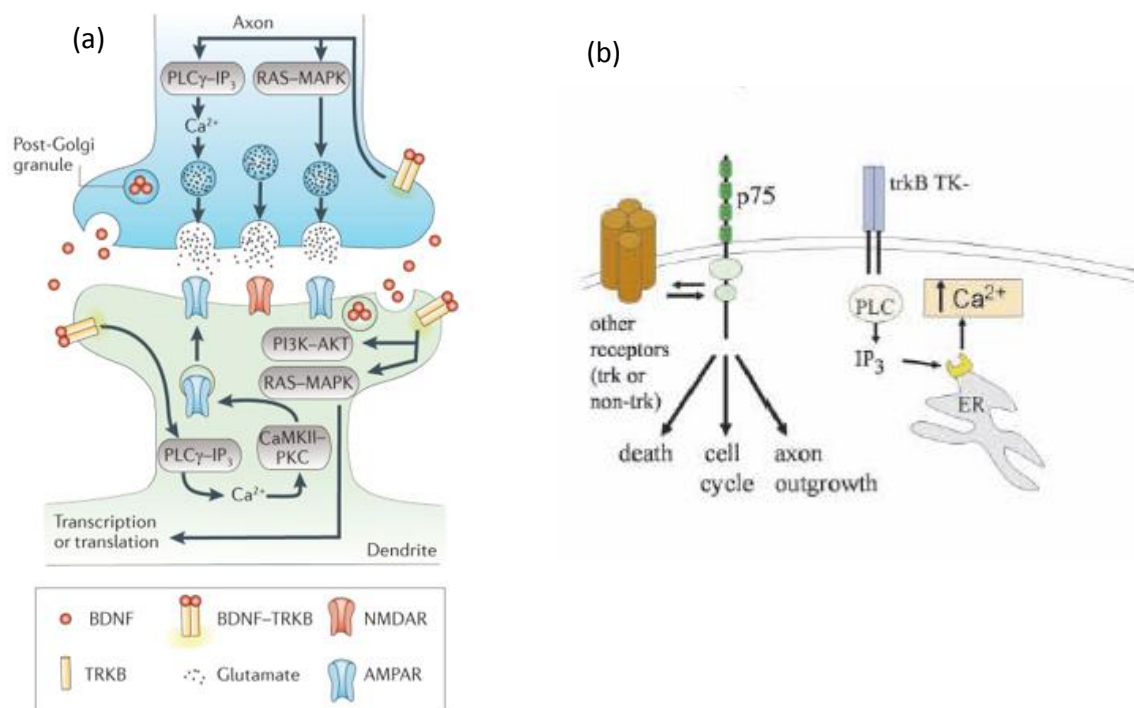


**Figure 6-1 (a) BDNF effects on synaptogenesis through TrkB receptor and downstream pathways. (b) Activation of truncated TrkB has the potential to modulate glial Ca<sup>2+</sup> signaling. A) Reproduced with permission from Nature Publishing Group (2013) B) Reproduced with permission from Taylor and Francis Group (2004)**

## 6. Incorporation of BDNF mimetic in PGS and effect on cardiomyocytes cell culturing

Despite intensive studies of BDNF functions in neurons, little is known about the role of BDNF in other organs and cells. A relatively high level of BDNF as well as their receptors are expressed in peripheral tissues, and can thus potentially contribute to both normal physiology and pathophysiology of several diseases. For example, BDNF expression and signalling mechanisms play an important role in early airway and lung development. BDNF production by resident airway cells such as epithelium and airway smooth muscle contributes to normal airway structure and function [248].

In the cardiovascular system, the role of BDNF is controversial. A study showed that a reduction in BDNF levels attenuated inflammation and angiogenesis and improved survival and cardiac function following myocardial infarction in mice [249]. Adverse roles of BDNF were also reported for the inflammation and injury in the aging heart [250]. However, more positive effects have been observed [251-254] and several hypotheses have been raised to explain the benefits of BDNF in the cardiovascular system. The protective effects could be provided by the central nervous system [251], activation of BDNF/VEGF/PI3K signaling pathways [252], or by enhancing cell viability of cardiomyocytes in hypoxic environments [253]. Recent studies showed that BDNF is an important protein for cardiomyocytes normal contraction and relaxation not only in conditions such as hypoxia and ischemia, but during normal physiological function [255, 256]. These two studies suggest that cardiomyocytes respond to BDNF, with  $\text{Ca}^{2+}$  as the possible downstream effector. It is not surprising that the role of BDNF in neurons is also activation and mobilization of the  $\text{Ca}^{2+}$  store [257]. The PLC $\gamma$ –IP3 pathway which activates  $\text{Ca}^{2+}$  mobilization in neurons also plays the same role in cardiomyocytes [258].

On the other hand, to provide a potential therapy for BDNF deficiency related disease, like Alzheimers disease, many BDNF mimetics (TrkB agonists) have been developed [259-261]. It has been demonstrated that those BDNF mimetics bind with specificity to the extracellular domain of TrkB. In an *in vitro* model

## 6. Incorporation of BDNF mimetic in PGS and effect on cardiomyocytes cell culturing

of neurodegenerative disease, they prevented neuronal degeneration with efficacy equal to that of native BDNF protein [259]. Among them, a BDNF mimetic referred to LM224-A (Fig. 6-2c) showed the best binding ability. *In vivo* studies have also shown LM224-A to provide protective effects on injured spinal cord nerves [262], slow down the progression of common neurodegenerative diseases [263] and promote recovery after hypoxic-ischemic stroke [264]. The studies are not limited to neuronal cells. The compound regulates cementoblast differentiation via TrkB-ERK/Akt signalling cascade [265]. But similar studies have not been carried out with cardiac cells or diseases related to TrkB deficiency.

In this chapter poly(glycerol sebacate) (PGS) was used as a substrate to study cardiomyocytes  $\text{Ca}^{2+}$  transients in the presence or absence of BDNF mimetic (the BDNF mimetic incorporated PGS is abbreviated to PGSB). To maintain the BDNF mimetic at a potentially therapeutic level for a long period, the BDNF mimetic was polymerised into the PGS chain. As PGS undergoes surface degradation via hydrolysis, it is postulated that the BDNF mimetic could be slowly released.

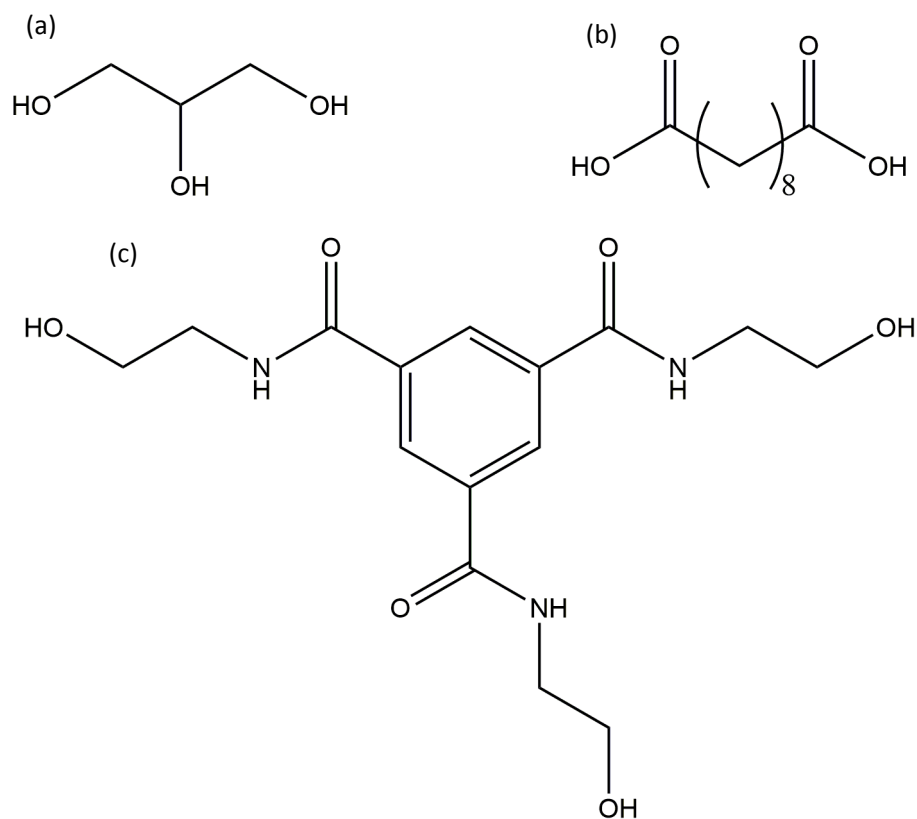


**Figure 6-2 Chemical structures of (a) glycerol (b) sebacate and (c) BDNF mimetic (LM224-A)**

## **6.2 Material and methods**

### **6.2.1 Synthesis of PGS and BDNF incorporated PGS (PGSB)**

The PGS was synthesized in the same way as described in Chapter 3. The BDNF mimetic monomer was thoroughly mixed with glycerol and sebacate at different molar ratios (1:99:100, 2:98:100 and 10:90:100, respectively). The molar concentration of BDNF mimetic and glycerol used was equated to the molar amount of sebacate. The monomers underwent polycondensation at 130 °C under 130 cm<sup>3</sup>.min<sup>-1</sup> flow of nitrogen for 24 hr with a cryogenic trap to condense any BDNF mimetic. The prepolymer was then cast on sucrose coated PDMS moulds at 150 °C on a hot plate to form a film. The cast PGSB sheets were cured at 160 °C under vacuum using a cryopump for 8 h. The solvent in the trap was transferred in fume hood and evaporated overnight.

### **6.2.2 Mechanical characterization of PGSB**

Mechanical specimens with a thickness of approximately 300 µm were cut from a cured, unpatterned PGSB sheet using a dumbbell shaped mould with a gauge length of 12.5 mm and a width of 3.25 mm. The thickness of each specimen was measured using an electronic vernier caliper. Tensile and cyclic tests were performed at room temperature using an Instron 5860 mechanical tester equipped with a 100 N load cell. Extension rates of 10 mm.min<sup>-1</sup> and 25 mm.min<sup>-1</sup> were applied for the tensile and cyclic tests respectively, to be consistent with earlier studies [48, 187, 231]. Specimens for the tensile tests were stretched to failure.

### **6.2.3 Thermal characterization**

The thermal behaviour of pure PGS, BDNF mimetic and PGSB was characterized using a Perkin Elmer Pyris1 Differential Scanning Calorimeter (DSC) under a nitrogen atmosphere. The nitrogen flow rate was 20 ml/min. All the specimens were crimp-sealed in aluminium pans and had a typical weight of about 6 mg. All specimens were heated from ambient temperature to 180 °C at a heating rate of 40 °C/min, and then held for 2 min to erase previous thermal history. Then the specimens were cooled to -50 °C at a cooling rate of 40 °C/min. After reaching thermal equilibrium, the specimens were further heated from -50 to 180 °C at a heating rate of 20 °C/min to study the thermal behavior.

### **6.2.4 Degradation characterization of PGSB**

The degradation was carried out in Milli-Q (MQ) water based and DME based solution. For MQ water based degradation, about 1g of the PGS or 5% PGSB thin films with a surface area of 2 cm<sup>2</sup> were soaked in 20 ml of MQ water or 1 mol/L hydrochloric acid for 1 week. For DMEM based degradation, PGSB thin films were cut into a round shape with a surface area of 70 mm<sup>2</sup> (around 50 mg) and soaked in 500 µl DMEM in 48 well culture plates with or without porcine liver esterase 2 µl (1366 units/ ml) (Sigma) based on previous studies [266] and each group was comprised of 3 samples. 1 unit of esterase is defined by the supplier, as the amount of esterase needed to hydrolyze 1 µM ethyl butyrate per min at pH 8.0 and 25 °C. The culture plate was placed in an environmental shaker (37 °C) with a rotating rate of 70 rpm. 100 µl media was extracted from the wells every three days. The same amount of fresh media was added in the extracted wells. 6 units of porcine liver esterase was added in the extracted wells with enzyme treatment. The extracted media were carefully sealed and stored at 4 °C.

### **6.2.5 UV-vis spectroscopy characterization**

UV-vis absorption spectra were recorded on a UV-4100 (Shimadzu) spectrophotometer between 180 nm and 500 nm with a scanning speed of 100 nm/min. The MQ water based degradation samples were heated on a hot plate at 60 °C overnight and redissolved in 1L MQ water for the tests. About 1 ml solution for each sample was added into a quartz cell. MQ water was used as the background.

### **6.2.6 Nuclear Magnetic Resonance (NMR) characterization**

Spectra were recorded for the BDNF mimetic and the degradation products of PGSB soaked in 1 mol/L hydrochloric acid solution. The PGS degradation products were heated at 60°C overnight to evaporate the water and hydrochloric acid in fume hood. The remaining compounds were dissolved in deuterated tetrahydrofuran. Chemical shifts ( $\delta$ ) reported as parts per million (ppm) from an external tetramethylsilane using a Bruker Avance III 400 NMR spectrometer. Samples of either PGS or PGSB before and after soaking in MQ water overnight were dried in a vacuum oven and then cryogenically ground into a fine powder.

### **6.2.7 HPLC characterization**

High performance liquid chromatography (HPLC) analysis was performed on a Hewlett-Packard 1100 series HPLC system (Agilent Technologies, CA) with a reverse-phase Vydac<sup>TM</sup> analytical (C18, 300 Å, 5  $\mu$ m, 4.6 mm x 150 mm) column. The eluent gradient was 0% to 25% solvent B (solvent A: 0.1% trifluoroacetic acid (TFA)/H<sub>2</sub>O; solvent B: 0.1% TFA/CH<sub>3</sub>CN) for the first 25 min. The flow rate was 1 mL min<sup>-1</sup>. A UV detector was used and the wavelength was set to 214 nm to detect the amide of BDNF mimetic. The DMEM based degradation products were characterized by HPLC. Visual examination was

## 6. Incorporation of BDNF mimetic in PGS and effect on cardiomyocytes cell culturing

carried for the PGSB degradation DMEM media at different time points with or without porcine liver esterase.

### 6.2.8 BDNF treatment and calcium transient imaging

Cardiomyocytes were cultured and maintained in the same way as described in Chapter 5 (page 98). Cardiomyocytes were cultured on unpatterned and 20  $\mu\text{m}$  micropatterned thin PGS or PGSB films. The cardiomyocytes cultured on both patterned and unpatterned PGS films were treated with 60 nM BDNF mimetic or 20 nM BDNF full protein. 4 days after isolation and seeding, the cardiomyocytes were treated after a media change, and examined 48 hr after BDNF treatment. No additional treatment was applied for the cardiomyocytes cultured on PGSB films. Calcium ion transients were recorded using fluorescence microscopy (Nikon Eclipse TS 100) (excitation at 485 nm, emission at 520 nm). Fluo-4 AM (Thermofisher Scientific™) was dissolved in dimethyl sulfoxide at 10 mM and diluted to a final concentration of 2  $\mu\text{M}$  in DMEM as an indicator of  $\text{Ca}^{2+}$  change. Three repeated experiments for each kind of treatment or sample were performed and compared with the cardiomyocytes cultured on PGS films without any treatment. Cardiomyocytes were incubated in DMEM with Fluo-4 for 30 min at 37 °C/5%  $\text{CO}_2$  in incubator. Whole-frame images obtained at 1360 × 1024 pixels were continuously recorded to produce image sequences. The image sequences were corrected for darkening over time (caused by condensation of water vapour on the lens) using ImageJ's bleach correction tool, and were then analyzed using the ImageJ software plugin LC Pro and previously reported R code [234]. The region of interest (ROI) was defined as a circle with a diameter of 40 pixels with an area similar to a cardiomyocyte size.

### 6.2.9 Viability assay

Cardiomyocytes were seeded into 96-well plates at  $1.5 \times 10^4$  cells/well and  $5 \times 10^4$  cells/well overnight, and serum starved for 48h. Cells were treated with BDNF mimetic (10–1000 nM). After 48hr incubation,

## 6. Incorporation of BDNF mimetic in PGS and effect on cardiomyocytes cell culturing

3-(4,5-dimethyl-2thiazoyl)-2,5-diphenyl-2H-tetrazolium bromide (MTT) assay was performed to examine the effect of BDNF mimetic on cell proliferation and cell viability. 10 µl of MTT stock solution (5mg/ml) was added to each well and incubated in the dark in a 37 °C incubator, 5% CO<sub>2</sub> for 4 hr. The media was removed from the wells, and 100 µl isopropanol added to each well. Plates were returned to the incubator for 20 mins or until blue formazan crystals dissolved into the isopropanol. The absorbance were measured with SpectroNano at 595nm using 655 nm as reference for background correction.

### 6.2.10 Cardiacmyocyte hypertrophy assay

Purified neonatal cardiac myocytes were seeded at  $3 \times 10^5$  cells/well in gelatin-coated 12-well plates, and maintained in serum-free DMEM media (Invitrogen, NY, USA) supplemented with 2 µg/ml insulin and 10 µg/ml transferrin. Cardiomyocytes hypertrophy was determined by <sup>3</sup>H- leucine incorporation. Cardiomyocytes were serum starved for 48 h before pretreatment (2 h) with BDNF mimetic (0.1–3 µM), cells were stimulated with 100 nM angiotensin II (AngII) for 60 h, in the presence of 1 µCi <sup>3</sup>H-leucine. After stimulation, cells were harvested by precipitation with 10% trichloroacetic acid (500 µl) for 30 min on ice and solubilized with 1 M NaOH (200 µl) overnight at 4 °C. The samples were then neutralized with 1 M HCl (200 µl), and <sup>3</sup>H levels were counted in scintillation fluid on a beta counter to determine levels of <sup>3</sup>H-leucine incorporation. All sample conditions were run in triplicate and compared with unstimulated and stimulated controls. A minimum of 3 repeated experiments were performed for each assay.



### 6.2.11 Statistical analysis

The data were analyzed using one-way analysis of variance followed by Tukey's post-hoc test. Results are presented as the mean  $\pm$  standard deviation (SD) and a p value of 0.05 was considered as significant. Significant changes in parameter variance were determined using a Brown-Forsythe test.

## 6.3 Results and Discussion

### 6.3.1 Mechanical properties of PGSB

For the synthesis of PGSB, the molar concentration of BDNF mimetic and glycerol used was equal to the molar amount of sebacate. BDNF mimetic and glycerol both possess three hydroxyl groups (Fig. 6-2a, 6-2b), so the substitution of BDNF mimetic with glycerol does not change the ratio between the hydroxyl and carboxyl groups. This does however assume that the hydroxyl groups of the glycerol and BDNF mimetic have equal reactivity. The flexibility and softness of PGS were maintained in PGSB, and the PGSB had maintained elastomeric stress-strain behaviour [16] (Fig. 6-3a). As reported previously, the relationship between network density and Young's modulus of an elastomer follows the following equation, [173]

$$n = E_0 / 3RT$$

where  $n$  is the strand density,  $E_0$  is the modulus,  $R$  is the universal gas constant and  $T$  is the temperature. No significant statistical difference in Young's modulus was found in the PGSB compared with PGS with a substitution of BDNF mimetic to glycerol of up to 5% (Fig. 6-3b), suggesting that the crosslinking density was not significantly different and that the hydroxyl groups of the BDNF mimetic had similar reactivity as glycerol. The Young's moduli of all PGSB samples were around 500 kPa, which covers the whole range of the human dilated heart [235].

## 6. Incorporation of BDNF mimetic in PGS and effect on cardiomyocytes cell culturing

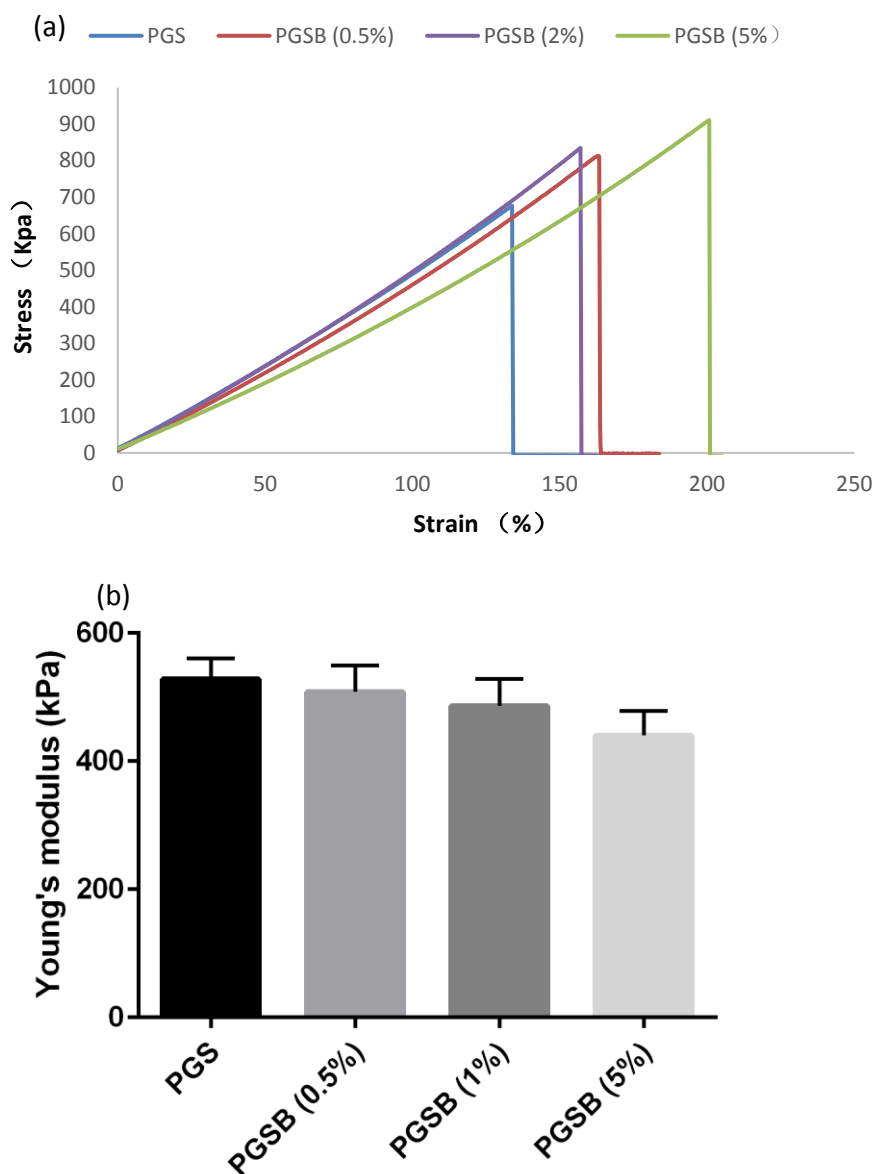


**Figure 6-3 (a) Stress-strain curves of PGS and PGSB. (b) The Young's modulus of PGS and PGSB. No significant difference in moduli was observed with incorporation of the BDNF mimetic (the percentage indicates the molar ratio of BDNF mimetic in the copolymer)**

### 6.3.2 Thermal properties of PGSB

The low glass transition temperature ( $T_g$ ) is the key factor which ensures the elasticity of PGS at room temperature. Previous studies have reported that PGS (glycerol:sebacic acid molar ratio of 1:1) is semi-crystalline with a glass transition temperature ( $T_g$ ) near  $-25\text{ }^{\circ}\text{C}$  and a melting point between  $0$  and  $10\text{ }^{\circ}\text{C}$ . The tiny change in PGSB compared to PGS was confirmed by DSC. The similar  $T_g$  was found in PGSB but

## 6. Incorporation of BDNF mimetic in PGS and effect on cardiomyocytes cell culturing

the melting behavior shows two peaks at a slightly lower temperature than reported previously (Fig. 6-4). The BDNF mimetic has a melting endotherm as indicated by a DSC peak around 135 °C (dashed line in Fig. 6-4). For the 5% BDNF mimetic incorporated PGSB, a glass transition is near -25 °C is observed however, no melting endotherm corresponding to BDNF was found. This suggests that either the BDNF mimetic is dissolved in the PGS network or it is covalently bonded in the elastomer network as suggested above. There is a small drop in the melting temperature of PGSB compared with PGS (solid line in the Fig. 6-4) which could be attributed to the BDNF mimetic incorporation, which decreased the regularity of the crystal structure.

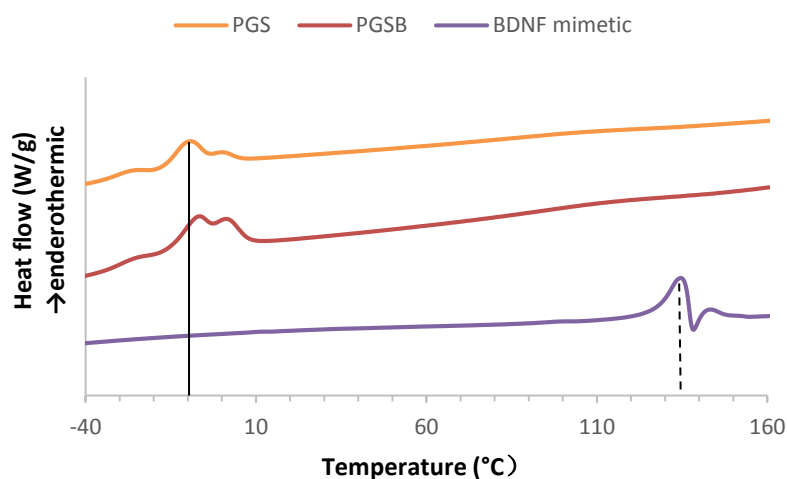


**Figure 6-4 DSC results of BDNF mimetic, PGS and PGSB.**

### 6.3.3 Degradation of PGSB and UV-Vis spectroscopy

Indirect evidence of incorporation of BDNF mimetic in PGS was demonstrated by the release studies. However more direct evidence of the BDNF mimetic in the PGS structure needs to be provided by analysing the PGS degradation products. The PGS/PGSB soaked in MQ water kept its integrity after one week while the PGSB soaked in 1 mol/L hydrochloric acid degraded without

## 6. Incorporation of BDNF mimetic in PGS and effect on cardiomyocytes cell culturing

any macroscopic residue. The amount of PGS/PGSB degradation products in MQ water was too small to be analysed by UV- Vis spectroscopy. This indicated that the BDNF mimetic was chemically incorporated into the network.

However, the UV- Vis spectra showed that  $24.3 \pm 1.7\%$  BDNF mimetic was released in the HCl degraded PGSB polymer (Fig. 6-5a,6-5b). The UV-vis spectrum of the PGSB degradation product showed the peak at 210 nm due to the BDNF mimetic overlapped with another lower wavelength peak which might due to the oligomers containing BDNF mimetic in the water. The percentage of BDNF recovered from the HCl-degraded PGSB polymer is low compared with the BDNF mimetic added to the polymerization mixture. The reduction in the amount of BDNF mimetic may be accounted for by evaporation from the high temperatures during the PGSB synthesis (which was undertaken at low pressure and high temperature). For the PGSB soaked in MQ water (Fig. 6-5c), only a small peak at 202 nm was observed in the UV-vis spectrum indicating that the amount of BDNF mimetic extracted by the water from the PGSB gel was not significant, suggesting that the BDNF mimetic was covalently bonded in the network structure of the polymer.

While BDNF mimetic was detected as the final degradation products in the UV-vis spectra, the degradation in MQ water and in 1 mol/L HCL solvent does not match the real environment and the real-time release of the BDNF mimetic. To simulate an *in vivo* environment, esterase from porcine liver was used as previously reported [267]. The enzymatic effect of esterase on the degradation of polyester polymers has been thoroughly examined *in vitro* [268, 269]. The PGSB samples degraded much faster in the presence of the enzyme. The colour remained bright pink in DMEM only solutions after 30 days. While the colour changed from bright pink to yellow indicating the pH drop due to the pH indicator phenol red in the DMEM (Fig. 6-6). The yellow colour indicated the additional proton from the ketone group is lost in acid environment while the pink/red colour indicated phenol's hydroxide group loses its

## 6. Incorporation of BDNF mimetic in PGS and effect on cardiomyocytes cell culturing

proton [270]. The color of DMEM with enzyme was bright pink at the beginning, but became orange 15 days later. At day 21, the color was yellow indicating an acidic environment. The acidity could be introduced by the degradation product of sebacate [271].

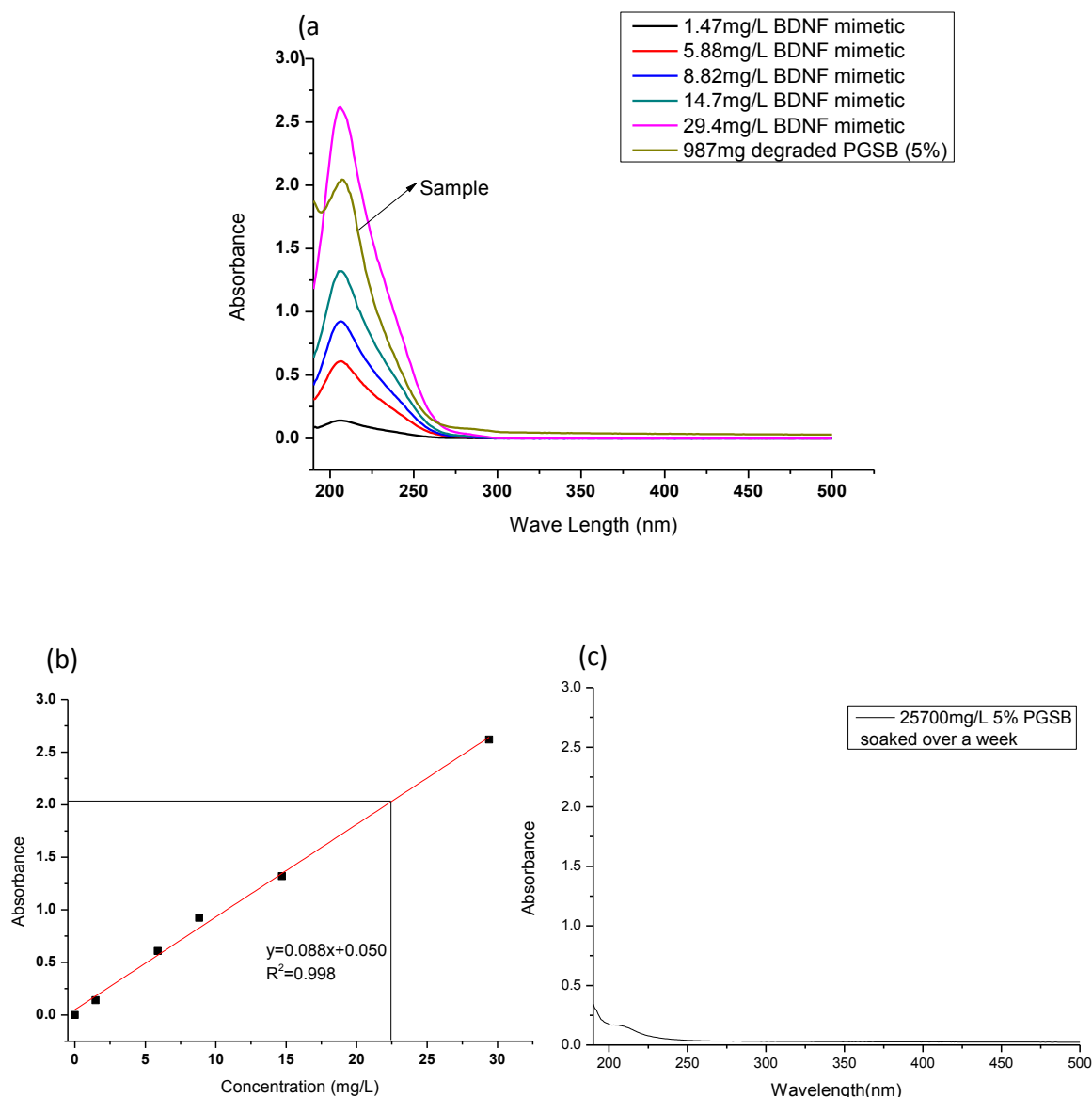


**Figure 6-5 UV-vis spectra of the BDNF mimetic and PGSB degradation products shown in (a). The typical BDNF mimetic absorption peak was at 202 nm. The concentration of the BDNF mimetic released was calculated based on the calibration curve (b). The peak of BDNF mimetic was not obvious for PGSB soaked for a week in MQ water (c).**

## 6. Incorporation of BDNF mimetic in PGS and effect on cardiomyocytes cell culturing

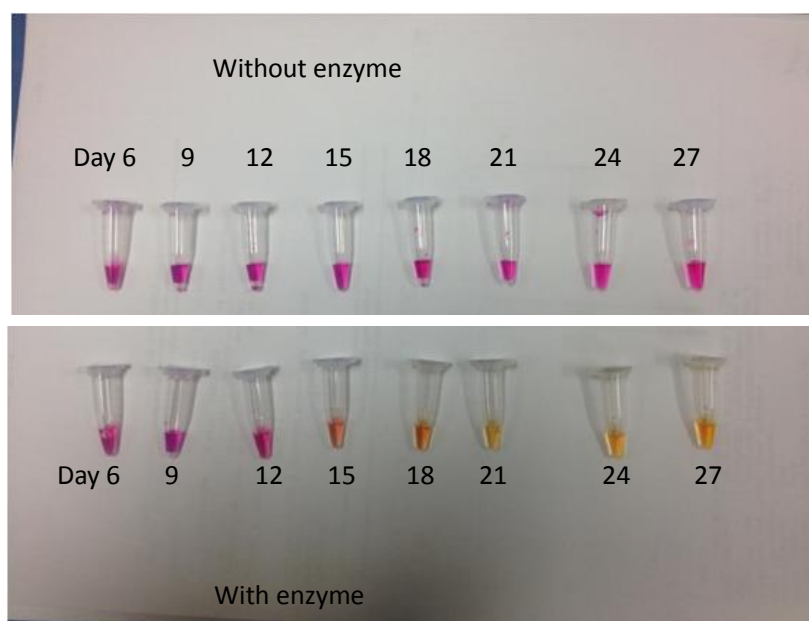


**Figure 6-6 Visual inspection of the PGSB degradation DMEM solutions with or without enzyme at different time points.**

### 6.3.4 Analysis of degradation products of PGSB by HPLC

HPLC of a BDNF solution showed the BDNF mimetic peak at 15.1 min (Fig. 6-7a). The peak area was proportional to the concentration of the BDNF mimetic (Fig. 6-7a). Acid accelerated degradation product (74.1 mg) was taken from the total amount of PGSB (475.2 mg) and dissolved in DMEM. However, only 2.2% of the total BDNF was detected in the accelerated degradation products (Fig. 6-7b). The value is quite different from that calculated from the UV-vis spectrum of the acid degraded product. The difference might be caused by the detection methods. All of the partially degraded PGSB soluble

## 6. Incorporation of BDNF mimetic in PGS and effect on cardiomyocytes cell culturing

fragments will be detected by the UV-Vis as they also contain an aromatic ring. However, using HPLC, PGSB fragments with different molecular species will be eluted at different times (peaks at 17.1 min, 27.4 min) and so the HPLC method may provide an underestimate of the amount of BDNF-based oligomers released during degradation. As the mimetic was designed to form a similar structure of the BDNF protein variable loop IIb (sequence SKGQL) which is considered to be the interacting part with TrkB [259], any change in the molecular structure of the BDNF mimetic, such as its oligomerization might impede its binding properties. Here we only regard the neat BDNF mimetic as the effective compound.

The amount of BDNF mimetic released from the PGSB degraded in DMEM without porcine liver esterase enzyme was below the detection limit of the HPLC until day 12. However, for the experiment with DMEM containing enzyme, at day 3, the peak area was significant. The BDNF mimetic peak area of PGSB degraded in DMEM with enzyme was consistently larger than that in DMEM at different time points (Fig. 6-7c). The amount of BDNF mimetic released from DMEM with enzyme, accelerated with time due to the reduction in pH which further caused the acidity-catalyzed degradation [231]. At day 30, the concentrations of BDNF mimetic in the test using the porcine liver esterase enzyme were over 2 times larger than for the test using DMEM without enzyme (193  $\mu\text{M}$  vs. 73  $\mu\text{M}$ ).

6. Incorporation of BDNF mimetic in PGS and effect on cardiomyocytes cell culturing

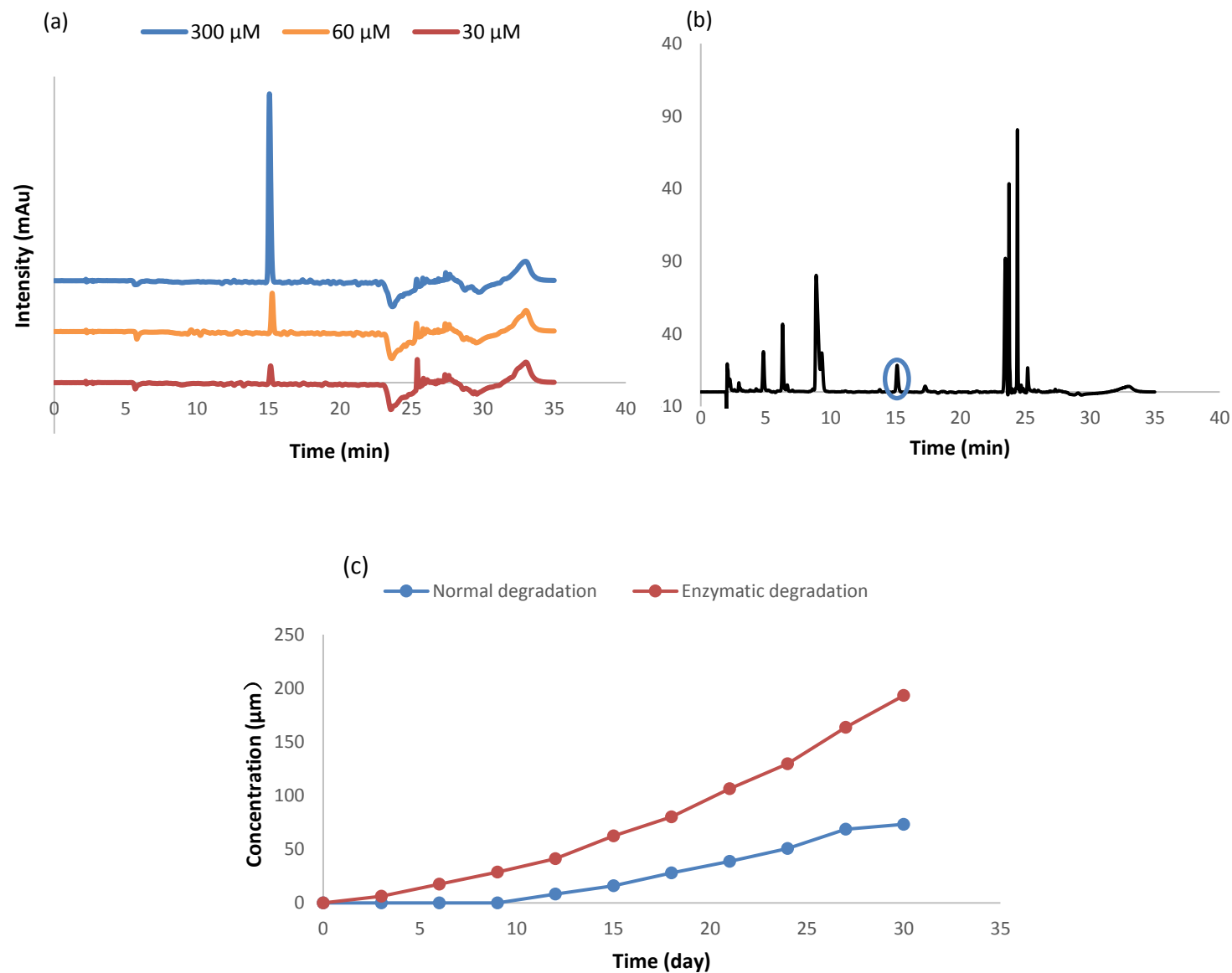


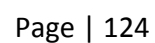
**Figure 6-7** (a) BDNF mimetic HPLC peak at 15.1 min at different concentrations (mAu = milliabsorbance units). (b) The peak (circled) was found in PGSB degraded in 1mol/L hydrochloric acid. (c) The released BDNF mimetic concentration in DEME with and without porcine liver esterase enzyme at different time points.



### **6.3.5 $^1\text{H}$ NMR of degradation products**

The presence of the BDNF mimetic within the elastomer was also confirmed by  $^1\text{H}$  NMR. The peaks indicating amides and aromatic rings were found in the PGSB gel degraded in 1 mol/L hydrochloric acid (Fig. 6-8a). However, compared with the pure BDNF mimetic peaks, the 8.51 ppm (aromatic ring) and 8.68 ppm (amide) (Fig. 6-8b), there is a small shift in the degradation products 8.43 (aromatic ring) and 8.82 (amide). The reason for this shift may be due to incomplete degradation of the PGSB, as mentioned above, so that the BDNF mimetic was esterified with the sebacic acid rather than being in its pure state.

(a)



### **6.3.6 Calcium transients in cardiomyocytes in presence of BDNF full protein or BDNF mimetic**

$\text{Ca}^{2+}$  elevation can trigger excitation-contraction coupling which is critical for optimal contractility, so  $\text{Ca}^{2+}$  transient over time reflects the condition of cardiomyocytes. As previously reported, BDNF elevates the amplitude (given as fluorescence intensity relative to baseline  $F/F_0$ ) of the calcium transient in cardiomyocytes [255, 256]. A similar finding with the BDNF mimetic was found in this study. However, not only did the amplitude increase, but more regular beating was also found. For the flat unpatterned PGS samples, only isolated cardiomyocytes showed calcium transients which were randomly flashed without any treatment (Fig. 6-9a). However, cells cultured on unpatterned PGS with BDNF full length protein, BDNF mimetic or on PGSB, a vague trend of synchronous calcium transient could be observed (Fig. 6-9c-6-9d). For the cardiomyocytes cultured micropatterned PGS with 20  $\mu\text{m}$  channels samples, the regular calcium transients were found without any treatment, so the improvement in regularity was not significant in presence of BDNF mimetic or BDNF protein (Fig. 6-10a-6-10d).

In addition, the increase in amplitude and improvement regularity, more cardiomyocytes were involved in the calcium transient with BDNF full protein treatment indicated by more regions of interests both on patterned and unpatterned samples (Fig. 6-11b, 6-12b). Similar results were also found for cardiomyocytes cultured on PGSB patterned (Fig. 6-11c) and unpatterned (Fig. 6-12c) films but not cardiomyocytes treated with BDNF mimetic (Fig. 6-11d, 6-12d). Although the concentration of the BDNF mimetic was three times higher than the BDNF full protein (60 nM vs. 20 nM), the difference in amplitude and number of cardiomyocytes involved was not significant compared with negative control groups especially on micropatterned samples (Fig. 6-13a, 6-13b). The BDNF mimetic has been reported to have a maximum levels of activity 80%-89% of the binding ability compared with BDNF full protein. However, normally it did not bind as efficiently as the BDNF full protein [259]. For the PGSB sample, the release of BDNF mimetic was caused by continual degradation. Calcium transient amplitude was greater

## 6. Incorporation of BDNF mimetic in PGS and effect on cardiomyocytes cell culturing

compared with BDNF mimetic treated samples (Fig. 6-14a, 6-14b). One possibility is that the concentration of BDNF mimetic released from PGSB in media was more than the treated concentration (60nM). The more significant change in amplitude would be caused by the higher concentration. However, the concentration of BDNF mimetic released from PGSB in media is still below the detection limit of the HPLC (the minimum detectable amount was around 10  $\mu$ M). The other possibility would be the continuous stimulation by the BDNF mimetic for a longer time. Compared with the other two treated groups which the treatment started at day 4 for 48 hr, the cardiomyocytes cultured on PGSB films would be exposed at the beginning of cell culture. The longer treatment time might lead to a greater amplitude.

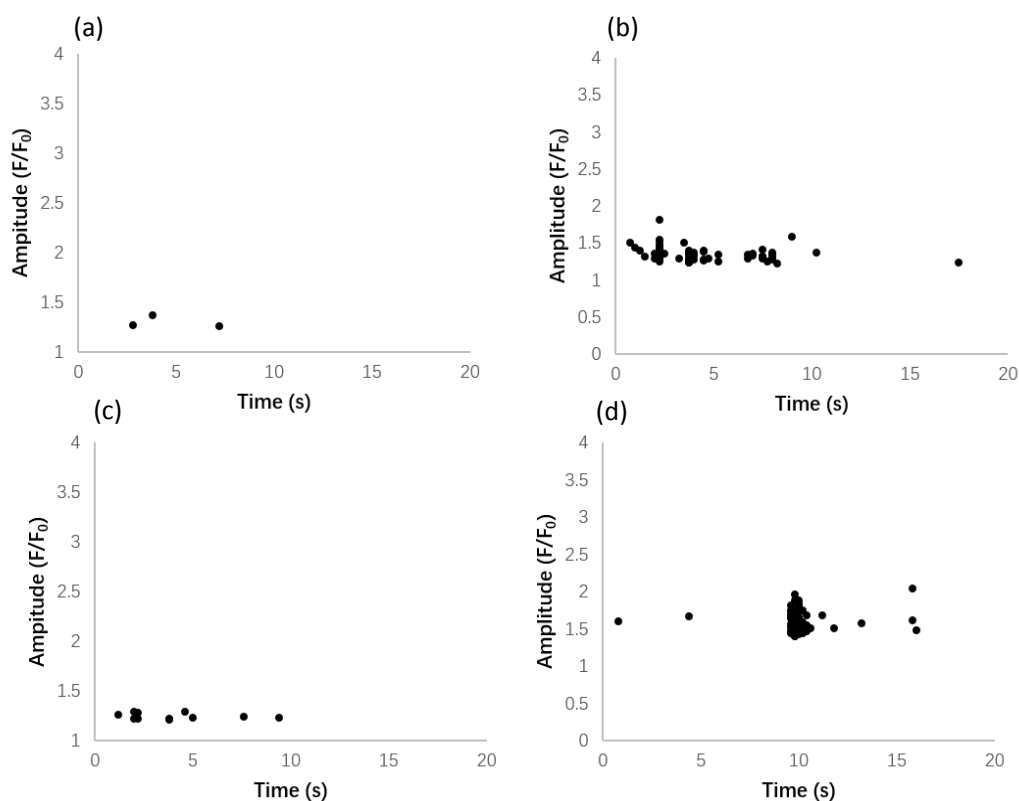


**Figure 6-9 Scattergrams of calcium transients of cardiomyocytes cultured on unpatterned substrates (a) PGS without any treatment (b) PGS treated with 20 nM BDNF full protein (c) PGS treated with 60 nM BDNF mimetic (d) 5% PGSB.**

## 6. Incorporation of BDNF mimetic in PGS and effect on cardiomyocytes cell culturing

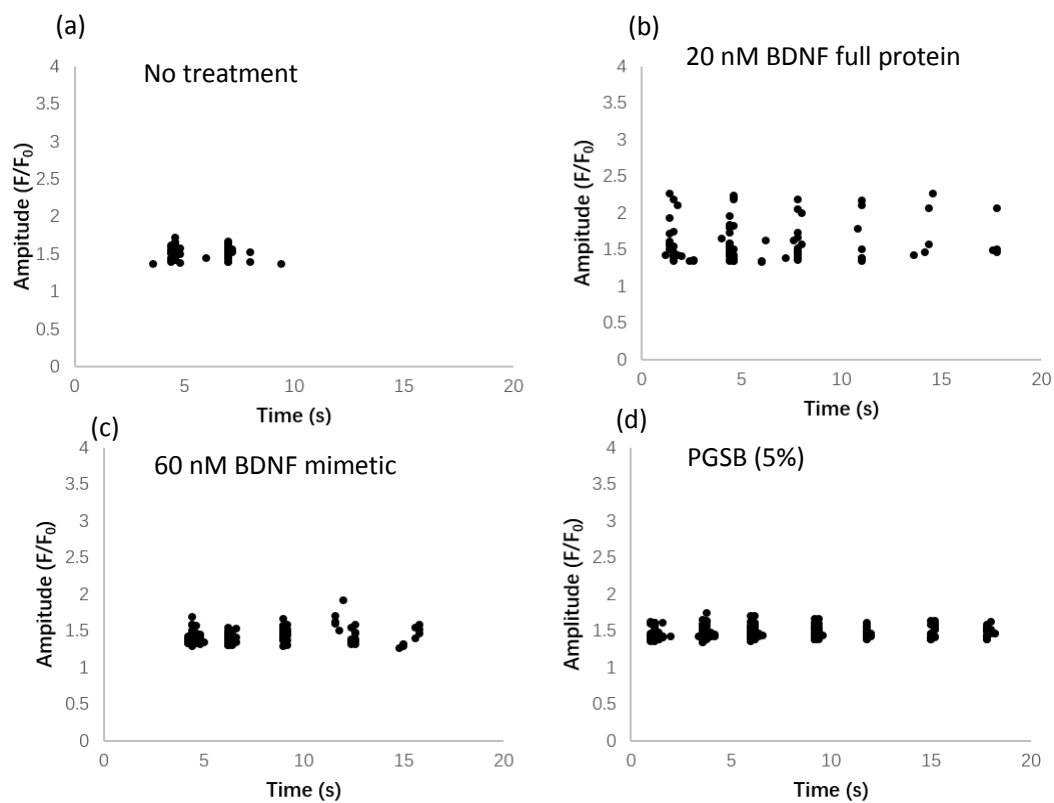


**Figure 6-10 Scattergrams of calcium transients of cardiomyocytes cultured on 20  $\mu$ m patterned substrates (a) PGS without any treatment (b) PGS treated with 20 nM BDNF full protein (c) PGS treated with 60 nM BDNF mimetic (d) 5% PGSB**

6. Incorporation of BDNF mimetic in PGS and effect on cardiomyocytes cell culturing

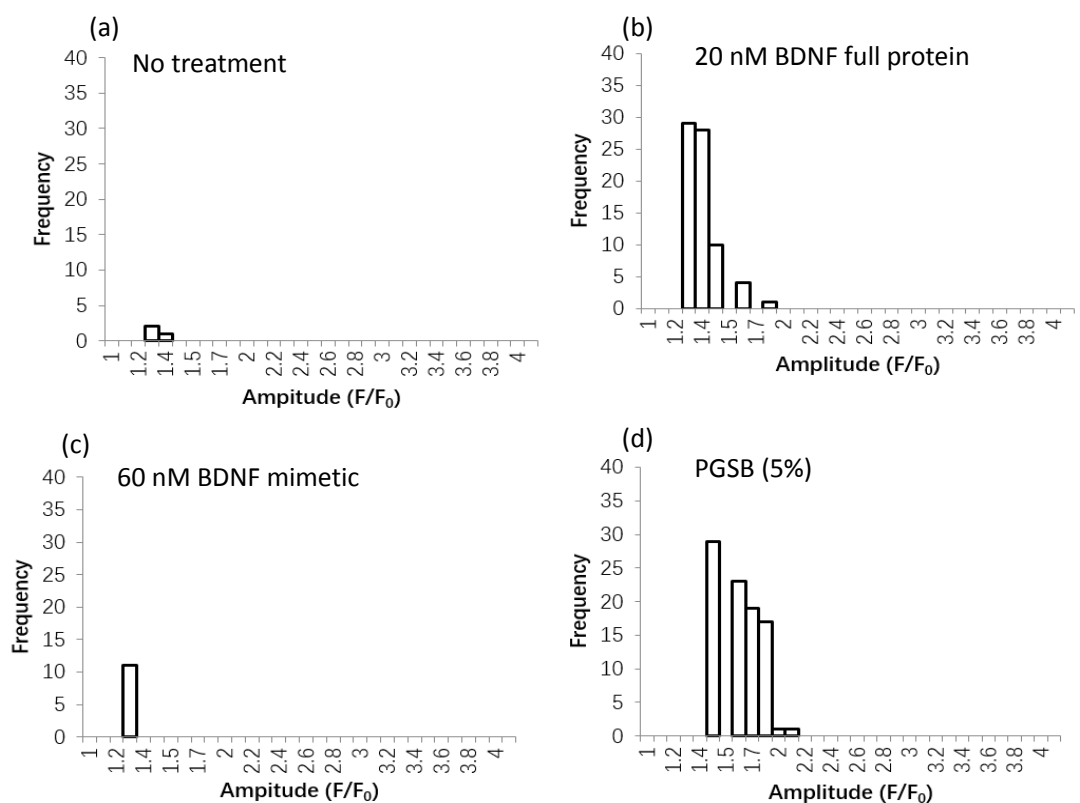


**Figure 6-11 Histogram of cardiomyocytes calcium transients amplitudes cultured on unpatterned substrates (a) PGS without any treatment (b) PGS treated with 20 nM BDNF full protein (c) PGS treated with 60 nM BDNF mimetic (d) 5% PGSB.**

6. Incorporation of BDNF mimetic in PGS and effect on cardiomyocytes cell culturing

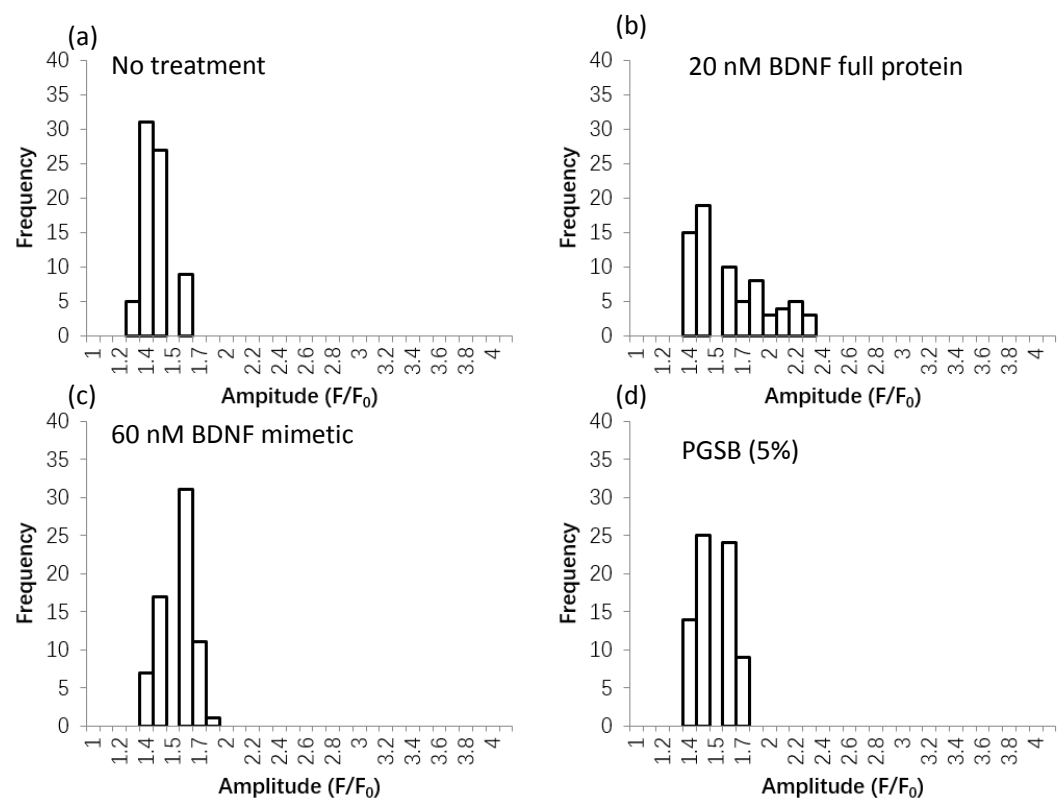


**Figure 6-12 Histogram of cardiomyocytes calcium transients amplitudes cultured on 20 μm patterned substrates (a)PGS without any tratment (b)PGS treated with 20 nM BDNF full protein (c)PGS treated with 60 nM BDNF mimetic (d) 5% PGSB.**

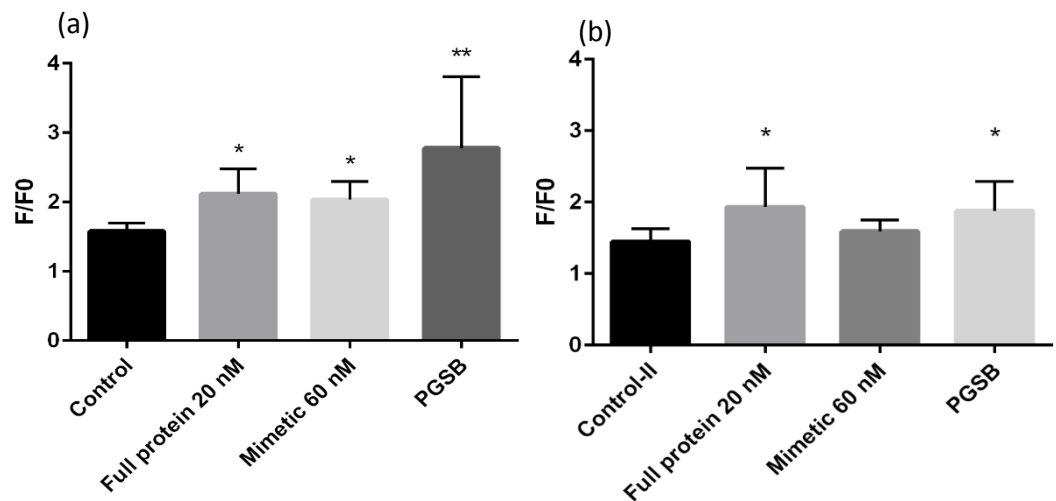


**Figure 6-13 The calcium transient amplitude comparasion between the drug treated and control goupes of unpatterned (e) and 20 μm patterned (f) samples.**

### **6.3.7 Cardiac cellular viability and cardiomyocyte hypertrophy**

The use of BDNF mimetic for cardiovascular disease treatment should be made under the premise that it would not reduce the normal functions of cardiomyocytes. The viability of cardiomyocytes was tested in the presence of BDNF mimetic at different concentrations. No differences in the viability of cardiomyocytes were found with or without BDNF mimetic treatment indicating that BDNF mimetic did not affect cell death (Fig. 6-15a).

Renin–angiotensin–aldosterone system (RAAS) plays a fundamental role in heart failure pathophysiology, and drugs inhibiting key components of the RAAS have become a cornerstone of contemporary cardiovascular drug therapy [20]. Angiotensin II is the protein which causes cardiomyocytes hypertrophy in RAAS. If BDNF full protein or BDNF mimetic could inhibit the effects of Ang II on cardiomyocytes, it would be a promising treatment for the myocardial hypertrophy after MI. By counting the  $^3\text{H}$ -leucine incorporation in cardiomyocytes, the proteins synthesized in cardiomyocytes can be quantified and give us information about the cardiomyocyte hypertrophy condition. By adding 100nM AngII, the  $^3\text{H}$ -leucine incorporation in cardiomyocytes increased significantly ( $p < 0.01$ ). However, by introducing BDNF full protein and BDNF, though it seems that the means of  $^3\text{H}$ -leucine incorporation in cardiomyocytes were reduced, no significant difference were found compared with that in Ang II stimulated cardiomyocytes. It seems that BDNF mimetic or BDNF full protein could not affect the downstream signalling pathways of Ang II.



6. Incorporation of BDNF mimetic in PGS and effect on cardiomyocytes cell culturing

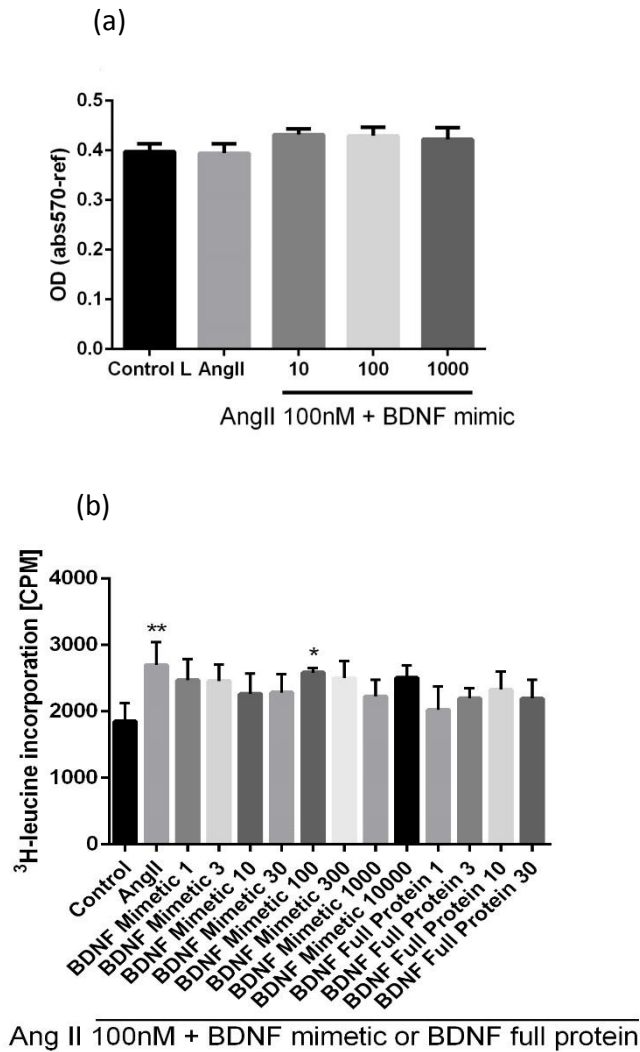


**Figure 6-14 The 100 nmol/L BDNF mimetic did not affect the viability of cardiomyocytes (a) BDNF mimetic or BDNF full protein at different concentrations did not clearly reveal any inhibition effects to Ang II(b) (\* indicates significant difference from control group).**

6.4 Conclusion

The BDNF mimetic was successfully incorporated into the PGS network structure to prolong the duration of continuous release. For the BDNF incorporated PGS, there was no significant change in mechanical

## 6. Incorporation of BDNF mimetic in PGS and effect on cardiomyocytes cell culturing

and thermal properties compared with PGS synthesized under the same conditions. Pork liver esterase was added in DMEM to mimic the in vivo condition and acceleration in the release of BDNF mimetic from the network was found. Cardiomyocyte's calcium transient amplitude was elevated in the presence of BDNF mimetic and BDNF full protein. However, the mimetic, either added separately or released from the polymer network, did not work as efficiently as the full protein. The increase in calcium transient amplitude was also found in PGSB due to the BDNF mimetic release. Stronger and more coordinated  $\text{Ca}^{2+}$  transients were found in presence of BDNF full protein and BDNF mimetic. PGSB showed potential to be used as cardiac patch because it can provide both mechanical support and a platform to deliver a mimetic of BDNF to maintain constitutive beating of the cardiomyocytes. However, it is still not clear what is the ideal concentration of BDNF mimetic for cardiomyocytes function, thus making it unable to determine the amount of BDNF incorporated in PGSB.

# 7 Conclusions and future work

## Declaration for Thesis Chapter [7]

### Declaration by candidate

In the case of Chapter [7], the nature and extent of my contribution to the work was the following:

Nature of contribution	Extent of contribution (%)
Major research and writing	90

The following co-authors contributed to the work.

Name	Nature of contribution	Extent of contribution (%) for student co-authors only
John Forsythe	Provided corrections	N/A

The undersigned hereby certify that the above declaration correctly reflects the nature and extent of the candidate's and co-authors' contributions to this work\*.

**Candidate's  
Signature**

	<b>Date</b> 26 <sup>th</sup> /08/2016
---	--

**Main  
Supervisor's  
Signature**

	<b>Date</b> 26 <sup>th</sup> /08/2016
---	--

### 7.1 Conclusions

To improve the performance of PGS as a biomaterial for myocardial tissue engineering, new methods and techniques were studied in designing and fabricating PGS based biomaterials. Although the tuneable mechanical properties enabled its potential as a myocardial tissue, the formation of fully biomimetic tissue was limited due to the imperfections in degradation, structure and signalization. The four sub-projects were designed to extend the potentialities of PGS in the area of myocardial tissue engineering.

Though PGS showed similar mechanical properties as myocardial tissue, the degradation of PGS is too fast with over 70% PGS degraded at day 35 [186]. On the other hand, the recovery for MI occurs over a long period. In chapter 3, to provide more enduring mechanical support to myocardial tissue, P34HB was blended into PGS. Single phase was found in the blends when P34HB content was below 50%, with elasticities like PGS. The stiffness increases with weight percentage of P34HB. P34HB could slow down the degradation speed of blends even at a relatively low percentage compared with pure PGS attribute to the surface degradation mechanism of PGS. These blends could be potentially used as matrix for cardiomyocytes cell culture.

In chapter 4, the optimization of PGS microcontact printing was studied. It has been established that micropatterning could provide topological cues for aligning cardiomyocytes. As a straightforward way to fabricate microstructure with a relatively high resolution, microcontact printing has not been carried for PGS as myocardial tissue. Direct print PGS from the photoresist on silicon wafer was not successful, with substantial PGS loss. The stickiness of PGS made it hard to be separate from the SU-8 photoresist mould. The improvement was limited for the resolution of PGS separated from hydrophobic PDMS mould. Other than the hydrophilicity, the nature stickiness of PGS was another cause for the difficulty in separation. Sucrose coating could be a potential solution. However, uneven dispersion of sucrose

## 7. Conclusions and future work

solution was found on PDMS mould. Hence, plasma treatment was applied for PDMS to form a relatively hydrophilic surface. The thickness of sucrose layer was thin and would not affect the depth of channels on PGS, but facilitate the separation.

The influence of microstructure on cardiomyocytes alignment and beating behavior was discussed in chapter 5. The results proved the hypothesis that the channel widths closest to the rat cardiomyocytes lateral size (around 20  $\mu\text{m}$ ) could provide best guidance. Best cardiomyocytes alignment was found on 20  $\mu\text{m}$  micropatterned PGS. Cardiomyocytes were found grown on both channels and crests. The cardiomyocytes grown on crests enabled communications of cells proved by the presence of gap junctions connexin 43. The two proteins for cardiomyocytes beating, troponin I and  $\alpha$ -actinin were also found widely spread in cardiomyocytes cultured on PGS. In consists of alignment, synchronized beating behavior with more coordinated calcium transients was almost exclusively found on micropatterned samples. The cardiomyocytes with better alignment facilitate the calcium transients between them and evoke the synchronized beating.

In chapter 6, the potential of BDNF mimetic to elevate the  $\text{Ca}^{2+}$  transient and contract ability was studied. Though BDNF RNA expression is found in cardiomyocytes at a higher concentration than the nervous system [272], the role is not well established. The  $\text{Ca}^{2+}$  transients elevation was the downstream effect of BDNF binding. In this study, the BDNF mimetic showed that it could provide similar effect as BDNF full protein. Other than the previous study which BDNF effects on a single cardiomyocyte, the cardiomyocytes cultured on PGS were observed as a whole for the drug treatment. More cardiomyocytes involved in  $\text{Ca}^{2+}$  transients, indicating the elevation of could reach the threshold for communication between cells. The BDNF mimetic was incorporated in the PGS network and released for a longer time. The release was accompanied with the degradation of PGS. Though the concentration was high in the PGSB compared with the treatment. It is not likely to happen *in vivo* with blood circulation.

## 7. Conclusions and future work

In this study, the scope and applications of PGS based biomaterials for myocardial tissue was expanded. As in specific applications and experiments, each biomaterial has its own respective advantages, it is hard to say that which one is the best. The softness and elasticity of PGS enables its application in the soft tissue engineering fields such as myocardial tissue engineering, vascular tissue engineering, nerve conduits, retina and tympanic membrane perforations. In light of the research in these areas since PGS was developed, the findings and systems reported in the study have contributed new designs and methodologies as well as applications towards myocardial tissue creating controllable environments to direct and exert influence on cell alignment. The medical applications of PGS are expanding further to include also targeted drug delivery. Other than biomaterials undergo bulk degradation which has limited ability of control release, the surface degradation mechanism of PGS enables long and steady release of the drug incorporated in PGS.

### **7.2 Limitations of the study and future work**

While the study has made a contribution towards PGS based biomaterials for myocardial tissue engineering, the systems themselves are not without limitations, and part of this has driven research in subsequent chapters to address the shortfalls.

All cardiomyocytes are cultured on the surface of PGS and the fabrication of 3-dimensional (3D) scaffolds is required. 3D scaffold biomaterials could delivery more cardiomyocytes to the infarcted myocardial tissue with multiple layers. As oxygen governed by molecular diffusion can only support a thin (few hundreds  $\mu\text{m}$ ) surface layer of functional tissue [273], angiogenesis needs to be promoted to support multilayer cardiomyocytes. Thus, interconnected pores with desired size should be evenly distributed in the scaffolds. Besides cardiomyocytes, other cells such as endothelial cells should be co-cultured in the

## 7. Conclusions and future work

3D scaffold system. The best ratio between cardiomyocytes and endothelial cells needs to be established to form a functional myocardial tissue.

How to maintain the aligned structure in 3D scaffolds is another challenge for myocardial tissue engineering. Though electrospinning could partially solve this problem, the pore size is too small and lack of proper cellular infiltration inside the fibres [230]. Another way is stack PGS thin films layer by layer [45]. However, the cardiomyocytes communications between layers are isolated and the cardiomyocytes density along vertical direction is less than the other two. Currently, there are no easy ways to create functional, fully perfusable biomimetic microvascular systems. PGS with a network of channels and interconnected pores to facilitate vascular network could be a potential solution but still need further investigation.

The cardiomyocytes used in this study were neonatal rat cardiomyocytes. However, to reduce the risk of rejection and provide accessible cell sources, cardiomyocytes derived from other cell sources such as embryonic stem cell derivatives, induced pluripotent stem cell derivatives and adult cardiac progenitor cells should be applied [6]. It is expected that the cardiomyocytes derived from other cell sources will have the same performance cultured on PGS based biomaterials. The *in vivo* application for such system is worth studying as well.

$\text{Ca}^{2+}$ , a downstream effector of BDNF-mediated activation on cardiomyocytes, elevates the cardiomyocytes  $\text{Ca}^{2+}$  transients and contraction amplitude. The complete and clear downstream pathways of BDNF signaling on cardiomyocytes is still unknown. The comprehensive understanding of BDNF signaling pathways is still required to better control the side effects especially combined with other therapies.

## 7. Conclusions and future work

BDNF mimetic was incorporated in PGS network, but whether it is polymerized or evenly distributed in the PGS network is unknown. As PGS undergoes surface degradation, the BDNF mimetic incorporation in these two ways could all provide slow release with degradation of PGS. The release difference detected by UV spectroscopy and HPLC could provide indirect evidence. Due to the low concentration and the harsh synthesis environment, the amount of BDNF mimetic in the PGSB was quite low and could not be detected by solid state NMR. PGS does not swell in water, it could swell in many organic solvents such as chloroform. It might be possible to swell PGS in deuterated solvents and analyse the solvents by NMR. Though it is not important to identify the incorporation ways of BDNF mimetic in PGS network in this project as it is released as a final degradation product, it might be helpful in other applications.



# Reference

- [1] Steg PG, James SK, Atar D, Badano LP, Lundqvist CB, Borger MA, et al. ESC Guidelines for the management of acute myocardial infarction in patients presenting with ST-segment elevation. *European heart journal*. 2012;ehs215.
- [2] Swirski FK, Nahrendorf M. Leukocyte behavior in atherosclerosis, myocardial infarction, and heart failure. *Science*. 2013;339:161-6.
- [3] Thygesen K, Alpert JS, Jaffe AS, Simoons ML, Chaitman BR, White HD. Third universal definition of myocardial infarction. *Circulation*. 2012;126:2020-35.
- [4] Flather MD, Yusuf S, Køber L, Pfeffer M, Hall A, Murray G, et al. Long-term ACE-inhibitor therapy in patients with heart failure or left-ventricular dysfunction: a systematic overview of data from individual patients. *The Lancet*. 2000;355:1575-81.
- [5] Chen Q-Z, Ishii H, Thouas GA, Lyon AR, Wright JS, Blaker JJ, et al. An elastomeric patch derived from poly (glycerol sebacate) for delivery of embryonic stem cells to the heart. *Biomaterials*. 2010;31:3885-93.
- [6] Fukuda K, Yuasa S. Stem cells as a source of regenerative cardiomyocytes. *Circulation research*. 2006;98:1002-13.
- [7] Müller-Ehmsen J, Peterson KL, Kedes L, Whittaker P, Dow JS, Long TI, et al. Rebuilding a damaged heart long-term survival of transplanted neonatal rat cardiomyocytes after myocardial infarction and effect on cardiac function. *Circulation*. 2002;105:1720-6.
- [8] Tanaka T, Tohyama S, Murata M, Nomura F, Kaneko T, Chen H, et al. In vitro pharmacologic testing using human induced pluripotent stem cell-derived cardiomyocytes. *Biochemical and biophysical research communications*. 2009;385:497-502.
- [9] Vunjak-Novakovic G, Tandon N, Godier A, Maidhof R, Marsano A, Martens TP, et al. Challenges in cardiac tissue engineering. *Tissue Engineering Part B: Reviews*. 2009;16:169-87.
- [10] McDevitt TC, Angello JC, Whitney ML, Reinecke H, Hauschka SD, Murry CE, et al. In vitro generation of differentiated cardiac myofibers on micropatterned laminin surfaces. *Journal of biomedical materials research*. 2002;60:472-9.
- [11] Jalil JE, Doering CW, Janicki JS, Pick R, Shroff SG, Weber KT. Fibrillar collagen and myocardial stiffness in the intact hypertrophied rat left ventricle. *Circulation research*. 1989;64:1041-50.
- [12] Chaturvedi RR, Herron T, Simmons R, Shore D, Kumar P, Sethia B, et al. Passive stiffness of myocardium from congenital heart disease and implications for diastole. *Circulation*. 2010;121:979-88.
- [13] Veress AI, Gullberg GT, Weiss JA. Measurement of strain in the left ventricle during diastole with cine-MRI and deformable image registration. *Journal of biomechanical engineering*. 2005;127:1195-207.
- [14] Zimmermann W-H, Didié M, Wasmeier GH, Nixdorff U, Hess A, Melnychenko I, et al. Cardiac grafting of engineered heart tissue in syngenic rats. *Circulation*. 2002;106:I-151-I-7.
- [15] Pryor HI, O'doherty E, Hart A, Owens G, Hoganson D, Vacanti JP, et al. Poly (glycerol sebacate) films prevent postoperative adhesions and allow laparoscopic placement. *Surgery*. 2009;146:490-7.
- [16] Chen Q-Z, Bismarck A, Hansen U, Junaid S, Tran MQ, Harding SE, et al. Characterisation of a soft elastomer poly (glycerol sebacate) designed to match the mechanical properties of myocardial tissue. *Biomaterials*. 2008;29:47-57.
- [17] Bian W, Jackman CP, Bursac N. Controlling the structural and functional anisotropy of engineered cardiac tissues. *Biofabrication*. 2014;6:024109.
- [18] Venugopal JR, Prabhakaran MP, Mukherjee S, Ravichandran R, Dan K, Ramakrishna S. Biomaterial strategies for alleviation of myocardial infarction. *Journal of The Royal Society Interface*. 2012;9:1-19.

- [19] Krijnen P, Nijmeijer R, Meijer C, Visser C, Hack C, Niessen H. Apoptosis in myocardial ischaemia and infarction. *Journal of clinical pathology*. 2002;55:801-11.
- [20] Von Lueder TG, Sangaralingham SJ, Wang BH, Kompa AR, Atar D, Burnett JC, et al. Renin–Angiotensin Blockade Combined With Natriuretic Peptide System Augmentation Novel Therapeutic Concepts to Combat Heart Failure. *Circulation: Heart Failure*. 2013;6:594-605.
- [21] Young JB, Mills RM. Clinical management of heart failure: Professional Communications; 2004.
- [22] Zammaretti P, Jaconi M. Cardiac tissue engineering: regeneration of the wounded heart. *Current opinion in biotechnology*. 2004;15:430-4.
- [23] Kelley ST, Malekan R, Gorman JH, Jackson BM, Gorman RC, Suzuki Y, et al. Restraining infarct expansion preserves left ventricular geometry and function after acute anteroapical infarction. *Circulation*. 1999;99:135-42.
- [24] Christman KL, Lee RJ. Biomaterials for the treatment of myocardial infarction. *Journal of the American College of Cardiology*. 2006;48:907-13.
- [25] Fan L, Yao J, Yang C, Wu Z, Xu D, Tang D. Material stiffness parameters as potential predictors of presence of left ventricle myocardial infarction: 3D echo-based computational modeling study. *Biomedical engineering online*. 2016;15:34.
- [26] Li R-K, Jia Z-Q, Weisel RD, Mickle DA, Zhang J, Mohabeer MK, et al. Cardiomyocyte transplantation improves heart function. *The Annals of Thoracic Surgery*. 1996;62:654-61.
- [27] Berry MF, Engler AJ, Woo YJ, Pirolli TJ, Bish LT, Jayasankar V, et al. Mesenchymal stem cell injection after myocardial infarction improves myocardial compliance. *American Journal of Physiology-Heart and Circulatory Physiology*. 2006;290:H2196-H203.
- [28] Robinson SW, Cho PW, Levitsky HI, Olson JL, Hruban RH, Acker MA, et al. Arterial delivery of genetically labelled skeletal myoblasts to the murine heart: long-term survival and phenotypic modification of implanted myoblasts. *Cell transplantation*. 1996;5:77-91.
- [29] Yang J, Yamato M, Okano T. Cell-sheet engineering using intelligent surfaces. *MRS bulletin*. 2005;30:189-93.
- [30] Parker KK, Ingber DE. Extracellular matrix, mechanotransduction and structural hierarchies in heart tissue engineering. *Philosophical Transactions of the Royal Society of London B: Biological Sciences*. 2007;362:1267-79.
- [31] Zong X, Bien H, Chung C-Y, Yin L, Fang D, Hsiao BS, et al. Electrospun fine-textured scaffolds for heart tissue constructs. *Biomaterials*. 2005;26:5330-8.
- [32] Carrier RL, Rupnick M, Langer R, Schoen FJ, Freed LE, Vunjak-Novakovic G. Perfusion improves tissue architecture of engineered cardiac muscle. *Tissue engineering*. 2002;8:175-88.
- [33] Park H, Radisic M, Lim JO, Chang BH, Vunjak-Novakovic G. A novel composite scaffold for cardiac tissue engineering. *In Vitro Cellular & Developmental Biology-Animal*. 2005;41:188-96.
- [34] Pego A, Siebum B, Van Luyn M, Gallego y Van Seijen X, Poot A, Grijpma D, et al. Preparation of degradable porous structures based on 1, 3-trimethylene carbonate and D, L-lactide (co) polymers for heart tissue engineering. *Tissue engineering*. 2003;9:981-94.
- [35] Lesman A, Habib M, Caspi O, Gepstein A, Arbel G, Levenberg S, et al. Transplantation of a tissue-engineered human vascularized cardiac muscle. *Tissue Engineering Part A*. 2009;16:115-25.
- [36] Fukuhara S, Tomita S, Nakatani T, Fujisato T, Ohtsu Y, Ishida M, et al. Bone marrow cell-seeded biodegradable polymeric scaffold enhances angiogenesis and improves function of the infarcted heart. *Circulation journal: official journal of the Japanese Circulation Society*. 2005;69:850-7.
- [37] Ke Q, Yang Y, Rana JS, Chen Y, Morgan JP, Xiao Y. Embryonic stem cells cultured in biodegradable scaffold repair infarcted myocardium in mice. *ACTA PHYSIOLOGICA SINICA-CHINESE EDITION*-. 2005;57:673.
- [38] Ozawa T, Mickle DA, Weisel RD, Koyama N, Ozawa S, Li R-K. Optimal biomaterial for creation of autologous cardiac grafts. *Circulation*. 2002;106:I-176-I-82.
- [39] Matsubayashi K, Fedak PW, Mickle DA, Weisel RD, Ozawa T, Li R-K. Improved left ventricular aneurysm repair with bioengineered vascular smooth muscle grafts. *Circulation*. 2003;108:II-219-II-25.
- [40] Jin J, Jeong SI, Shin YM, Lim KS, Lee YM, Koh HC, et al. Transplantation of mesenchymal stem cells within a poly (lactide - co -  $\epsilon$  - caprolactone) scaffold improves cardiac function in a rat myocardial infarction model. *European journal of heart failure*. 2009;11:147-53.

- [41] Hashizume R, Fujimoto KL, Hong Y, Guan J, Toma C, Tobita K, et al. Biodegradable elastic patch plasty ameliorates left ventricular adverse remodeling after ischemia–reperfusion injury: A preclinical study of a porous polyurethane material in a porcine model. *The Journal of thoracic and cardiovascular surgery*. 2013;146:391-9. e1.
- [42] Fujimoto KL, Tobita K, Merryman WD, Guan J, Momoi N, Stolz DB, et al. An elastic, biodegradable cardiac patch induces contractile smooth muscle and improves cardiac remodeling and function in subacute myocardial infarction. *Journal of the American College of Cardiology*. 2007;49:2292-300.
- [43] Siepe M, Giraud M-N, Pavlovic M, Recepto C, Beyersdorf F, Menasché P, et al. Myoblast-seeded biodegradable scaffolds to prevent post–myocardial infarction evolution toward heart failure. *The Journal of Thoracic and Cardiovascular Surgery*. 2006;132:124-31.
- [44] McDevitt TC, Woodhouse KA, Hauschka SD, Murry CE, Stayton PS. Spatially organized layers of cardiomyocytes on biodegradable polyurethane films for myocardial repair. *Journal of Biomedical Materials Research Part A*. 2003;66:586-95.
- [45] Engelmayer GC, Cheng M, Bettinger CJ, Borenstein JT, Langer R, Freed LE. Accordion-like honeycombs for tissue engineering of cardiac anisotropy. *Nature materials*. 2008;7:1003-10.
- [46] Guillemette MD, Park H, Hsiao JC, Jain SR, Larson BL, Langer R, et al. Combined technologies for microfabricating elastomeric cardiac tissue engineering scaffolds. *Macromolecular bioscience*. 2010;10:1330-7.
- [47] Ravichandran R, Venugopal JR, Sundarrajan S, Mukherjee S, Ramakrishna S. Poly (glycerol sebacate)/gelatin core/shell fibrous structure for regeneration of myocardial infarction. *Tissue Engineering Part A*. 2011;17:1363-73.
- [48] Xu B, Rollo B, Stamp LA, Zhang D, Fang X, Newgreen DF, et al. Non-linear elasticity of core/shell spun PGS/PLLA fibres and their effect on cell proliferation. *Biomaterials*. 2013;34:6306-17.
- [49] Masoumi N, Larson BL, Annabi N, Kharaziha M, Zamanian B, Shapero KS, et al. Electrospun PGS: PCL microfibers align human valvular interstitial cells and provide tunable scaffold anisotropy. *Advanced healthcare materials*. 2014;3:929-39.
- [50] Kharaziha M, Nikkhah M, Shin S-R, Annabi N, Masoumi N, Gaharwar AK, et al. PGS: Gelatin nanofibrous scaffolds with tunable mechanical and structural properties for engineering cardiac tissues. *Biomaterials*. 2013;34:6355-66.
- [51] Stuckey DJ, Ishii H, Chen Q-Z, Boccaccini AR, Hansen U, Carr CA, et al. Magnetic resonance imaging evaluation of remodeling by cardiac elastomeric tissue scaffold biomaterials in a rat model of myocardial infarction. *Tissue Engineering Part A*. 2010;16:3395-402.
- [52] Radisic M, Park H, Martens TP, Salazar - Lazaro JE, Geng W, Wang Y, et al. Pre - treatment of synthetic elastomeric scaffolds by cardiac fibroblasts improves engineered heart tissue. *Journal of biomedical materials research Part A*. 2008;86:713-24.
- [53] Dobner S, Bezuidenhout D, Govender P, Zilla P, Davies N. A synthetic non-degradable polyethylene glycol hydrogel retards adverse post-infarct left ventricular remodeling. *Journal of cardiac failure*. 2009;15:629-36.
- [54] Rane AA, Chuang JS, Shah A, Hu DP, Dalton ND, Gu Y, et al. Increased infarct wall thickness by a bio-inert material is insufficient to prevent negative left ventricular remodeling after myocardial infarction. *PLoS One*. 2011;6:e21571.
- [55] Yoon SJ, Fang YH, Lim CH, Kim BS, Son HS, Park Y, et al. Regeneration of ischemic heart using hyaluronic acid - based injectable hydrogel. *Journal of Biomedical Materials Research Part B: Applied Biomaterials*. 2009;91:163-71.
- [56] Shapira-Schweitzer K, Habib M, Gepstein L, Seliktar D. A photopolymerizable hydrogel for 3-D culture of human embryonic stem cell-derived cardiomyocytes and rat neonatal cardiac cells. *Journal of molecular and cellular cardiology*. 2009;46:213-24.
- [57] Singelyn JM, DeQuach JA, Seif-Naraghi SB, Littlefield RB, Schup-Magoffin PJ, Christman KL. Naturally derived myocardial matrix as an injectable scaffold for cardiac tissue engineering. *Biomaterials*. 2009;30:5409-16.
- [58] Seif-Naraghi SB, Singelyn JM, Salvatore MA, Osborn KG, Wang JJ, Sampat U, et al. Safety and efficacy of an injectable extracellular matrix hydrogel for treating myocardial infarction. *Science translational medicine*. 2013;5:173ra25-ra25.

- [59] Yanagawa B, Rao V, Yau TM, Cusimano RJ. Initial experience with intraventricular repair using CorMatrix extracellular matrix. *Innovations: Technology and Techniques in Cardiothoracic and Vascular Surgery*. 2013;8:348-52.
- [60] Gaballa MA, Sunkomat JN, Thai H, Morkin E, Ewy G, Goldman S. Grafting an acellular 3-dimensional collagen scaffold onto a non-transmural infarcted myocardium induces neo-angiogenesis and reduces cardiac remodeling. *The Journal of heart and lung transplantation*. 2006;25:946-54.
- [61] Chachques JC, Trainini JC, Lago N, Cortes-Morichetti M, Schussler O, Carpentier A. Myocardial assistance by grafting a new bioartificial upgraded myocardium (MAGNUM trial): clinical feasibility study. *The Annals of thoracic surgery*. 2008;85:901-8.
- [62] Yost MJ, Baicu CF, Stonerock CE, Goodwin RL, Price RL, Davis JM, et al. A novel tubular scaffold for cardiovascular tissue engineering. *Tissue engineering*. 2004;10:273-84.
- [63] Tsang K, Annabi N, Ercole F, Zhou K, Karst DJ, Li F, et al. Facile One - Step Micropatterning Using Photodegradable Gelatin Hydrogels for Improved Cardiomyocyte Organization and Alignment. *Advanced functional materials*. 2015;25:977-86.
- [64] Li R-K, Yau TM, Weisel RD, Mickle DA, Sakai T, Choi A, et al. Construction of a bioengineered cardiac graft. *The Journal of Thoracic and Cardiovascular Surgery*. 2000;119:368-75.
- [65] Shin SR, Jung SM, Zalabany M, Kim K, Zorlutuna P, Kim Sb, et al. Carbon-nanotube-embedded hydrogel sheets for engineering cardiac constructs and bioactuators. *ACS nano*. 2013;7:2369-80.
- [66] Kofidis T, Lenz A, Boublik J, Akhyari P, Wachsmann B, Mueller-Stahl K, et al. Pulsatile perfusion and cardiomyocyte viability in a solid three-dimensional matrix. *Biomaterials*. 2003;24:5009-14.
- [67] Birla RK, Borschel GH, Dennis RG, Brown DL. Myocardial engineering in vivo: formation and characterization of contractile, vascularized three-dimensional cardiac tissue. *Tissue engineering*. 2005;11:803-13.
- [68] Dahlmann J, Krause A, Möller L, Kensah G, Möwes M, Diekmann A, et al. Fully defined in situ cross-linkable alginate and hyaluronic acid hydrogels for myocardial tissue engineering. *Biomaterials*. 2013;34:940-51.
- [69] Lee KY, Mooney DJ. Alginate: properties and biomedical applications. *Progress in polymer science*. 2012;37:106-26.
- [70] Landa N, Miller L, Feinberg MS, Holbova R, Shachar M, Freeman I, et al. Effect of injectable alginate implant on cardiac remodeling and function after recent and old infarcts in rat. *Circulation*. 2008;117:1388-96.
- [71] Lee RJ, Hinson A, Helgersson S, Bauernschmitt R, Sabbah HN. Polymer-based restoration of left ventricular mechanics. *Cell transplantation*. 2013;22:529-33.
- [72] Liu Z, Wang H, Wang Y, Lin Q, Yao A, Cao F, et al. The influence of chitosan hydrogel on stem cell engraftment, survival and homing in the ischemic myocardial microenvironment. *Biomaterials*. 2012;33:3093-106.
- [73] Hussain A, Collins G, Yip D, Cho CH. Functional 3 - D cardiac co - culture model using bioactive chitosan nanofiber scaffolds. *Biotechnology and bioengineering*. 2013;110:637-47.
- [74] Reis LA, Chiu LL, Liang Y, Hyunh K, Momen A, Radisic M. A peptide-modified chitosan–collagen hydrogel for cardiac cell culture and delivery. *Acta biomaterialia*. 2012;8:1022-36.
- [75] Martins AM, Eng G, Caridade SG, Mano JoF, Reis RL, Vunjak-Novakovic G. Electrically conductive chitosan/carbon scaffolds for cardiac tissue engineering. *Biomacromolecules*. 2014;15:635-43.
- [76] Law C-H, Li J-M, Chou H-C, Chen Y-H, Chan H-L. Hyaluronic acid-dependent protection in H9C2 cardiomyocytes: A cell model of heart ischemia–reperfusion injury and treatment. *Toxicology*. 2013;303:54-71.
- [77] Boublik J, Park H, Radisic M, Tognana E, Chen F, Pei M, et al. Mechanical properties and remodeling of hybrid cardiac constructs made from heart cells, fibrin, and biodegradable, elastomeric knitted fabric. *Tissue engineering*. 2005;11:1122-32.
- [78] Marin E, Briceño MI, Caballero-George C. Critical evaluation of biodegradable polymers used in nanodrugs. *International journal of nanomedicine*. 2013;8:3071.
- [79] Ratner BD, Hoffman AS, Schoen FJ, Lemons JE. *Biomaterials science: an introduction to materials in medicine*: Academic press; 2004.

- [80] Papadaki M, Bursac N, Langer R, Merok J, Vunjak-Novakovic G, Freed L. Tissue engineering of functional cardiac muscle: molecular, structural, and electrophysiological studies. *American Journal of Physiology-Heart and Circulatory Physiology*. 2001;280:H168-H78.
- [81] Engelberg I, Kohn J. Physico-mechanical properties of degradable polymers used in medical applications: a comparative study. *Biomaterials*. 1991;12:292-304.
- [82] Jawad H, Ali N, Lyon A, Chen Q, Harding S, Boccaccini A. Myocardial tissue engineering: a review. *Journal of tissue engineering and regenerative medicine*. 2007;1:327-42.
- [83] Sorrell JM, Baber MA, Caplan AI. A self-assembled fibroblast-endothelial cell co-culture system that supports in vitro vasculogenesis by both human umbilical vein endothelial cells and human dermal microvascular endothelial cells. *Cells Tissues Organs*. 2007;186:157-68.
- [84] Pascual-Gil S, Garbayo E, Díaz-Herráez P, Prosper F, Blanco-Prieto MJ. Heart regeneration after myocardial infarction using synthetic biomaterials. *Journal of Controlled Release*. 2015;203:23-38.
- [85] Kim G, Son J, Park S, Kim W. Hybrid process for fabricating 3D hierarchical scaffolds combining rapid prototyping and electrospinning. *Macromolecular Rapid Communications*. 2008;29:1577-81.
- [86] Labet M, Thielemans W. Synthesis of polycaprolactone: a review. *Chemical Society Reviews*. 2009;38:3484-504.
- [87] Ishii O, Shin M, Sueda T, Vacanti JP. In vitro tissue engineering of a cardiac graft using a degradable scaffold with an extracellular matrix-like topography. *The Journal of thoracic and cardiovascular surgery*. 2005;130:1358-63.
- [88] Shin M, Ishii O, Sueda T, Vacanti J. Contractile cardiac grafts using a novel nanofibrous mesh. *Biomaterials*. 2004;25:3717-23.
- [89] Piao H, Kwon J-S, Piao S, Sohn J-H, Lee Y-S, Bae J-W, et al. Effects of cardiac patches engineered with bone marrow-derived mononuclear cells and PGCL scaffolds in a rat myocardial infarction model. *Biomaterials*. 2007;28:641-9.
- [90] Yin L, Bien H, Entcheva E. Scaffold topography alters intracellular calcium dynamics in cultured cardiomyocyte networks. *American Journal of Physiology-Heart and Circulatory Physiology*. 2004;287:H1276-H85.
- [91] Rogers JA, Nuzzo RG. Recent progress in soft lithography. *Materials today*. 2005;8:50-6.
- [92] Fromstein JD, Zandstra PW, Alperin C, Rockwood D, Rabolt JF, Woodhouse KA. Seeding bioreactor-produced embryonic stem cell-derived cardiomyocytes on different porous, degradable, polyurethane scaffolds reveals the effect of scaffold architecture on cell morphology. *Tissue Engineering Part A*. 2008;14:369-78.
- [93] Park H, Larson BL, Guillemette MD, Jain SR, Hua C, Engelmayr GC, et al. The significance of pore microarchitecture in a multi-layered elastomeric scaffold for contractile cardiac muscle constructs. *Biomaterials*. 2011;32:1856-64.
- [94] Xu B, Li Y, Zhu C, Cook WD, Forsythe J, Chen Q. Fabrication, mechanical properties and cytocompatibility of elastomeric nanofibrous mats of poly (glycerol sebacate). *European Polymer Journal*. 2015;64:79-92.
- [95] Kenar H, Kose G, Hasirci V. Design of a 3D aligned myocardial tissue construct from biodegradable polyesters. *Journal of Materials Science: Materials in Medicine*. 2010;21:989-97.
- [96] Chaussade S. Mechanisms of action of low doses of polyethylene glycol in the treatment of functional constipation. *Italian journal of gastroenterology and hepatology*. 1999;31:S242-4.
- [97] Li Z, Guan J. Hydrogels for cardiac tissue engineering. *Polymers*. 2011;3:740-61.
- [98] Chen S, Li L, Zhao C, Zheng J. Surface hydration: principles and applications toward low-fouling/nonfouling biomaterials. *Polymer*. 2010;51:5283-93.
- [99] Zhu J. Bioactive modification of poly (ethylene glycol) hydrogels for tissue engineering. *Biomaterials*. 2010;31:4639-56.
- [100] Rafat M, Li F, Fagerholm P, Lagali NS, Watsky MA, Munger R, et al. PEG-stabilized carbodiimide crosslinked collagen-chitosan hydrogels for corneal tissue engineering. *Biomaterials*. 2008;29:3960-72.
- [101] Jongpaiboonkit L, King WJ, Lyons GE, Paguirigan AL, Warrick JW, Beebe DJ, et al. An adaptable hydrogel array format for 3-dimensional cell culture and analysis. *Biomaterials*. 2008;29:3346-56.

- [102] Smith AW, Segar CE, Nguyen PK, MacEwan MR, Efimov IR, Elbert DL. Long-term culture of HL-1 cardiomyocytes in modular poly (ethylene glycol) microsphere-based scaffolds crosslinked in the phase-separated state. *Acta biomaterialia*. 2012;8:31-40.
- [103] Badylak SF. The extracellular matrix as a biologic scaffold material. *Biomaterials*. 2007;28:3587-93.
- [104] Roura S, Gálvez - Montón C, Bayes - Genis A. Fibrin, the preferred scaffold for cell transplantation after myocardial infarction? An old molecule with a new life. *Journal of tissue engineering and regenerative medicine*. 2016.
- [105] Nieponice A, Gilbert TW, Badylak SF. Reinforcement of esophageal anastomoses with an extracellular matrix scaffold in a canine model. *The Annals of thoracic surgery*. 2006;82:2050-8.
- [106] Sepantafar M, Maheronnaghsh R, Mohammadi H, Rajabi-Zeleti S, Annabi N, Aghdami N, et al. Stem cells and injectable hydrogels: synergistic therapeutics in myocardial repair. *Biotechnology advances*. 2016;34:362-79.
- [107] Van Luyn M, Tio R, y van Seijen XG, Plantinga J, De Leij L, DeJongste M, et al. Cardiac tissue engineering: characteristics of in unison contracting two-and three-dimensional neonatal rat ventricle cell (co)-cultures. *Biomaterials*. 2002;23:4793-801.
- [108] Radisic M, Euloth M, Yang L, Langer R, Freed LE, Vunjak - Novakovic G. High - density seeding of myocyte cells for cardiac tissue engineering. *Biotechnology and bioengineering*. 2003;82:403-14.
- [109] Kofidis T, Akhyari P, Wachsmann B, Mueller-Stahl K, Boublik J, Ruhparwar A, et al. Clinically established hemostatic scaffold (tissue fleece) as biomatrix in tissue-and organ-engineering research. *Tissue engineering*. 2003;9:517.
- [110] Kofidis T, Akhyari P, Boublik J, Theodorou P, Martin U, Ruhparwar A, et al. In vitro engineering of heart muscle: artificial myocardial tissue. *The Journal of Thoracic and Cardiovascular Surgery*. 2002;124:63-9.
- [111] Radisic M, Park H, Shing H, Consi T, Schoen FJ, Langer R, et al. Functional assembly of engineered myocardium by electrical stimulation of cardiac myocytes cultured on scaffolds. *Proceedings of the National Academy of Sciences*. 2004;101:18129-34.
- [112] Gómez-Guillén M, Giménez B, López-Caballero Ma, Montero M. Functional and bioactive properties of collagen and gelatin from alternative sources: A review. *Food Hydrocolloids*. 2011;25:1813-27.
- [113] Veis A, Anesey J, Cohen J. The long range reorganization of gelatin to the collagen structure. *Archives of biochemistry and biophysics*. 1961;94:20-31.
- [114] Wang Z-G, Wan L-S, Xu Z-K. Surface engineerings of polyacrylonitrile-based asymmetric membranes towards biomedical applications: An overview. *Journal of Membrane Science*. 2007;304:8-23.
- [115] Jin R, Teixeira LM, Krouwels A, Dijkstra P, Van Blitterswijk C, Karperien M, et al. Synthesis and characterization of hyaluronic acid-poly (ethylene glycol) hydrogels via Michael addition: An injectable biomaterial for cartilage repair. *Acta biomaterialia*. 2010;6:1968-77.
- [116] Akhyari P, Fedak PW, Weisel RD, Lee T-YJ, Verma S, Mickle DA, et al. Mechanical stretch regimen enhances the formation of bioengineered autologous cardiac muscle grafts. *Circulation*. 2002;106:I-137-I-42.
- [117] Shaikh FM, Callanan A, Kavanagh EG, Burke PE, Grace PA, McGloughlin TM. Fibrin: a natural biodegradable scaffold in vascular tissue engineering. *Cells Tissues Organs*. 2008;188:333-46.
- [118] Ruvinov E, Cohen S. Alginate biomaterial for the treatment of myocardial infarction: progress, translational strategies, and clinical outlook: from ocean algae to patient bedside. *Advanced drug delivery reviews*. 2016;96:54-76.
- [119] Bai X, Zheng H, Fang R, Wang T, Hou X, Li Y, et al. Fabrication of engineered heart tissue grafts from alginate/collagen barium composite microbeads. *Biomedical Materials*. 2011;6:045002.
- [120] Leor J, Aboulafia-Etzion S, Dar A, Shapiro L, Barbash IM, Battler A, et al. Bioengineered cardiac grafts a new approach to repair the infarcted myocardium? *Circulation*. 2000;102:lii-56-iii-61.
- [121] Dar A, Shachar M, Leor J, Cohen S. Optimization of cardiac cell seeding and distribution in 3D porous alginate scaffolds. *Biotechnology and bioengineering*. 2002;80:305-12.
- [122] Lin Y-D, Yeh M-L, Yang Y-J, Tsai D-C, Chu T-Y, Shih Y-Y, et al. Intramyocardial peptide nanofiber injection improves postinfarction ventricular remodeling and efficacy of bone marrow cell therapy in pigs. *Circulation*. 2010;122:S132-S41.

- [123] French KM, Somasuntharam I, Davis ME. Self-assembling peptide-based delivery of therapeutics for myocardial infarction. *Advanced drug delivery reviews*. 2016;96:40-53.
- [124] Fraser J, Laurent T, Laurent U. Hyaluronan: its nature, distribution, functions and turnover. *Journal of internal medicine*. 1997;242:27-33.
- [125] Stern R. Hyaluronan in cancer biology: Academic Press; 2009.
- [126] Dang AB, Guccione JM, Zhang P, Wallace AW, Gorman RC, Gorman JH, et al. Effect of ventricular size and patch stiffness in surgical anterior ventricular restoration: a finite element model study. *The Annals of thoracic surgery*. 2005;79:185-93.
- [127] Efe JA, Hilcove S, Kim J, Zhou H, Ouyang K, Wang G, et al. Conversion of mouse fibroblasts into cardiomyocytes using a direct reprogramming strategy. *Nature cell biology*. 2011;13:215-22.
- [128] Pijnappels DA, Schaliij MJ, Ramkisoensing AA, van Tuyn J, de Vries AA, van der Laarse A, et al. Forced alignment of mesenchymal stem cells undergoing cardiomyogenic differentiation affects functional integration with cardiomyocyte cultures. *Circulation research*. 2008;103:167-76.
- [129] Sosnovik DE, Wang R, Dai G, Wang T, Aikawa E, Novikov M, et al. Diffusion spectrum MRI tractography reveals the presence of a complex network of residual myofibers in infarcted myocardium. *Circulation: Cardiovascular Imaging*. 2009;2:206-12.
- [130] Hsiao C-W, Bai M-Y, Chang Y, Chung M-F, Lee T-Y, Wu C-T, et al. Electrical coupling of isolated cardiomyocyte clusters grown on aligned conductive nanofibrous meshes for their synchronized beating. *Biomaterials*. 2013;34:1063-72.
- [131] Orlova Y, Magome N, Liu L, Chen Y, Agladze K. Electrospun nanofibers as a tool for architecture control in engineered cardiac tissue. *Biomaterials*. 2011;32:5615-24.
- [132] Yu J, Lee A-R, Lin W-H, Lin C-W, Wu Y-K, Tsai W-B. Electrospun PLGA fibers incorporated with functionalized biomolecules for cardiac tissue engineering. *Tissue Engineering Part A*. 2014;20:1896-907.
- [133] Castellano D, Blanes M, Marco B, Cerrada I, Ruiz-Saurí A, Pelacho B, et al. A comparison of electrospun polymers reveals poly (3-hydroxybutyrate) fiber as a superior scaffold for cardiac repair. *Stem cells and development*. 2014;23:1479-90.
- [134] Hussain A, Collins G, Cho CH. Electrospun chitosan-based nanofiber scaffolds for cardiac tissue engineering applications. *Proceedings of the 2010 IEEE 36th Annual Northeast Bioengineering Conference (NEBEC): IEEE; 2010*. p. 1-2.
- [135] Rockwood DN, Akins RE, Parrag IC, Woodhouse KA, Rabolt JF. Culture on electrospun polyurethane scaffolds decreases atrial natriuretic peptide expression by cardiomyocytes in vitro. *Biomaterials*. 2008;29:4783-91.
- [136] Kantawong F, Burchmore R, Gadegaard N, Oreffo RO, Dalby MJ. Proteomic analysis of human osteoprogenitor response to disordered nanotopography. *Journal of the Royal Society Interface*. 2009;6:1075-86.
- [137] Aubin H, Nichol JW, Hutson CB, Bae H, Sieminski AL, Cropek DM, et al. Directed 3D cell alignment and elongation in microengineered hydrogels. *Biomaterials*. 2010;31:6941-51.
- [138] Hahn MS, Miller JS, West JL. Three - dimensional biochemical and biomechanical patterning of hydrogels for guiding cell behavior. *Advanced Materials*. 2006;18:2679-84.
- [139] Tsai W-B, Lin J-H. Modulation of morphology and functions of human hepatoblastoma cells by nano-grooved substrata. *Acta biomaterialia*. 2009;5:1442-54.
- [140] Wójciak-Stothard B, Curtis A, Monaghan W, Macdonald K, Wilkinson C. Guidance and activation of murine macrophages by nanometric scale topography. *Experimental cell research*. 1996;223:426-35.
- [141] Salick MR, Napiwocki BN, Sha J, Knight GT, Chindhy SA, Kamp TJ, et al. Micropattern width dependent sarcomere development in human ESC-derived cardiomyocytes. *Biomaterials*. 2014;35:4454-64.
- [142] Feinberg AW, Ripplinger CM, Van Der Meer P, Sheehy SP, Domian I, Chien KR, et al. Functional differences in engineered myocardium from embryonic stem cell-derived versus neonatal cardiomyocytes. *Stem cell reports*. 2013;1:387-96.
- [143] Vandemburgh HH, Solerssi R, Shansky J, Adams JW, Henderson SA, Lemaire J. Response of neonatal rat cardiomyocytes to repetitive mechanical stimulation in vitro. *Annals of the New York Academy of Sciences*. 1995;752:19-29.
- [144] Simpson D, Majeski M, Borg T, Terracio L. Regulation of cardiac myocyte protein turnover and myofibrillar structure in vitro by specific directions of stretch. *Circulation Research*. 1999;85:e59-e69.

- [145] Matsuda T, Takahashi K, Nariai T, Ito T, Takatani T, Fujio Y, et al. N-cadherin-mediated cell adhesion determines the plasticity for cell alignment in response to mechanical stretch in cultured cardiomyocytes. *Biochemical and biophysical research communications*. 2004;326:228-32.
- [146] Tulloch NL, Muskheli V, Razumova MV, Korte FS, Regnier M, Hauch KD, et al. Growth of engineered human myocardium with mechanical loading and vascular coculture. *Circulation research*. 2011;109:47-59.
- [147] Nitsan I, Drori S, Lewis YE, Cohen S, Tzliil S. Mechanical communication in cardiac cell synchronized beating. *Nature Physics*. 2016.
- [148] Berger H-J, Prasad SK, Davidoff A, Pimental D, Ellingsen O, Marsh J, et al. Continual electric field stimulation preserves contractile function of adult ventricular myocytes in primary culture. *American Journal of Physiology-Heart and Circulatory Physiology*. 1994;266:H341-H9.
- [149] Holt E, Lunde P, Sejersted O, Christensen G. Electrical stimulation of adult rat cardiomyocytes in culture improves contractile properties and is associated with altered calcium handling. *Basic research in cardiology*. 1997;92:289-98.
- [150] Ivester CT, Tuxworth WJ, Cooper G, McDermott PJ. Contraction accelerates myosin heavy chain synthesis rates in adult cardiocytes by an increase in the rate of translational initiation. *Journal of Biological Chemistry*. 1995;270:21950-7.
- [151] Au HTH, Cheng I, Chowdhury MF, Radisic M. Interactive effects of surface topography and pulsatile electrical field stimulation on orientation and elongation of fibroblasts and cardiomyocytes. *Biomaterials*. 2007;28:4277-93.
- [152] Feuerstein GZ, Young PR. Apoptosis in cardiac diseases: stress-and mitogen-activated signaling pathways. *Cardiovascular research*. 2000;45:560-9.
- [153] He S, Song H-F, Wu J, Weisel RD, Li R-K. A Conductive Biomaterial Patch to Repair a Cardiac Defect. *Am Heart Assoc*; 2016.
- [154] Park J, Park S, Ryu S, Bhang SH, Kim J, Yoon JK, et al. Graphene–Regulated Cardiomyogenic Differentiation Process of Mesenchymal Stem Cells by Enhancing the Expression of Extracellular Matrix Proteins and Cell Signaling Molecules. *Advanced healthcare materials*. 2014;3:176-81.
- [155] Qazi TH, Rai R, Dippold D, Roether JE, Schubert DW, Rosellini E, et al. Development and characterization of novel electrically conductive PANI–PGS composites for cardiac tissue engineering applications. *Acta biomaterialia*. 2014;10:2434-45.
- [156] Mooney E, Mackle JN, Blond DJ-P, O'Cearbhaill E, Shaw G, Blau WJ, et al. The electrical stimulation of carbon nanotubes to provide a cardiomimetic cue to MSCs. *Biomaterials*. 2012;33:6132-9.
- [157] Freier T. Biopolyesters in tissue engineering applications. *Polymers for Regenerative Medicine*. 2006:1-61.
- [158] Spaans CJ, Belgraver VW, Rienstra O, De Groot JH, Pennings AJ. Biomedical polyurethane-amide, its preparation and use. *Google Patents*; 2001.
- [159] Dumas JE, Davis T, Holt GE, Yoshii T, Perrien DS, Nyman JS, et al. Synthesis, characterization, and remodeling of weight-bearing allograft bone/polyurethane composites in the rabbit. *Acta Biomaterialia*. 2010;6:2394-406.
- [160] Yoshii T, Hafeman AE, Nyman JS, Esparza JM, Shinomiya K, Spengler DM, et al. A sustained release of lovastatin from biodegradable, elastomeric polyurethane scaffolds for enhanced bone regeneration. *Tissue Eng Part A*. 2010;16:2369-79.
- [161] Sudesh K, Abe H, Doi Y. Synthesis, structure and properties of polyhydroxyalkanoates: Biological polyesters. *Progress in Polymer Science (Oxford)*. 2000;25:1503-55.
- [162] Reusch RN, Sparrow AW, Gardiner J. Transport of poly- $\beta$ -hydroxybutyrate in human plasma. *Biochimica et Biophysica Acta - Lipids and Lipid Metabolism*. 1992;1123:33-40.
- [163] Kaufman E, Relkin N, Nelson T. Regulation and Properties of an NADP+ Oxidoreductase Which Functions as a  $\gamma$  - Hydroxybutyrate Dehydrogenase. *Journal of Neurochemistry*. 1983;40:1639-46.
- [164] Williams SF, Martin DP. Applications of PHAs in medicine and pharmacy. *Biopolymers*. 2002;4:91-127.
- [165] Sodian R, Hoerstrup SP, Sperling JS, Daebritz S, Martin DP, Moran AM, et al. Early in vivo experience with tissue-engineered trileaflet heart valves. *Circulation*. 2000;102:lii-22-iii-9.
- [166] Zhao K, Deng Y, Chen JC, Chen GQ. Polyhydroxyalkanoate (PHA) scaffolds with good mechanical properties and biocompatibility. *Biomaterials*. 2003;24:1041-5.



- [167] Li M, Gao S. Properties of poly(3-hydroxybutyrate-co-4-hydroxybutyrate)/polylactic acid blend. *Zhongguo Suliao*. 2008;22:36-41.
- [168] Luo R, Xu K, Chen G-Q. Study of miscibility, crystallization, mechanical properties, and thermal stability of blends of poly(3-hydroxybutyrate) and poly(3-hydroxybutyrate-co-4-hydroxybutyrate). *J Appl Polym Sci*. 2007;105:3402-8.
- [169] Rao U, Kumar R, Balaji S, Sehgal PK. A novel biocompatible poly (3-hydroxy-co-4-hydroxybutyrate) blend as a potential biomaterial for tissue engineering. *J Bioact Compat Polym*. 2010;25:419-36.
- [170] Tang Y, Liang D, Lou B. Crystallization and rheological behavior of poly(butylene succinate)/poly(3-hydroxybutyrate-4-hydroxybutyrate) blends. *Gaofenzi Cailiao Kexue Yu Gongcheng*. 2012;28:28-31,5.
- [171] Wang X, Chen Z, Chen X, Pan J, Xu K. Miscibility, crystallization kinetics, and mechanical properties of poly(3-hydroxybutyrate-co-3-hydroxyvalerate)(PHBV)/poly(3-hydroxybutyrate-co-4-hydroxybutyrate)(P3/4HB) blends. *J Appl Polym Sci*. 2010;117:838-48.
- [172] Zhu W, Wang X, Chen X, Xu K. Miscibility, crystallization, and mechanical properties of poly(3-hydroxybutyrate-co-4-hydroxybutyrate)/poly(butylene succinate) blends. *J Appl Polym Sci*. 2009;114:3923-31.
- [173] Wang Y, Ameer GA, Sheppard BJ, Langer R. A tough biodegradable elastomer. *Nature Biotechnology*. 2002;20:602-6.
- [174] Veress AI, Gullberg GT, Weiss JA. Measurement of strain in the left ventricle during diastole with cine-MRI and deformable image registration. *TRANSACTIONS-AMERICAN SOCIETY OF MECHANICAL ENGINEERS JOURNAL OF BIOMECHANICAL ENGINEERING*. 2005;127:1195.
- [175] Lv S, Dudek DM, Cao Y, Balamurali M, Gosline J, Li H. Designed biomaterials to mimic the mechanical properties of muscles. *Nature*. 2010;465:69-73.
- [176] Bellingham CM, Lillie MA, Gosline JM, Wright GM, Starcher BC, Bailey AJ, et al. Recombinant human elastin polypeptides self - assemble into biomaterials with elastin - like properties. *Biopolymers*. 2003;70:445-55.
- [177] Pinner SH. A practical course in polymer chemistry: Pergamon New York; 1961.
- [178] Berchtold MW, Brinkmeier H, Müntener M. Calcium ion in skeletal muscle: Its crucial role for muscle function, plasticity, and disease. *Physiological Reviews*. 2000;80:1215-65.
- [179] Woodcock EA, Wang BH, Arthur JF, Lennard A, Matkovich SJ, Du X-J, et al. Inositol polyphosphate 1-phosphatase is a novel antihypertrophic factor. *Journal of Biological Chemistry*. 2002;277:22734-42.
- [180] Autelitano DJ, Woodcock EA. Selective Activation of  $\alpha$  1A-adrenergic Receptors in Neonatal Cardiac Myocytes is Sufficient to Cause Hypertrophy and Differential Regulation of  $\alpha$  1-adrenergic Receptor Subtype mRNAs. *Journal of molecular and cellular cardiology*. 1998;30:1515-23.
- [181] Liang S, Cook WD, Chen Q. Physical characterization of poly (glycerol sebacate)/Bioglass® composites. *Polymer International*. 2012.
- [182] Ferreira V, Douglas J, Amis E. Phase ordering in blend films of semi - crystalline and amorphous polymers. *Macromolecular Symposia: Wiley Online Library*; 2001. p. 73-88.
- [183] Alfonso G, Russell T. Kinetics of crystallization in semicrystalline/amorphous polymer mixtures. *Macromolecules*. 1986;19:1143-52.
- [184] Jayasuriya AC, Ghosh S, Scheinbeim JI, Lubkin V, Bennett G, Kramer P. A study of piezoelectric and mechanical anisotropies of the human cornea. *Biosensors and Bioelectronics*. 2003;18:381-7.
- [185] Maikos JT, Elias RA, Shreiber DI. Mechanical properties of dura mater from the rat brain and spinal cord. *Journal of neurotrauma*. 2008;25:38-51.
- [186] Wang Y, Kim YM, Langer R. In vivo degradation characteristics of poly (glycerol sebacate). *Journal of biomedical materials research Part A*. 2003;66:192-7.
- [187] Xu B, Li Y, Fang X, Thouas GA, Cook WD, Newgreen DF, et al. Mechanically tissue-like elastomeric polymers and their potential as a vehicle to deliver functional cardiomyocytes. *Journal of the mechanical behavior of biomedical materials*. 2013;28:354-65.
- [188] Li Y, Cook WD, Moorhoff C, Huang W-C, Chen Q-Z. Synthesis, characterization and properties of biocompatible poly(glycerol sebacate) pre-polymer and gel. *Polymer International*. 2013;62:534-47.
- [189] Barrick CJ, Rojas M, Schoonhoven R, Smyth SS, Threadgill DW. Cardiac response to pressure overload in 129S1/SvImJ and C57BL/6J mice: temporal-and background-dependent development of concentric left

ventricular hypertrophy. *American Journal of Physiology-Heart and Circulatory Physiology*.

2007;292:H2119-H30.

[190] Brower GL, Gardner JD, Forman MF, Murray DB, Voloshenyuk T, Levick SP, et al. The relationship between myocardial extracellular matrix remodeling and ventricular function. *European Journal of Cardiothoracic surgery*. 2006;30:604-10.

[191] Giraud M-N, Armbruster C, Carrel T, Tevaearai HT. Current state of the art in myocardial tissue engineering. *Tissue engineering*. 2007;13:1825-36.

[192] Edith D, Six J-L. Surface characteristics of PLA and PLGA films. *Applied Surface Science*. 2006;253:2758-64.

[193] Zhang P, Tian R, Lv R, Na B, Liu Q. Water-permeable polylactide blend membranes for hydrophilicity-based separation. *Chemical Engineering Journal*. 2015;269:180-5.

[194] Falconnet D, Csucs G, Grandin HM, Textor M. Surface engineering approaches to micropattern surfaces for cell-based assays. *Biomaterials*. 2006;27:3044-63.

[195] Hubbell JA. *Biomaterials in tissue engineering*. Bio/technology (Nature Publishing Company). 1995;13:565-76.

[196] Tirrell M, Kokkoli E, Biesalski M. The role of surface science in bioengineered materials. *Surface Science*. 2002;500:61-83.

[197] Rajagopalan P, Marganski WA, Brown XQ, Wong JY. Direct comparison of the spread area, contractility, and migration of balb/c 3T3 fibroblasts adhered to fibronectin-and RGD-modified substrata. *Biophysical journal*. 2004;87:2818-27.

[198] Maheshwari G, Brown G, Lauffenburger DA, Wells A, Griffith LG. Cell adhesion and motility depend on nanoscale RGD clustering. *Journal of Cell Science*. 2000;113:1677-86.

[199] Lord MS, Foss M, Besenbacher F. Influence of nanoscale surface topography on protein adsorption and cellular response. *Nano Today*. 2010;5:66-78.

[200] Roach P, Eglin D, Rohde K, Perry CC. Modern biomaterials: a review—bulk properties and implications of surface modifications. *Journal of Materials Science: Materials in Medicine*. 2007;18:1263-77.

[201] Higuchi A, Ling Q-D, Chang Y, Hsu S-T, Umezawa A. Physical cues of biomaterials guide stem cell differentiation fate. *Chemical reviews*. 2013;113:3297-328.

[202] McBeath R, Pirone DM, Nelson CM, Bhadriraju K, Chen CS. Cell shape, cytoskeletal tension, and RhoA regulate stem cell lineage commitment. *Developmental cell*. 2004;6:483-95.

[203] Thomas CH, Collier JH, Sfeir CS, Healy KE. Engineering gene expression and protein synthesis by modulation of nuclear shape. *Proceedings of the National Academy of Sciences*. 2002;99:1972-7.

[204] Bietsch A, Michel B. Conformal contact and pattern stability of stamps used for soft lithography. *Journal of Applied Physics*. 2000;88:4310-8.

[205] Armani D, Liu C, Aluru N. Re-configurable fluid circuits by PDMS elastomer micromachining. *Micro Electro Mechanical Systems, 1999 MEMS'99 Twelfth IEEE International Conference on: Ieee; 1999*. p. 222-7.

[206] Subramani K, Birch MA. Fabrication of poly (ethylene glycol) hydrogel micropatterns with osteoinductive growth factors and evaluation of the effects on osteoblast activity and function. *Biomedical Materials*. 2006;1:144.

[207] Sundback CA, Shyu JY, Wang Y, Faquin WC, Langer RS, Vacanti JP, et al. Biocompatibility analysis of poly (glycerol sebacate) as a nerve guide material. *Biomaterials*. 2005;26:5454-64.

[208] Neeley WL, Redenti S, Klassen H, Tao S, Desai T, Young MJ, et al. A microfabricated scaffold for retinal progenitor cell grafting. *Biomaterials*. 2008;29:418-26.

[209] Microchem Corporation. [http://nano.columbia.edu/files/cise/SU8\\_2002-2025.pdf](http://nano.columbia.edu/files/cise/SU8_2002-2025.pdf).

[210] Li Y, Cook WD, Moorhoff C, Huang WC, Chen QZ. Synthesis, characterization and properties of biocompatible poly (glycerol sebacate) pre - polymer and gel. *Polymer International*. 2013;62:534-47.

[211] Bodas D, Khan-Malek C. Hydrophilization and hydrophobic recovery of PDMS by oxygen plasma and chemical treatment—An SEM investigation. *Sensors and Actuators B: Chemical*. 2007;123:368-73.

[212] Clark P, Connolly P, Curtis A, Dow J, Wilkinson C. Topographical control of cell behaviour: II. Multiple grooved substrata. *Development*. 1990;108:635-44.

[213] Vernon RB, Gooden MD, Lara SL, Wight TN. Microgrooved fibrillar collagen membranes as scaffolds for cell support and alignment. *Biomaterials*. 2005;26:3131-40.

- [214] Laflamme MA, Chen KY, Naumova AV, Muskheli V, Fugate JA, Dupras SK, et al. Cardiomyocytes derived from human embryonic stem cells in pro-survival factors enhance function of infarcted rat hearts. *Nature biotechnology*. 2007;25:1015-24.
- [215] van Laake LW, Passier R, Doevendans PA, Mummery CL. Human embryonic stem cell–derived cardiomyocytes and cardiac repair in rodents. *Circulation research*. 2008;102:1008-10.
- [216] Sekine H, Shimizu T, Dobashi I, Matsuura K, Hagiwara N, Takahashi M, et al. Cardiac cell sheet transplantation improves damaged heart function via superior cell survival in comparison with dissociated cell injection. *Tissue engineering Part A*. 2011;17:2973-80.
- [217] Segers VF, Lee RT. Stem-cell therapy for cardiac disease. *Nature*. 2008;451:937-42.
- [218] Seif-Naraghi SB, Salvatore MA, Schup-Magoffin PJ, Hu DP, Christman KL. Design and characterization of an injectable pericardial matrix gel: a potentially autologous scaffold for cardiac tissue engineering. *Tissue Engineering Part A*. 2010;16:2017-27.
- [219] Park H, Larson BL, Kolewe ME, Vunjak-Novakovic G, Freed LE. Biomimetic scaffold combined with electrical stimulation and growth factor promotes tissue engineered cardiac development. *Experimental cell research*. 2014;321:297-306.
- [220] Condorelli G, Borello U, De Angelis L, Latronico M, Sirabella D, Coletta M, et al. Cardiomyocytes induce endothelial cells to trans-differentiate into cardiac muscle: implications for myocardium regeneration. *Proceedings of the National Academy of Sciences*. 2001;98:10733-8.
- [221] Annabi N, Tsang K, Mithieux SM, Nikkhah M, Ameri A, Khademhosseini A, et al. Highly elastic micropatterned hydrogel for engineering functional cardiac tissue. *Advanced functional materials*. 2013;23:4950-9.
- [222] Alperin C, Zandstra P, Woodhouse K. Polyurethane films seeded with embryonic stem cell-derived cardiomyocytes for use in cardiac tissue engineering applications. *Biomaterials*. 2005;26:7377-86.
- [223] Wang P-Y, Yu J, Lin J-H, Tsai W-B. Modulation of alignment, elongation and contraction of cardiomyocytes through a combination of nanotopography and rigidity of substrates. *Acta biomaterialia*. 2011;7:3285-93.
- [224] Pilarczyk G, Raulf A, Gunkel M, Fleischmann BK, Lemor R, Hausmann M. Tissue-Mimicking Geometrical Constraints Stimulate Tissue-Like Constitution and Activity of Mouse Neonatal and Human-Induced Pluripotent Stem Cell-Derived Cardiac Myocytes. *Journal of functional biomaterials*. 2016;7:1.
- [225] Chen Y, Wang J, Shen B, Chan CW, Wang C, Zhao Y, et al. Engineering a Freestanding Biomimetic Cardiac Patch Using Biodegradable Poly (lactic - co - glycolic acid)(PLGA) and Human Embryonic Stem Cell - derived Ventricular Cardiomyocytes (hESC - VCMs). *Macromolecular bioscience*. 2015;15:426-36.
- [226] Gorgieva S, Kokol V. Collagen-vs. gelatine-based biomaterials and their biocompatibility: review and perspectives: INTECH open access publisher; 2011.
- [227] Chen Q, Liang S, Thouas GA. Elastomeric biomaterials for tissue engineering. *Progress in polymer science*. 2013;38:584-671.
- [228] Deutsch J, Motlagh D, Russell B, Desai TA. Fabrication of microtextured membranes for cardiac myocyte attachment and orientation. *Journal of biomedical materials research*. 2000;53:267-75.
- [229] Xu B, Cook WD, Zhu C, Chen Q. Aligned core/shell electrospinning of poly (glycerol sebacate)/poly (l - lactic acid) with tuneable structural and mechanical properties. *Polymer International*. 2016.
- [230] Bhardwaj N, Kundu SC. Electrospinning: a fascinating fiber fabrication technique. *Biotechnology advances*. 2010;28:325-47.
- [231] Liang S-L, Cook WD, Thouas GA, Chen Q-Z. The mechanical characteristics and in vitro biocompatibility of poly (glycerol sebacate)-Bioglass® elastomeric composites. *Biomaterials*. 2010;31:8516-29.
- [232] Lagerqvist E, Finnin B, Elliott D, Anderson D, Wu S, Pouton C, et al. Comparing mouse and human pluripotent stem cell derived cardiac cells: Both systems have advantages for pharmacological and toxicological screening. *Journal of pharmacological and toxicological methods*. 2015;74:17-25.
- [233] Xu F, Beyazoglu T, Hefner E, Gurkan UA, Demirci U. Automated and adaptable quantification of cellular alignment from microscopic images for tissue engineering applications. *Tissue Engineering Part C: Methods*. 2011;17:641-9.
- [234] Francis M, Waldrup J, Qian X, Taylor MS. Automated analysis of dynamic Ca<sup>2+</sup> signals in image sequences. *JoVE (Journal of Visualized Experiments)*. 2014:e51560-e.

- [235] Nagueh SF, Shah G, Wu Y, Torre-Amione G, King NM, Lahmers S, et al. Altered titin expression, myocardial stiffness, and left ventricular function in patients with dilated cardiomyopathy. *Circulation*. 2004;110:155-62.
- [236] Shapira-Schweitzer K, Seliktar D. Matrix stiffness affects spontaneous contraction of cardiomyocytes cultured within a PEGylated fibrinogen biomaterial. *Acta biomaterialia*. 2007;3:33-41.
- [237] Zimmermann W-H, Melnychenko I, Wasmeier G, Didié M, Naito H, Nixdorff U, et al. Engineered heart tissue grafts improve systolic and diastolic function in infarcted rat hearts. *Nature medicine*. 2006;12:452-8.
- [238] Boutin-Ganache I, Picard S, Deschepper CF. Distinct gene-sex interactions regulate adult rat cardiomyocyte width and length independently. *Physiological genomics*. 2002;12:61-7.
- [239] Du Y, Plante E, Janicki JS, Brower GL. Temporal evaluation of cardiac myocyte hypertrophy and hyperplasia in male rats secondary to chronic volume overload. *The American journal of pathology*. 2010;177:1155-63.
- [240] Jaafar IH, LeBlon CE, Wei M-T, Ou-Yang D, Coulter JP, Jedlicka SS. Improving fluorescence imaging of biological cells on biomedical polymers. *Acta biomaterialia*. 2011;7:1588-98.
- [241] Shenasa M. Arrhythmias in Cardiomyopathies, An Issue of Cardiac Electrophysiology Clinics: Elsevier Health Sciences; 2015.
- [242] Chao MV. Neurotrophins and their receptors: a convergence point for many signalling pathways. *Nature Reviews Neuroscience*. 2003;4:299-309.
- [243] Levi - Montalcini R, Hamburger V. Selective growth stimulating effects of mouse sarcoma on the sensory and sympathetic nervous system of the chick embryo. *Journal of experimental zoology*. 1951;116:321-61.
- [244] Acheson A, Conover JC, Fandl JP, DeChiara TM, Russell M, Thadani A, et al. A BDNF autocrine loop in adult sensory neurons prevents cell death. 1995.
- [245] Baxter GT, Radeke MJ, Kuo RC, Makrides V, Hinkle B, Hoang R, et al. Signal transduction mediated by the truncated trkB receptor isoforms, trkB. T1 and trkB. T2. *The Journal of neuroscience*. 1997;17:2683-90.
- [246] Klein R, Conway D, Parada LF, Barbacid M. The trkB tyrosine protein kinase gene codes for a second neurogenic receptor that lacks the catalytic kinase domain. *Cell*. 1990;61:647-56.
- [247] Rose CR, Blum R, Pichler B, Lepier A, Kafitz KW, Konnerth A. Truncated TrkB-T1 mediates neurotrophin-evoked calcium signalling in glia cells. *Nature*. 2003;426:74-8.
- [248] Prakash Y, Martin RJ. Brain-derived neurotrophic factor in the airways. *Pharmacology & therapeutics*. 2014;143:74-86.
- [249] Halade GV, Ma Y, Ramirez TA, Zhang J, Dai Q, Hensler JG, et al. Reduced BDNF attenuates inflammation and angiogenesis to improve survival and cardiac function following myocardial infarction in mice. *American Journal of Physiology-Heart and Circulatory Physiology*. 2013;305:H1830-H42.
- [250] Cai D, Holm JM, Duignan IJ, Zheng J, Xaymardan M, Chin A, et al. BDNF-mediated enhancement of inflammation and injury in the aging heart. *Physiological genomics*. 2006;24:191-7.
- [251] Okada S, Yokoyama M, Toko H, Tateno K, Moriya J, Shimizu I, et al. Brain-derived neurotrophic factor protects against cardiac dysfunction after myocardial infarction via a central nervous system-mediated pathway. *Arteriosclerosis, thrombosis, and vascular biology*. 2012;32:1902-9.
- [252] Katare RG, Kakinuma Y, Arikawa M, Yamasaki F, Sato T. Chronic intermittent fasting improves the survival following large myocardial ischemia by activation of BDNF/VEGF/PI3K signaling pathway. *Journal of molecular and cellular cardiology*. 2009;46:405-12.
- [253] Hang P, Zhao J, Cai B, Tian S, Huang W, Guo J, et al. Brain-derived neurotrophic factor regulates TRPC3/6 channels and protects against myocardial infarction in rodents. *International journal of biological sciences*. 2015;11:536.
- [254] Liu Y, Sun L, Huan Y, Zhao H, Deng J. Application of bFGF and BDNF to improve angiogenesis and cardiac function. *Journal of Surgical Research*. 2006;136:85-91.
- [255] Feng N, Huke S, Zhu G, Tocchetti CG, Shi S, Aiba T, et al. Constitutive BDNF/TrkB signaling is required for normal cardiac contraction and relaxation. *Proceedings of the National Academy of Sciences*. 2015;112:1880-5.
- [256] Fulgenzi G, Tomassoni-Ardori F, Babini L, Becker J, Barrick C, Puverel S, et al. BDNF modulates heart contraction force and long-term homeostasis through truncated TrkB. T1 receptor activation. *The Journal of cell biology*. 2015;210:1003-12.

- [257] Li H-S, Xu X-ZS, Montell C. Activation of a TRPC3-dependent cation current through the neurotrophin BDNF. *Neuron*. 1999;24:261-73.
- [258] Contreras-Ferrat AE, Toro B, Bravo R, Parra V, Vásquez C, Ibarra C, et al. An inositol 1, 4, 5-triphosphate (IP3)-IP3 receptor pathway is required for insulin-stimulated glucose transporter 4 translocation and glucose uptake in cardiomyocytes. *Endocrinology*. 2010;151:4665-77.
- [259] Massa SM, Yang T, Xie Y, Shi J, Bilgen M, Joyce JN, et al. Small molecule BDNF mimetics activate TrkB signaling and prevent neuronal degeneration in rodents. *The Journal of clinical investigation*. 2010;120:1774-85.
- [260] Nagahara AH, Tuszynski MH. Potential therapeutic uses of BDNF in neurological and psychiatric disorders. *Nature reviews Drug discovery*. 2011;10:209-19.
- [261] Gudasheva T, Logvinov I, Antipova T, Seredenin S. Brain-derived neurotrophic factor loop 4 dipeptide mimetic GSB-106 activates TrkB, Erk, and Akt and promotes neuronal survival in vitro. *Doklady Biochemistry and biophysics: Springer Science & Business Media*; 2013. p. 212.
- [262] Yu G, Wang W. Protective effects of LM22A-4 on injured spinal cord nerves. *International journal of clinical and experimental pathology*. 2015;8:6526.
- [263] Numakawa T. Possible protective action of neurotrophic factors and natural compounds against common neurodegenerative diseases. *Neural regeneration research*. 2014;9:1506.
- [264] Han J, Pollak J, Yang T, Siddiqui MR, Doyle KP, Taravosh-Lahn K, et al. Delayed administration of a small molecule tropomyosin-related kinase B ligand promotes recovery after hypoxic-ischemic stroke. *Stroke*. 2012;43:1918-24.
- [265] Kajiya M, Takeshita K, Kittaka M, Matsuda S, Ouhara K, Takeda K, et al. BDNF mimetic compound LM22A-4 regulates cementoblast differentiation via the TrkB-ERK/Akt signaling cascade. *International immunopharmacology*. 2014;19:245-52.
- [266] Li Y, Huang W, Cook WD, Chen Q. A comparative study on poly (xylitol sebacate) and poly (glycerol sebacate): mechanical properties, biodegradation and cytocompatibility. *Biomedical Materials*. 2013;8:035006.
- [267] Liang S-L, Yang X-Y, Fang X-Y, Cook WD, Thouas GA, Chen Q-Z. In vitro enzymatic degradation of poly (glycerol sebacate)-based materials. *Biomaterials*. 2011;32:8486-96.
- [268] Smith R, Williams D, Oliver C. The biodegradation of poly (ether urethanes). *Journal of biomedical materials research*. 1987;21:1149-65.
- [269] Smith R, Oliver C, Williams D. The enzymatic degradation of polymers in vitro. *Journal of biomedical materials research*. 1987;21:991-1003.
- [270] Tamura Z, Maeda M. [Differences between phthaleins and sulfonphthaleins]. *Yakugaku zasshi: Journal of the Pharmaceutical Society of Japan*. 1997;117:764-70.
- [271] Pomerantseva I, Krebs N, Hart A, Neville CM, Huang AY, Sundback CA. Degradation behavior of poly (glycerol sebacate). *Journal of biomedical materials research Part A*. 2009;91:1038-47.
- [272] Hiltunen JO, Laurikainen A, Väkevä A, Meri S, Saarma M. Nerve growth factor and brain - derived neurotrophic factor mRNAs are regulated in distinct cell populations of rat heart after ischaemia and reperfusion. *The Journal of pathology*. 2001;194:247-53.
- [273] Radisic M, Park H, Chen F, Salazar-Lazzaro JE, Wang Y, Dennis R, et al. Biomimetic approach to cardiac tissue engineering: oxygen carriers and channeled scaffolds. *Tissue engineering*. 2006;12:2077-91.